HYDROPHOBIC PAYLOAD ENCAPSULATION AND RELEASE CHARACTERISTICS IN SELF-ASSEMBLED PEPTIDE HYDROGELS

by

Jessie E.P. Sun

A dissertation submitted to the Faculty of the University of Delaware in partial fulfillment of the requirements for the degree of Doctor of Philosophy in Materials Science and Engineering

Fall 2015

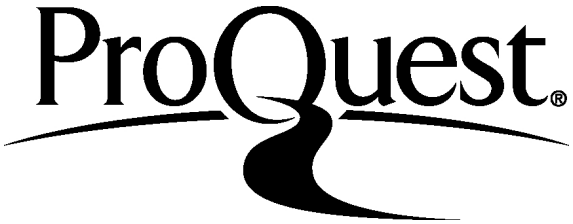

HYDROPHOBIC PAYLOAD ENCAPSULATION AND RELEASE CHARACTERISTICS IN SELF-ASSEMBLED PEPTIDE HYDROGELS

by

Jessie E.P. Sun

Approved: _____
Darrin J. Pochan, Ph.D.
Chair of the Department of Materials Science and Engineering

Approved: _____
Babatunde A. Ogunnaike, Ph.D.
Dean of the College of Engineering

Approved: _____
Ann L. Ardis, Ph.D.
Interim Vice Provost for Graduate and Professional Education

I certify that I have read this dissertation and that in my opinion it meets the academic and professional standard required by the University as a dissertation for the degree of Doctor of Philosophy.

Signed: _____

Darrin J. Pochan, Ph.D.
Professor in charge of dissertation

I certify that I have read this dissertation and that in my opinion it meets the academic and professional standard required by the University as a dissertation for the degree of Doctor of Philosophy.

Signed: _____

Xinqiao Jia, Ph.D
Member of dissertation committee

I certify that I have read this dissertation and that in my opinion it meets the academic and professional standard required by the University as a dissertation for the degree of Doctor of Philosophy.

Signed: _____

Kristi L. Kiick., Ph.D.
Member of dissertation committee

I certify that I have read this dissertation and that in my opinion it meets the academic and professional standard required by the University as a dissertation for the degree of Doctor of Philosophy.

Signed: _____

Sigrid A. Langhans, Ph.D.
Member of dissertation committee

ACKNOWLEDGEMENTS

There would be no thesis without my advisor, Professor Darrin Pochan. I am forever appreciative to have had the opportunity to join the group and performed the research I did. I am grateful for his patience, suggestions, discussions, and general knowledge. Under his guidance, I gained so much in my research, presentation, and conference skills. The bulk of this dissertation comes from a collaboration with Professor Sigrid Langhans at Nemours/AI duPont Hospital for Children. I would like to thank her for her guidance and instruction in proper *in vitro* and *in vivo* work. I would also like to thank Dr. Seung Joon Lee, Alisa Litan, and Dr. Stephan Lindsey for our collaborative work at Nemours. Through my years at UD, I have greatly appreciated Professor Kristi Kiick for her keen eye and discussions on how to improve and grow as a researcher. I am also grateful for Professor Xinqiao Jia's assistance with any questions that arose from cell work and hydrogels. In addition, special thanks to Dr. Joel Schneider and Katelyn Nagy for their help in peptide synthesis and purification. From my time at NIST, I am thankful for Dr. Paul Butler and Dr. Boualem Hammouda in their ready assistance and knowledge of SANS.

Of friends and family, I firstly have to thank my parents Chaomei Lin and Weijing Sun. Thank you for the seemingly endless patience with my absolutely endless deluge of inquiries throughout my life. I never stopped asking questions and my parents gave me all the answers with accompanying detailed explanations. I managed to break everything, myself included. I would not be here without every sacrifice they have ever made for me. I know that having me in the first years of living in America was not easy. I realize how hard they each have worked to afford me the opportunities I have now. I am forever grateful. Thank you for filling my life with songs, stories, and endless inspiration to be a better, smarter Jie Yaya. And of course, thank you Nini Meimei,

my sister Jenny, for listening to my complaints, sending me pictures of Andrew Luck, and going with me to Old Country Buffet.

Thank you Ben Emata, for everything ridiculous. A million thanks to Kate & Capt Andy (& Co-pilot Luke!) Stevens, for their never-ending belief in me (and Kelly). My forever gratitude to the teachers who motivated and built me up as a person, not just a student: Mark Linkins, Katie Shepard, Sherry Paris, Roberta Winemiller, and Jane Evans.

If it were not for Justin Vranic and the ridiculous hours; constant prodding and inspiration; and continued encouragement I would not have made it out of undergrad whole. Penn Women's Rugby, without you I would not have had found the confidence to be so comfortably myself. Thank you lovely ladies. In particular, thanks for still sticking by my ridiculous side, Krystyna Dereszowska.

I was incredibly lucky to have one of the most supportive and enthusiastic undergraduate research advisors. Professor Russ Composto has been one of the most positive influences in my life, and I can never thank him enough for being such a big part of my academic career. In kind, I would also like to thank Professor Karen Winey for her constant practical advice and kind encouragement.

"How To Commute Efficiently Without Losing Your Mind &
Strangling Everyone Around You:
A Guide to I-95's Mid-Atlantic Corridor"

The commuting has certainly added its own stress and health issues these past few years. It's also added a whole slew of people I have to thank for helping me while at UD. Thank you, my other roommate, Nandita Bhagwat: who slogged through the bad days, celebrated the good days, and watched ridiculous TV (*cough* Supernatural) with me. Thank you Lauren Hurd: my gym buddy, cupcake ally, general motivator, and adventure compadre. Thank you Mary Boggs and Karen Black for being my McKinley go-to's, for the easy conversation, and for solid friendships. While driving

to/from NIST this past year, without the wonderful folks at the NCNR (especially Kirby's, Krzywon, Katie, Kim, and Amanda) the traffic through Maryland would not have been worth it. A million thank you's to the Pochan group, old and new members: Aysegul, Congqi, Sean, Jiahua, Sameer, Yingchao, Brandon, Pete, Mike, Zach, Ziran, Yu, Jee, and Fränk.

And finally, to my husband, Michael JA Hore. Without you, I would be typing this in Word, frustrated with every equation. Without you, I am not entirely sure I would have gone to grad school or made it this far. Without you, there would not be Elvis & ELO filled adventures, hand-brake turns, or bulldog pictures. Thank you for sending me that strawberry pizza picture so many years ago and agreeing to be my best Powell. As is tradition, I strive to be a better person because of you and cannot wait to see all the awesome we're about to take on. Home, is where I want to be, but I guess I'm already there.

TABLE OF CONTENTS

LIST OF TABLES

LIST OF FIGURES

ABSTRACT

Peptide based hydrogels are an important class of polymeric materials, which have received a large amount of attention for their easy-to-tailor synthesis, biocompatibility, self-assembly into ordered structures and advantageous rheological properties. With twenty-one biologically-relevant amino acids and an ever growing number of synthetic amino acids, countless combinations of potential peptide sequences can be synthesized on the benchtop. The step-by-step synthesis of these peptides leads to precisely controlled amino acid sequences, with predictable physical properties, chemical characteristics and functionalities. In this dissertation, the MAX8 peptide hydrogel is used to encapsulate hydrophobic drugs within a self-assembled, fibrillar network. MAX8 peptide sequences self-assemble at physiological conditions into β-hairpins that form bilayer fibrils with natural branch and entanglement points. In particular, because of this physically crosslinked network, MAX8 is a shear-thinning injectable solid with immediate rehealing behavior.

Using rheometry, cytotoxicity assays, spectrophotometry, and liquid scintillation counting, this dissertation examines the successful encapsulation and continuous release of a hydrophobic drug, vincristine, over the course of a month from MAX8 peptide hydrogels. Vincristine, effective at low concentrations, is a commonly used chemotherapeutic that indiscriminately attacks any replicating cell. Despite a month of encapsulation in the aqueous MAX8 hydrogel environment, the vincristine concentrations released are non-zero and retain cytotoxicity. This sustained release of active vincristine, combined with the injectable solid properties of MAX8, demonstrate that MAX8 peptide hydrogels are ideal drug delivery vehicles. Finally, MAX8 hydrogels will have the ability to localize and deliver the potent chemotherapeutic, minimizing unwanted cytotoxicity, while also providing constant treatment.

To better characterize the relationship between the hydrophobic vincristine and MAX8 hydrogels, the final chapter of this dissertation utilizes small-angle neutron scattering (SANS) to investigate drug-gel nanostructure. SANS is a powerful technique that characterizes interparticle correlations, which is necessary for understanding the inner hydrogel environment in the presence and constantly changing surrounding concentration of vincristine. The SANS experimental conditions for defining the relationship of a hydrophobic payload in MAX8 hydrogel included time release in different sample environments and the introduction of cisplatin — another hydrophobic chemotherapeutic. Additionally, in this chapter, SANS is employed to quantify the dimensions of a multi-metal/ligand supramolecular gel.

Chapter 1

INTRODUCTION

This thesis details the encapsulation of vincristine in MAX8 hydrogels. The unique peptidic nature of MAX8 is important in its eventual use as a drug delivery vehicle. Here, the encapsulation and release of vincristine are characterized to better understand the drug's effect on the network of MAX8, the drug's effect on cell death over time while encapsulated, and the drug's own characteristics within the hydrogel network.

This chapter examines the importance of polymer hydrogels as drug delivery vehicles. The different types of polymer hydrogels will be highlighted, with a particular focus on peptide hydrogels. Peptides have distinct structures — primary, secondary, tertiary, quaternary, each capable of creating hydrogels. Of the structures, there is an emphasis on β-hairpin, the fundamental structure of MAX8. After exploring the methods of characterization and applications of the peptidic hydrogels, there is a more detailed examination of the MAX family of peptides and its unique desired characteristics. The MAX family of peptides have successfully encapsulated a variety of payloads. These successes pave the way for the bulk of the work of this thesis.

1.1 Hydrogels as Drug Delivery Vehicles

The fundamental definition of a hydrogel is a three-dimensional network of hydrated polymer chains. In practice, hydrogels are highly varied in assembly components and methods, resulting in a large range of gel structure, gelation, and biocompatibilty characteristics. Of the many possible hydrogel applications, such as cell scaffolding and tissue engineering or diagnostic sensors, the focus of this thesis will be on drug delivery.

Hydrogels used for drug delivery vehicles can be categorized by the composition of the hydrogel, whether from synthetic origins or biological origins.

1.1.1 Synthetic Polymer Hydrogels

Synthetic polymers can be viewed as polymers without natural inspirations, created purely within the lab. Because of its man-made nature, synthetic polymer hydrogels can be synthesized with specific desired characteristics and capabilities in mind. There are many synthetic polymers currently available for hydrogel drug delivery, including poly-(ethylene glycol)(PEG) and poly-(vinyl alcohol)(PVA). PVA hydrogels are stable and elastic hydrogels that can be physically or chemically crosslinked.[1–5] There are several ways of creating and modifying PVA hydrogels. With the wide availability of pendant hydroxy groups, the possible macromers and resultant characteristics, gives variability in payload encapsulation[6] or degradation of PVA hydrogels.[4,7–9]

Most notably, PEG is used for many biomaterial applications and is one of the most commonly studied and varied polymers for hydrogels. PEG is known for its protein adsorption resistance[10,11], useful in biomedical applications. There are an increasing number of applications using PEG, varying modifications to its surface[1,12–14] or to its overall composition as a block copolymer.[15–17] There are many more synthetic polymer hydrogels for drug delivery available for discussion. However, the line between synthetic and biology inspired polymer hydrogels blur as current applications and modifications of synthetic polymer hydrogels are increasingly incorporating the use of biologically inspired components.[4,15,18]

1.1.2 Biological Polymer Hydrogels

Biological polymers draw inspiration from the proteins and polysaccharides created in nature. Specifically, these hydrogels can be composed of chitosan — a linear polysaccharide found in crustacean exoskeletons[3,19–22], hyaluronic acid – a major component of the extracellular matrix[13,23,24], alginate — an anionic polysaccharide found mostly in algae[24–26], or many different types of proteins and protein derivatives found

naturally in the human body.[7,27–30] Because the hydrogels are composed of the nature-inspired materials, these biological polymer hydrogels are often cytocompatible. Cytocompatibility is a broad, general term that describes whether or not a cell is able to survive near, in, with, or on a hydrogel. This makes biological polymer hydrogels excellent candidates in providing growth conditions that mimic the natural, in vivo environment of cells. This cytocompatibility also means that the hydrogels alone are less likely to induce an adverse immune response.

As mentioned before, there is an increasing trend towards hybrid molecules produced through traditional organic or polymer chemistry methods with desired biologically inspired polymers attached to synthetic polymers, hydrocarbon chains, or even peptide chains as conjugates. One of the most common sequences used as a conjugate is the three amino acid sequence of RGD (arginine, glycine, aspartic acid). RGD is used because of its ability to trigger cell adhesion, a useful feature after delivery.[31–38] RGD and its many derivatives can also be synthesized by through non-traditional methods.[32,35,36,39–43] RGD does not create hydrogels itself; rather, RGD is incorporated into other polymer sequences that go on to create hydrogels through physical assembly or chemical reactions. Another biologically inspired molecule used to modify synthetic polymers to improve drug delivery is heparin, a linear polysaccharide used clinically for blood coagulation.[44] Heparin can be covalently attached or encapsulated for release in a hydrogel to promote anti-coagulation[45] or help collect needed proteins to sustain delivery after deposition.[46]

Specifically, this thesis focuses on peptide hydrogels, a type of biologically inspired polymer hydrogel. Peptide hydrogels, have shown exceptional cytocompatibility with many different cell lines such as mesenchymal stem cells (MSCs)[47–49], embryonic stem cells (ESCs)[50,51], rat adrenal pheochromocytoma cells[52], or macrophages.[53] Many of these cell types have not only stayed alive while encapsulated, but also continued to grow and proliferate, indicating a high degree of cytocompatibility in the peptide hydrogels.

Because of the nature-inspired origins of peptide hydrogels, the natural degradation of peptide hydrogels is also an important property. This is a feature that is inherent in peptide hydrogels that is less characteristic in polymeric hydrogels. Because of the amino acid origins of peptide hydrogels, there is natural degradation[47,54,55] that occurs from enzymes secreted by the body in vivo, without major immune reactions.[33,33,41,41,54,56–58] Macrophages and neutrophils are cells typically associated with an immune response in the body that are observed to have little or no reaction when cultured with hydrogels[50,53,59] or in vivo.[50] The interaction of enzyme with peptides to affect hydrogel properties is not surprising, since one of the possible triggers for self-assembly is the introduction of enzymes to linear peptides as seen by the Xu and Ulijn groups.[60,61] In degradation, however, instead of assembling short peptides into fibrils and hydrogels, the hydrogels are being broken down into smaller pieces through enzymolysis.[27,55,62] When designing the peptide sequences, specific segments that act as reaction substrates for enzymes such as MMP13[62] or MMP2.[27] can be incorporated into the initial peptide synthesis. The rest of this chapter explores the fundamentals of peptide hydrogels and the resultant advantages of using peptide hydrogels for drug delivery.

1.2 Peptide Hydrogels

Peptides in nature and biology are critical for structure and function and involved in every bodily process from cell reproduction and tissue generation to simple enzymatic reactions. In the design of synthetic peptides, the scientist and engineer has twenty one natural amino acids, in addition to a large and growing number of man-made amino acids to choose from for molecule formation. This amino acid toolbox provides for an almost limitless array of characteristics and function in new molecules and hydrogel materials. Amino acid attributes can include more traditional characteristics, such as hydrophobicity, polarity, or charge, or more exotic functionality such as the ability to crosslink with specificity in a click ligation reaction.[32,34,36,38,39,63–66] Therefore, these inherent amino acid characteristics are taken full advantage of in creating

a rich library of peptide hydrogel sequences with drastically varied chemistries.

The piece-by-piece amino acid chemical connection during peptide synthesis, combined with the range of amino acid properties, gives peptide hydrogels tunable characteristics and capabilities for a multitude of chemical, material or biological uses. After molecular peptide synthesis, many peptide hydrogels are constructed with solution assembly mechanisms and can be made in situ with the introduction of the proper trigger, or change in environment, such as changes in temperature, pH, or ionic concentration.[31,32,36,39,67–74] While the starting peptide sequences are straightforward to synthesize, the resulting structures after triggered molecular assembly can take on secondary, tertiary or quaternary structures like peptides and proteins in nature.

There are many different types of peptide hydrogels presently being researched, from those created from short peptide sequences that exist as conjugates with other synthetic polymer constructs.[28,54,60,67,70,71,75–80] to hydrogels made from high molecular weight, protein-like molecules.[73,81–88] The focus on peptide hydrogels will be mainly on shorter peptide sequences that can be triggered in situ to form higher order structure and, consequently, form supramolecular, physical hydrogels.[31,33,35,37,69] These sequences are shorter than typical proteins, and their solution self-assembling capabilities to form higher order, intra- and intermolecular structures can result in a variety of hydrogels with beneficial and interesting material properties such as shear-thinning capabilities for injectable solid behavior for therapy delivery.[35,39–43,69,75,89–91]

The structural hierarchy of peptide hydrogel sets them apart from synthetic polymer hydrogels. Peptides, and their resultant shapes after folding and intermolecular assembly, are categorized by four different levels of structure: primary, secondary, tertiary, and quaternary. With adaptable and precise synthesis methods, peptide structures have the ability to achieve naturally-inspired structures such as those observed in known protein crystal structures as well as completely new, de novo designed structures by proper design of a peptide sequence. Starting with a designed sequence, peptides can be constructed faithfully into a final, desired structure and function. Additional functional groups or amino acids can be added, exchanged, or removed from a

known natural or designed sequence to change the final material structure, the kinetics of intermolecular assembly, the material properties or other behaviors (*e.g.* biological properties) of the resultant peptide hydrogel. The molecular assembly processes designed into peptide hydrogels can be readily made to be efficient, fast, and easily modified based on the desired hydrogel performance environment. From synthesis to assembly, a considerable amount of organization of intermolecular and intramolecular interactions is needed. Each structure and its final properties as a hydrogel is defined and affected by these interactions.

Regardless of final hydrogel structure, the driving forces of peptide assembly into hierarchical structures and materials are physical, non-covalent interactions such as hydrogen bonding and π-stacking, hydrophobicity, van der Waals interactions, as well as electrostatic interactions. In aqueous solutions, all of these interactions have been used, primarily in concert, to bring peptides together and to hold the assembled structure together after assembly and gelation.[60,61,67,70,71,77,79,80,86,87,92,93] Changing the pH, ionic concentration, or temperature of a solution can be used to trigger the solution assembly of the peptide sequences. These changes force single molecules to intramolecularly fold into desired secondary structures, such as β-sheets or α-helices, and/or collections of molecules that begin intermolecularly assembling to form local nanostructure such as nanofibrils or nanotubes. The entire process results in a hydrogel with quaternary structure (*i.e.* hydrogel network structure) organization.[31,32,35,36,39,60,67–74,81,82,84,87,88,93–95]

1.2.1 Primary Structures

Primary structure is the first order peptide structure resulting from the amino acid linear sequence. The diversity in the natural amino acids as well as numerous synthetic, non-natural amino acids allows for a great and constantly growing number of possibilities of primary sequences. Linked together with amide bonds between the carboxylic acid and amine ends of neighboring amino acids, peptides are predominantly linear in architecture. However, chemistry can be designed to make

branched peptides, particularly when peptides are combined as a hybrid with other organic molecules. For example, peptide primary structure can also be seen in hybrid polymer-peptide or aliphatic hydrocarbon conjugates that can introduce new architecture and other characteristics (*e.g.* peptide amphiphiles that exhibit branches or helical behavior.[28,54,60,67,70–72,75–80,86,96–100]); or polymer-peptide conjugates that have star or branched architecture.[56,73,74,81–88,101–106]

Previously, the synthesis of peptidic materials was seen as a cumbersome and expensive method that lacked the precision of other polymeric synthesis methods.[31,33,35,37,63,69,72,74,86,107] Synthesis of peptides has quickly advanced with cheaper methods, larger yield quantities, greater precision, and more adaptive equipment and methodology. There are two main pathways of creating a large number of customized peptide sequences: a.) engineered/recombinant DNA synthesis or b.) synthetic solid phase peptide synthesis (SPPS).[35,39–43,69,74,75,86,89–91,108,109] These synthetic methods are preferred to traditional methods because of the yield, automation, and time saved when compared to manual organic synthesis.

The main method of peptide synthesis used in this thesis is SPPS. This method allows for more straightforward incorporation of noncanonical amino acids than with recombinant DNA.[33,41,49,59,60,75,78,82,110,111] Additionally, the synthesis process can be done by automation through machine or by hand. The convenience of using a machine is the automated process of many repeat steps for longer peptide sequences. The ease of use allows for a greater number of novel peptide sequences to be created. Synthesis begins with a resin support made of small, porous polymer beads that are functionalized so that the amino acid attaches with an amide bond. The functionalization of the bead depends on the protection group used for the attaching amino acids and cleavage conditions.[112] Amino acids are added sequentially onto the solid phase-supported growing sequence, c-terminus to n-terminus. To ensure only one coupling reaction per amino acid, the n-terminus of each amino acid added to the reaction vessel has one of two possible protection groups, fluorenylmethyloxycarbonyl chloride (Fmoc) or tert-butyloxycarbonyl (Boc). Traditionally, Boc was the protection group, but the need for

hydrogen fluoride (HF) in the final cleavage step brought about the Fmoc group for protection.[112,113] The system is washed after each coupling step to remove unattached amino acids, after which, the n-terminus of the growing peptide chain is deprotected for the next amino acid. After the desired sequence is created, the resin and attached amino acids are filtered to remove unwanted amino acids. The desired peptide sequence is finally cleaved from the resin. As mentioned before, HF, an acid, is needed in the cleavage step for Boc protected synthesis, while a base such as piperidine is needed for Fmoc protected synthesis. Because of the sequential definition of amino acids, peptide hydrogels can be readily designed with different characteristics by specifically altering the primary sequence. This primary structure design can directly affect the solution conditions in which the peptides intermolecularly assemble, and the nanostructure formed after assembly. Hydrogel properties such as the solution conditions desired for encapsulated payload release are also dependent on primary structures.

With the ease of synthesis, there are a vast number of possible combinations of natural and non-natural amino acids with varying sequence lengths. The length of a peptide sequence affects many of the characteristics of the hydrogel created. Shorter peptide sequences will generally assemble faster intermolecularly with less defective assembly than longer sequences that can coil and entangle during assembly. Mono-[75], di-[114,115], and tri-peptide.[35,60,73,90] sequences that are created as supramolecular gelators tend to be made of amino acids with naturally hydrophobic or polar but uncharged functional groups.[33,35,67,87,88,90] Some mono-, di- and tri-peptide sequences retain the Fmoc protection group at the end of the n-terminus, which is observed to be an integral part in hydrogel formation with π-stacking from the aromatic rings. Changing pH[56,75,90,91,102,104] to force hydrophobic collapse or the addition of enzymes[60,61,63,72,86,107] can be used to induce hydrogelation. Figure 1.1 shows two di-peptides used in combination to create three different hydrogels and the TEM images of the fibrils formed.[115]

When triggered, short amino acid sequences can form long fibril networks of peptides to form hydrogels. The peptides generally start as primary structures soluble in solution, but then self assemble intermolecularly into higher order structures and

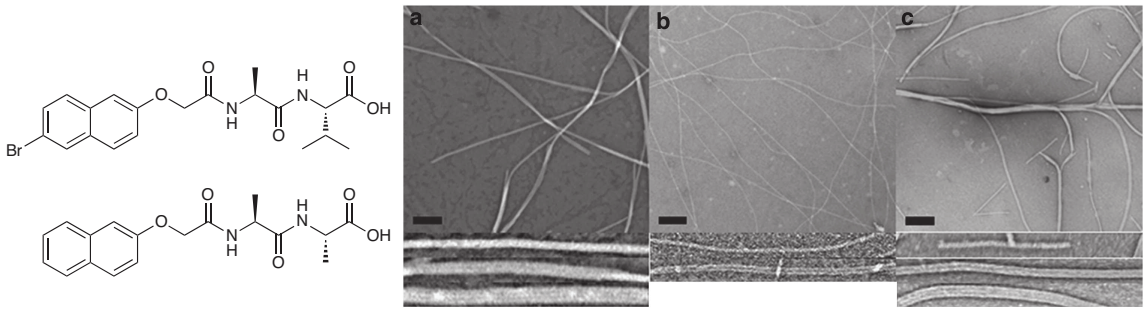

Figure 1.1: Shown are two monopeptide structures, the top (**I**) and bottom (**II**) alone or in combination using TEM. The inset beneath image shows local fibril structure more clearly. The scale bar is 200nm. **a.**) **I** alone. **b.**) **II** alone **c.**) Combination of **I** and **II**.[115]

hydrogels.[39,82,84,86–88,93,95,108,109,116,117] In order for longer sequences to self-assemble, longer peptide sequences generally have both hydrophobic, uncharged amino acids, and hydrophilic, polar groups to help drive secondary bonding and hydrophobic collapse of sequences. The trigger for longer sequences to intermolecularly assemble into higher order structures will usually be a change in pH, temperature or ion concentration although many other stimuli have been designed and will be discussed later in the chapter. The properties and applications of these higher order structures will be discussed in greater detail further on with quaternary structures. Figure 1.2 is an example from the Hartgerink group, showing fibril formation and hydrogel formation.[95] First, the primary order peptide structures assembled into fibrous quaternary structures. The introduction of multivalent ions triggers gelation, inducing interfibrillar assembly. The barely entangled or branched fibril structures between the short sequence peptide hydrogels of Figure 1.1 is visibly different from the longer sequence fibrils after gelation in Figure 1.2.

1.2.2 Secondary Structures

Secondary structures in peptides display a specific conformation of the peptide chain. The two main secondary structures are the α-helix and the β-sheet. For both structures, there has been extensive research to define, dictate, and predict structural and folding behaviors of primary sequences of peptides.[35] Before a triggering event

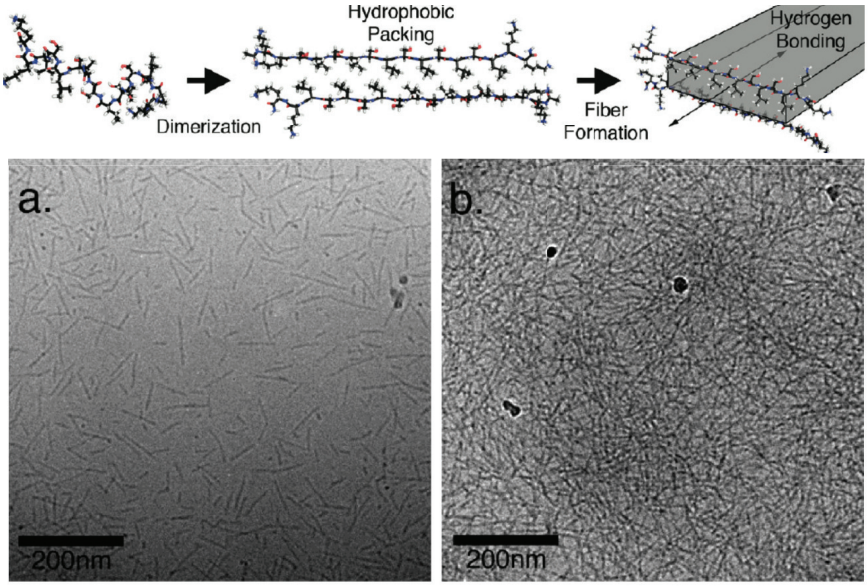

Figure 1.2: Dimers and folding mechanism of primary peptide sequences. TEM images show $E(QL)_6E$ from the Hartgerink group **a.**) before gelation and **b.**) after gelation, triggered with Mg^{+2}. [95]

for secondary structure formation (*i.e.* intramolecular folding), the unfolded peptide sequence may be a random coil, lacking specific three-dimensional structure. Figure 1.3 shows the secondary order structures discussed in this chapter and their potential quaternary order structures.[35]

As indicated by the name, α-helices form a unimolecular helix when triggered to fold. Figure 1.3b shows an external model of an α-helix and Figure 1.4 shows a top down view of the helix[35,69] Each turn of an α-helix is 3.6 amino acid residues. The α-helical structure is held together by hydrogen bonds between backbone CO and NH functionalities along the helix, holding the helix together tightly, and creating a fairly rigid secondary structure.[35,69] A common helix design for gelation involves helices that are composed of amino acid heptads labeled **bcdefg**, where the first and fourth amino acids are typically hydrophobic while the remaining amino acids are polar.[31,69,87] This design places the hydrophobic residues alternatingly 3 or 4 residues apart along the chain, giving the helix a hydrophobic face that winds around the surface of the helix. The exposed hydrophobic face after helix formation is one of the

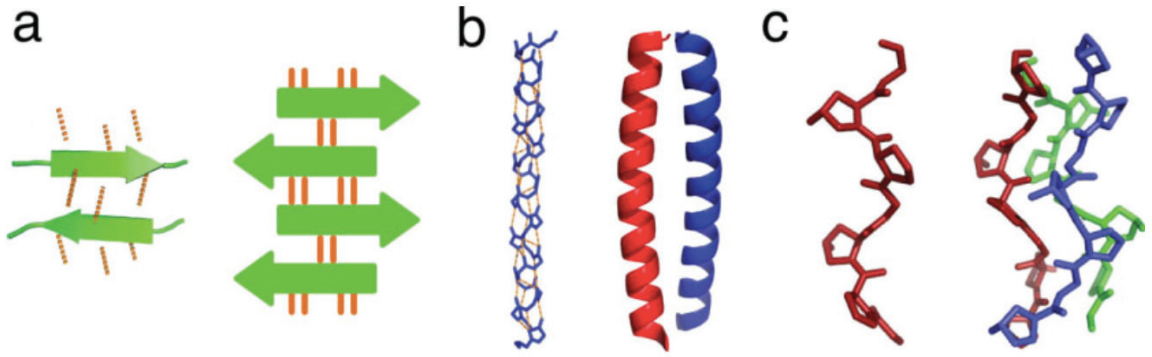

Figure 1.3: Basic secondary structure schematics **a.**) β-strands; extended peptide chains held together by hydrogen bonds shown in orange between CO and NH groups in the peptide backbones, and resultant β-sheets formed by several or more β strands (actually an example of quaternary structure). **b.**) An α-helix with orange hydrogen bonds along the length of the helix and a coiled coil quaternary structure made of two alpha-helices. **c.**) A proline helix that goes on to form a collagen helix with other proline helices.[35]

driving forces for higher order structure formation and gelation. This driving force is discussed further in the quaternary structure section, as helices collapse into what are called coiled-coils and, ultimately, into fibrils and hydrogels (*cf.* Figure 1.3b and Figure 1.4)[69,87] Certain amino acids are more likely to be found in α-helices such as lysine, glutamine, glutamic acid, or alanine[39,42] α-helices can be left or right-handed[35] and can be modified with additional functional groups[39] For example, the Woolfson group uses peptide customization to functionalize α-helices with sticky ends designed to link helices together to propagate longer fibrils upon self-assembly.[31,39,68,69]

The other dominant secondary structure is the β-strand that can further hydrogen bond together to form β-sheets. Strictly speaking, the strand is the intramolecular secondary structure while interstrand sheet formation is a quaternary structure. β-sheets have a distance of 4.7$\mathring{A}$ between each neighboring strand, since hydrogen bonds form laterally between the CO and NH functionalities of opposite β-strand backbones, as shown schematically in Figure 1.3a. Just as there are certain amino acids primarily associated with α-helices, hydrophobic and aromatic amino acids such as phenylalanine, valine, and isoleucine are associated with the formation of β-sheets.[35,42,69,118]

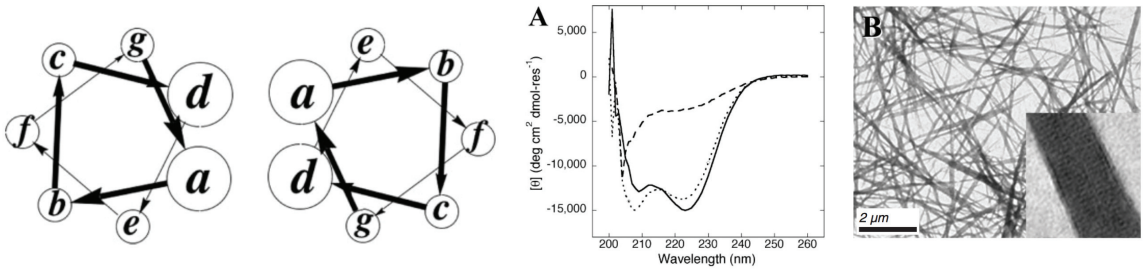

Figure 1.4: Diagram of typical α-helical heptad organization for coiled-coil formation and the protection of hydrophobic residues at a and d for two coiled-coils. **a.**) CD data proving alpha helix confirmation (two minima at 208 and 222nm) for the peptide at 37°C (solid line) when cooled to 37°C from 85°C (dotted line); 85°C (broken line) shows typical random coil behavior. **b.**) shows TEM of the resultant larger fibril organization with higher magnification to show striations.[69]

The presence of hydrophobic residues in a β-sheet can create hydrophobic faces that build up as β-sheet formation occurs, causing the β-sheet fibrils to collapse forming hierarchical fibrillar and fiber nanostructures, further examined later in quaternary structures.[81]

A variation of the β-sheet is the β-hairpin formed by two β-strands held together by short amino acid sequence known as a β-turn. The Schneider and Pochan groups created the family of MAX β-hairpin structures that intramolecularly fold and intermolecularly assemble into nanofibrils with a hydrophobic core. Figure 1.5 shows an example of the β-hairpin structure from the group's flagship MAX1 peptide sequence that collapses to protect hydrophobic valines when triggered.[81,94] The hairpin collapse throughout the solution creates a bilayer fibril, where hydrogen bonds between carboxyl and amine groups of opposing amino acid backbones stabilize the parallel structures (dotted lines in the Figure 1.5.[81,94]).

The β-hairpin structure and its resultant assemblies are important to the remaining chapters of this thesis. Later in the chapter, the MAX peptide quaternary structure and molecular self-assembly are discussed more in-depth. The β-hairpin is integral to the properties exhibited in the MAX family of peptidic hydrogels.

Figure 1.6 shows AFM images of two very similar primary sequences that appear similar after quaternary structure formation and gelation, but one forms α-helices while

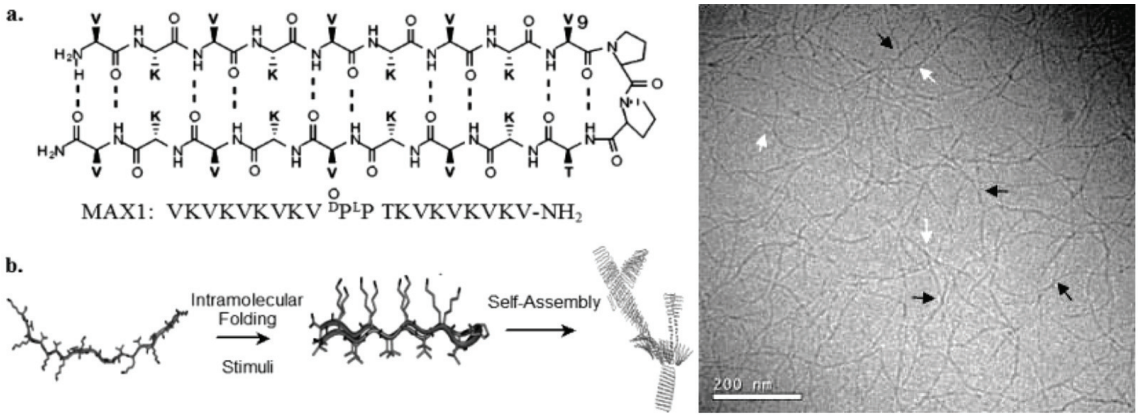

Figure 1.5: A diagram of a β-hairpin molecule, showing the hydrogen bonds (dotted lines) that stabilize the folded conformation between carboxyl and amide groups.[81] On folding, the hydrophobic, valine side chain-rich face collapses together with a neighbor to form a bilayered fibril cross-section. The hairpins also hydrogen bond with neighbors to form fibrils that branch and entangle with physical crosslinks as indicated by the arrows in the Cryo-TEM image.[94]

the other forms β-sheets.[42] Beyond the most common α-helices and β-sheets, there are other secondary structures that are less observed in peptide hydrogels.[35,54,87] One example is the polyproline helix seen in Figure 1.3c, a common secondary structure observed in collagen materials and hydrogels.[50]

A benefit of peptide synthesis is that one can easily fine tune amino acid content (*i.e.* primary structure) of peptides to customize final molecular conformations, gelation times, or other molecular interactions. This allows the creation of an array of peptides with minute differences in sequences but vast differences in final properties. Characterization is important to understanding the secondary structures formed by individual peptides and, consequently, the higher order structures that are formed during gelation. To confirm and characterize second order structure, two spectroscopic methods, circular dichroism spectroscopy (CD) and Fourier-transform infrared spectroscopy (FTIR) are frequently used. Both methods examine light absorption by molecular bonds to identify the presence of random coils, α-helices, or β-sheets. Figure 1.4 shows CD measurements with typical α-helical characteristics (two minima at 208 and 222 nm) when the peptide is at 37°C (solid line) or when cooled to 37°C from

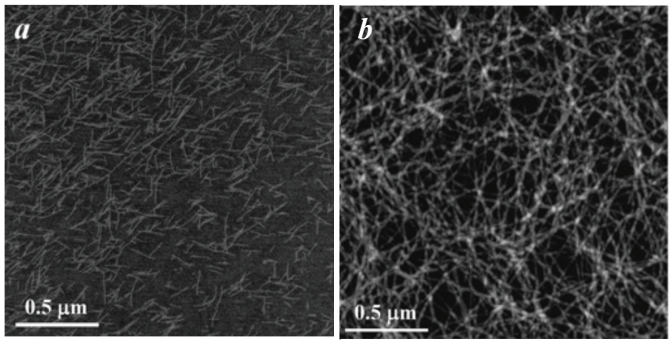

Figure 1.6: AFM micrographs on negatively charged mica of freshly prepared **a.**) α-helix forming AEAKAEAK solution and (b) β-sheet forming FEFEFKFK. Alanine based peptide sequence to phenylalanine changes folding properties. Both form secondary structures that go on to create fibrils into a higher order structures.[42]

85°C (dotted line). The broken line demonstrates the sequence exhibiting random coil behavior at 85°C[69,89] Figure 1.7 shows CD data with an FTIR inset of the Schneider and Pochan groups' MAX1 along with varying ratios of its stereoisomer DMAX1.[119] The FTIR inset confirms β-sheet structure that was not clear in the CD due to a G mixture of both D and L peptide stereoisomers, eliminating a clear CD signal. The inset shows clear absorption at 1615 and 1680 cm^{-1} indicative of β-strand behavior. These spectroscopy methods are used for confirming and analyzing secondary structures, but as the peptide sequences go on to form desired intermolecular structures, microscopy and rheology techniques are required. These techniques for examining quaternary structures are discussed later in the chapter.

Most of the peptide hydrogels that currently exist exhibit a specific secondary structure before and during gelation. While there are many secondary structures available, only those that are able to induce intermolecular assembly into quaternary structure formation are important to the formation of peptide hydrogels. In current peptide hydrogels, the secondary structure utilized most frequently in peptide hydrogel design is the β-sheet due to its propensity to form fibrillar intermolecular nanostructure and, thus, entangled and branched fibrillar networks for hydrogel formation. The examples presented herein contain hydrogels of both major secondary structures but focus mostly on β-sheet constructions.

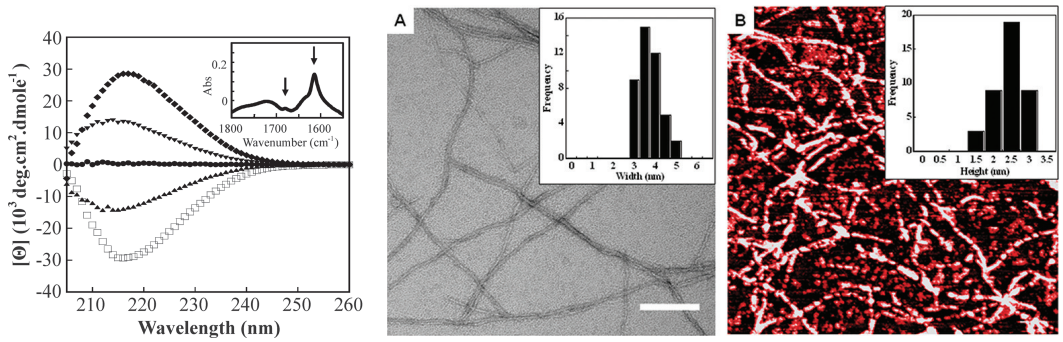

Figure 1.7: Left: CD spectra of 1wt% hydrogels containing (from top to bottom) pure DMAX1, 3:1DMAX1:MAX1, 1:1DMAX1:MAX1, 1:3DMAX1:MAX1, and pure MAX1. The inset shows the IR spectra of 1:1DMAX1:MAX to prove β-strand behavior. **Right**: 1wt% 1:1DMAX1:MAX1gel as **a.**) TEM and **b.**) AFM images, with insets of average fibrillar widths. Scale bar is 100nm.[119]

1.2.3 Tertiary Structures

Tertiary structures, like primary and secondary structures, are observed within single peptide chains. Unlike primary or secondary structures, tertiary structures can exhibit primary and/or secondary structures all within the same molecule. Tertiary structures are stabilized by a wide variety of intramolecular interactions in addition to hydrogen bonding and hydrophobic interactions. These bonds, including salt-bridges or disulfide cysteine bonds, can also be covalent bonds unlike primary or secondary structures.[72,86,96] Figure 1.8 shows a protein example of tertiary structure from the serpin family of proteins naturally found in the body.[120] In the diagram there are visible α-helices, one of which is highlighted in purple, and there are β-strands highlighted in red and blue all within the same molecule.

While there are many proteins that exhibit tertiary order in their globular,

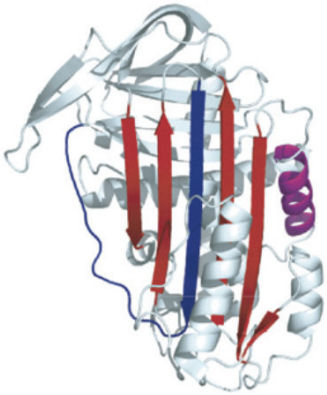

Figure 1.8: Serpin molecule with tertiary order. β-strands are represented by arrows with visible α-helices throughout the entire protein as well as disordered, random coils and turns that connect the areas of more regular secondary structure.[120]

functional form, in peptide hydrogels currently there are very few tertiary order structures. Inspirations for some synthetic globular proteins come from naturally occurring tertiary structures such as bovine serum albumin, β-lactoglobulin, or ovalalbumin.[74,101,103,105,106] Assembling globular proteins into quaternary structures for hydrogels are examined later in the chapter. As the field of peptide hydrogels grows and more complex sequences are created, there may be more tertiary order structures for peptide hydrogels on the horizon.[121]

1.2.4 Quaternary Structures

While previous sections described molecular structures peptide sequences can adopt before interacting with other sequences, the actual peptide hydrogel network itself has an intermolecular quaternary structure. When exposed to the proper triggers in solution, the previously mentioned primary, secondary, and tertiary structures create quaternary structures. The solution triggers include, but are not limited to, changes in pH[33,54,56–58,91] or ionic concentration.[43,58,93] The desired hydrogel characteristics and properties dictate the solution and triggering conditions sought for gel formation as peptide sequences fold and assemble into the network quaternary structure. The dominant peptide hydrogel network quaternary structure is the peptide nanofibril.

Fibrils and fibrillar structure are critical for peptide hydrogel formation; the entanglement and branching of fibrils define the quaternary structures of most peptide hydrogel networks. The fibrils formed during gelation can be well-defined nanofibrils alone that entangle or branch. Nanofibrils can also hierarchically assemble into larger fibrils or fibers to form a network. Non-covalent crosslinking is a critical attribute of physical peptide hydrogels. As the fibrils develop, natural entanglement of the fibrils with themselves as well as physical crosslinking of hydrogen bonds along the backbones of the fibrils and hydrophobic interactions between fibrils, form networks of the peptide hydrogel. The kinetics of the hydrogel formation can affect fibril widths and branching as well as ultimate hydrogel properties.

The kinetics of β-sheet fibril formation and growth can be strongly affected by the hydrophobic interactions of the constituent amino acids.[33,40,73,91,93] The hydrogen bonding and hydrophobic collapse during β-sheet formation and gelation can form homogeneous fibrillar nanostructures with a hydrophobic core[81,95,111] or can lead to hierarchical assembly of nanofibrils into fibers of a wide variety of length scales.[109,122,123] For peptide sequences that assume other secondary structure before fibrillar growth, such as α-helices, hydrophobic collapse can also cause a rather specific intermolecular interaction to form supramolecular structure. For α-helices, two or more helices can collapse together to form what are known as coiled-coils[124–127] Figure 1.4 demonstrates how two α-helices would interact to form a coiled-coil by burying their hydrophobic faces.[33,40,54,111] The number of helices that come together in fibril formation to form the coiled-coil dictates the width of assembled fibrils. As mentioned previously, the α-helices can be functionalized with sticky ends, altering the mechanical strengths of the overall hydrogel[31,39,68,69]

Changing the peptide primary structure itself can alter the kinetics and structure of fibril formation. With gelation/peptide folding and assembly dependent on the peptide charge and hydrophobicity, faster gelation kinetics can be realized by reducing the overall charge of the peptide sequence. For example, the Schneider and Pochan groups substitute a single glutamic acid for a lysine forming a slightly less charged

MAX8 hydrogel, rather than the MAX1 hydrogel shown in Figure 1.10.[49] This change greatly increases the speed of hydrogel formation as compared to MAX1 in identical solution conditions. An increase in the rate of intramolecular folding leads to a faster intermolecular assembly with more branched fibrils and more fibrillar entanglements overall in the quaternary structure. Consequently, this leads to stiffer hydrogels, assembling more quickly than more highly charged MAX1 networks show affects on the distribution of encapsulated payloads. The faster gelation prevents heavier items, such as cells, from sinking due to gravity before the fibrillar network finishes gelation, as seen in Figure 1.10. The fibrillar network and resultant molecular diffusion properties within the gel do not change significantly between peptide gels because the method of fibrillar growth does not change.[96] One can also change the solution peptide folding and assembly triggering conditions in order to change the amount of branching of the gel, which changes the number of physical crosslinks of the gel, ultimately affecting the stiffness of the MAX hydrogel created.[49,128,129] The Schneider group has also looked at substituting all L-amino (left handed) acids for D-amino acids (right handed), thereby reversing the natural chirality of MAX1.[119] The assembly kinetics and mechanical stiffness of the hydrogel were found to depend on the chirality of the peptide. Combining equal amounts of MAX1 and its stereoisomer resulted in a racemic hydrogel that was an order of magnitude stiffer than the individual stereoisomer gels. Clearly, there is ample opportunity to alter quaternary structure in peptide hydrogels through new primary structure design in peptide molecules.

Rheology is an important technique to identify if a hydrogel network is present and to measure properties such as mechanical rigidity and timing of gelation. Unlike the other characterization techniques, which examine the static structure of the hydrogel, rheology subjects the hydrogel to shear forces in order to better understand bulk gel mechanical properties and structure such as gel stiffness, flow properties, assembly time and overall network structure. For the same peptide sequences, the solution conditions and peptide concentration can cause drastic differences in gelation time and ultimate gel properties. A simple example of the utility of rheology is shown in Figure

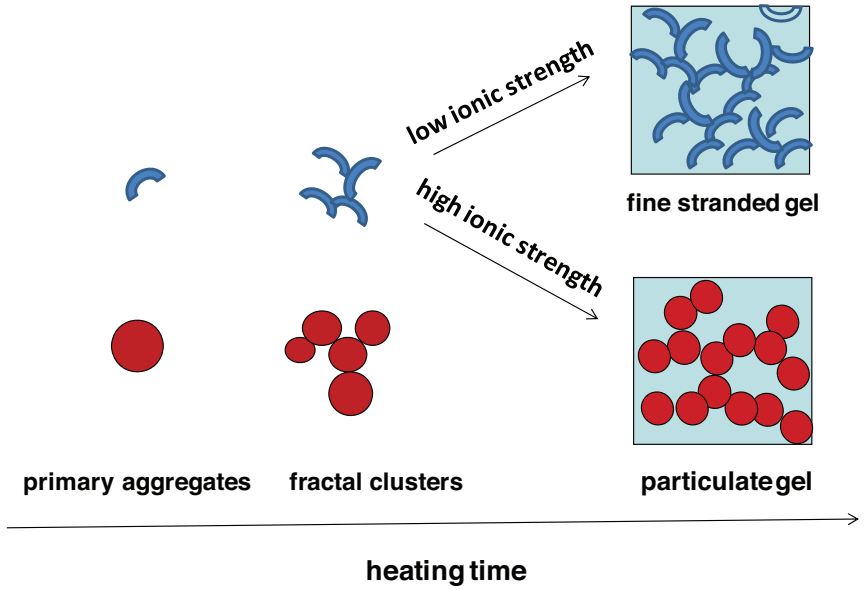

Figure 1.9: Different pathways to form a globular protein hydrogel; a tertiary structure as it gels into a hydrogel with quaternary structure.[74]

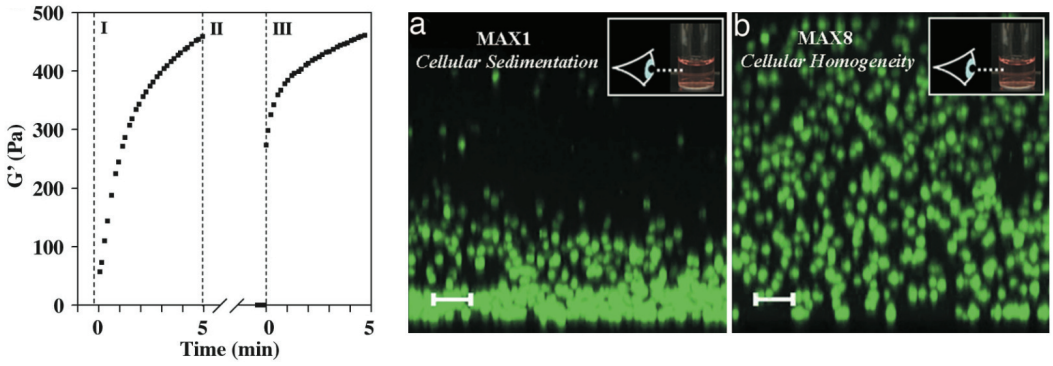

Figure 1.10: Left: Rheology data showing the storage modulus of 0.5wt% MAX8 I.) during initial gelation, II.) as MAX8 undergoes steady-state shear, it becomes liquid like. III.) When shear ceases, the gel immediately displays solid like behavior with G > 250 Pa and quickly recovers original storage modulus. **Right**: MAX1 and MAX8 are both 20 amino acids, where MAX8 has a single substitution difference from MAX1, reducing overall charge of peptide sequence. The reduced charge leads to faster kinetics and gelation time for MAX8, as evidenced by the effects of gravity on encapsulated MSCs in the MAX1 gel.[49] Copyright (2007) National Academy of Sciences, U.S.A.

1.8.[120] MAX1 peptide is assembled with the same peptide concentration but different salt concentration in Figure 1.11a showing clear differences in gel stiffness as indicated by different storage moduli, G′, when hydrogelation occurs with a higher salt concentration in solution.[81] The higher the salt concentration, the faster the intramolecular folding and secondary structure formation and the faster the intermolecular quaternary structure hydrogel network formation. Consequently, the faster the assembly, the more crosslinks in the gel and the stiffer the final network. This observation is only possible with rheology during and after the gelation process. In Figure 1.11b, the stiffness (G′) and viscous properties (G″ or loss modulus) are measured for a MAX1 gel as a function of frequency in order to gain insight into the material properties relative to time scale of shear applied to the gel. Rheology is a critical tool to defining quaternary structures and ultimately peptide hydrogel properties. Yan et al. have defined and examined the importance and uses for rheology to better understand peptide hydrogels as the field expands.[37]

An exciting property of some physical peptide hydrogels due to the entangled and branched nanostructure is the ability of the solid gel to flow like a liquid when under stress, otherwise known as shear-thinning. The property allows a gel network quaternary structure to be set and subsequently processed (*i.e.* injected from a syringe) to a secondary site. Rheology is an important tool in understanding and confirming shear-thinning behavior. Many of these materials after the cessation of shear are able to fully recover into solid hydrogel materials similar to the preshear state.[33,41,49,111] The Pochan group studied at length the causes for shear-thinning behavior in β-hairpin peptide hydrogels and how the hydrogel is able to recover into a solid. The shear-thinning capability comes from the physical crosslinking, primarily the fibril branching present in the quaternary order. When the gel experiences shear forces, the fibril network can fracture, breaking the gel into domains that are able to move past each other. When shear forces cease, the gel domains come into contact with each other and immediately percolate to reform a gel network.[111] Figure 1.10 shows an example of rheology data for MAX8 where it first gels, then shear-thins under steady-state

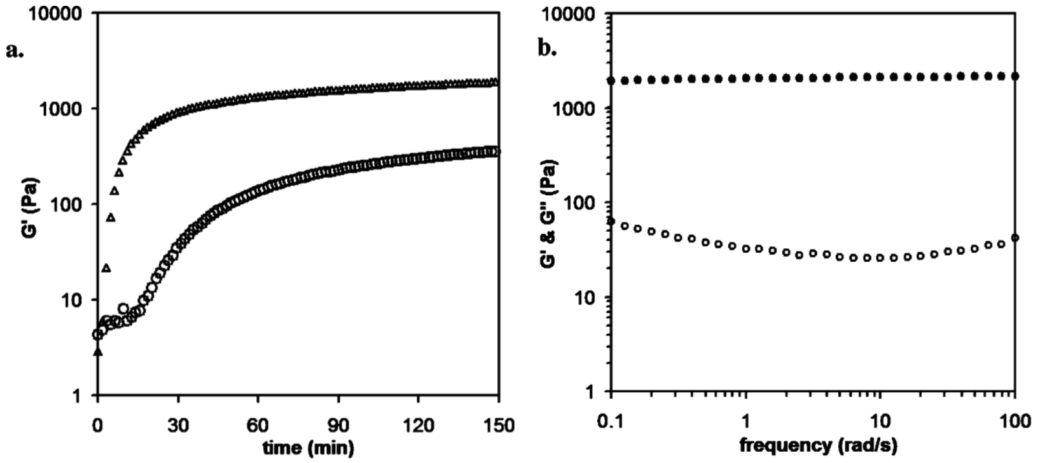

Figure 1.11: The difference in rheology data is shown here in a 2wt%MAX1 hydrogel in a **a.**)— dynamic time sweep at 20°C (circles) and at 37°C (triangles), and **b.**) a frequency sweep at 37°C showing G′(filled) and G″(empty).[81]

shear, exhibits solid properties directly after shear has ceases and ultimately recovers to preshear stiffness after a short amount of time. This property is critical in defining the properties of hydrogel-encapsulated payload constructs where one would like to know the exact properties of the construct, *e.g.* drug delivery profile[130] or encapsulated cell state, after in vivo injection.[48,49]

1.3 Peptide Hydrogel Properties

Peptide hydrogels have many properties that allow for a wide range of possible applications from drug delivery to tissue scaffolding. In addition, the customizable synthesis of peptide sequences for use as hydrogels allows for the tailoring of hydrogel properties. Some of these supramolecular hydrogel properties, like cytocompatibility or customizable gelation conditions, are properties seen regularly in peptide hydrogels and are necessary for biomedical peptide hydrogel applications.

The Zhang group encapsulated biologically native proteins of varying charge and hydrophobicity to better understand diffusion kinetics through the Ac-$(RADA)_4$-$CONH_2$ peptide hydrogels in vitro.[131] Measuring a single molecule at a time, the kinetics showed potential for sustained release of proteins, where diffusion of the protein was dependent on size and not charge. To study bulk release of drug molecules, the Pochan

group has encapsulated hydrophobic curcumin, a derivative of the naturally occurring Indian spice turmeric.[130] In this study, the hydrophobic curcumin was encapsulated and protected from quick degradation in a mostly aqueous situation in the MAX8 peptide hydrogel. The encapsulated curcumin remained active after release well beyond its chemical stability half-life of 8 hours. In addition, the compound continued very low, sustained concentrations of release over two weeks, enough for cancer cell eradication in vitro. Since many chemotherapeutics can be equally detrimental to healthy cells, this ability to release chemotherapeutic compounds locally and at low but effective concentrations is advantageous for minimizing side effects while maintaining meaningful treatments. Peptide hydrogels can be delivered into the body through several different methods, depending on the gel assembly mechanism and desired application of the hydrogel. Peptide hydrogels can be introduced by injection[43,58,80,86,87,93,111] or surgical placement.[33,60,82] While injection is a common delivery tactic, most polymer material hydrogels are injected as liquids that are designed to be crosslinked covalently in vivo.[43,58] This requires additional external stimuli to trigger gelation after injection. For example, a gel pre-cursor is injected, and gelation is then triggered using UV.[132,133], a crosslinking chemical, or infrared light.[134] Not only do external stimuli increase the possibility of contamination or side effects, these delayed crosslinking steps do not guarantee uniformity in gel structures or payload distribution. In the cases when peptides are injected as a liquid, usually a biological stimulus in vivo is used to cause desired secondary and quaternary structure formation *i.e.* gelation. These gelation stimuli include using body temperature[135], cell environments[71,100], or native enzymes.[136]

An alternative to liquid injection that is made possible by some physical peptide hydrogels is the idea of an injectable solid. The Pochan and Schneider groups are able to take advantage of the structural organization of MAX gels to inject solids that have already assembled because the hydrogels have shear-thinning behavior and reheal at the cessation of shear forces. This advantage is the result of the physical crosslinking of the hydrogel nanostructures, causing the hydrogel to break up into smaller domains of intact gel when undergoing shear. Because the system is not chemically cross-linked,

when shear forces cease, the nanofibrils re-form physical crosslink contacts and do not need the introduction of another trigger to reform a hydrogel network. As a shear-thinning and rehealing hydrogel is injected through a syringe, only the hydrogel at the edges, along the surface of the syringe, experiences shear, leaving the rest of the hydrogel intact. This creates a plug flow of hydrogel.[33,40] The resultant plug flow allows the hydrogel to protect payloads from shear and maintain the distribution and viability of cells, drugs, or proteins encapsulated within.[33,40,82,111] Besides drugs and large molecules, peptide hydrogels are also used in the delivery of cells.[40,41,43,47–49,51,130] MSCs are encapsulated for injection in hopes of influencing or better understanding stem cell differentiation, with the goal of depositing the cells in a specific-cell type deficient area.[47–49] Instead of encapsulating cells for cell growth, the Hartgerink group cultures ESCs and their $E_2(SL)_6E_2$GRGDS hydrogel separated by a permeable membrane.[41] The separated peptide hydrogels act as sponges, harnessing secreted growth factors and secretomes from ESCs. Then, the protein-infused peptide hydrogels are injected in vivo or used for tissue culture at a later time with concurrent release of or metabolism of the infused ESC proteins.

In addition to delivery, peptide hydrogels are ideal for tissue scaffolding and 3D cell growth environments. 3D environments can be used to provide a working model of systems within the body that may be hard to observe and difficult to mimic in vitro. Some of these systems include the culture of endothelial stem cells[84], blood vessel formation[107], chondrocyte development[67], and stem cells of many types.[47,49] 3D environments also provide a more natural environment than 2D cell culturing methods with ability to control material details in 3D such as morphology and matrix stiffnesses.[39,56,137–140] Extracellular matrix (ECM) mimetic 3D structures are also highly desirable to better understand the intricate physical networks that cells need for growth and replication. The inherent fibrillar network of the gels provides a similar ECM-like structure on which cells may anchor, as well as a hydrogel porous enough for growth factors and important biochemical signals to diffuse through.[33,55,67,87,88,141–143] Some of the many encapsulated cell lines include MSCs[47,49], endothelial cells[84], chondrocytes.[144], or

fibroblasts[51] The Schneider and Pochan groups have successfully encapsulated MSCs in a 3D environment as seen in Figure 1.10, showing homogenous distribution of cells with desired cell density and spacing – a feature unavailable in 2D growth environments.[48,49] Additionally, the 3D environment also provides the starting structure for the cells to deposit ECM[48,49] with the opportunity to observe in vivo-like behavior recreated in the 3D peptide hydrogel construct.

This chapter examined polymer hydrogels as delivery vehicles with a focus on exploring the importance of peptide hierarchical structures. Peptide hydrogels are great candidates in the ever-growing field of biological and medical applications. Not only are peptide sequences easy to synthesize, the synthesis process allows for customizable molecular and material features such as peptide length, amino acid substitution, gelation time, mechanical properties (*e.g.* stiffness), or functionalities for cell targeting or encapsulations. The natural cytocompatibility and degradability of peptides make peptide hydrogels great candidates for cell encapsulation, 3D growth environments, tissue scaffolding, and injectable payload delivery. Peptide hydrogels are not only able to successfully encapsulate cells, but also able to encapsulate proteins and drugs of varying charge, size, or hydrophobicity. Unlike traditional liquid-based delivery systems that rely on gelation after injection while simultaneously delivering encapsulated payloads, some peptide hydrogels can be injected as solids without need of external stimuli or interactions to reform into a solid similar to the preinjected material. It is clear that the future is bright for the discovery of new peptide molecules to make new hydrogel materials with both designed properties as well as unanticipated, excellent properties.

1.4 MAX Family of Hydrogels

1.4.1 Properties

MAX8 is a peptidic hydrogel that forms a β-hairpin when folding, a variation of the β-sheet. Its peptidic nature is important for its assembly and overall hydrogel

properties. Similar to other peptidic hydrogels, MAX8 is cytocompatible. Additionally, MAX8 is shear-thinning and release capabilities. The Pochan and Schneider groups began studying the MAX family of peptide hydrogels. MAX1, (VKVKVKVK-V^{D}PPT-KVKVKVKV-NH_2), is the flagship peptide studied extensively by the Pochan group. MAX1's sequence contains two β strands of alternating hydrophobic valines (V) and hydrophilic, charged lysine (K) residues, covalently bonded to a turn sequence (V^{D}PPT).[70] Because of the repulsion between lysine side groups, when dissolved in a neutral pH solution, the peptide is unfolded and has a random coil-like configuration. Folding of the peptide sequence is induced by increasing pH to deprotonate the lysines, adding salt to screen electrostatic interaction, and increasing temperature to cause a hydrophobic collapse. Once triggered, self-assembly begins as the turn sequence pushes the peptides to fold into a β-hairpin shape. The β-hairpin shape is held in place, and receives its name, from the hydrogen bonds between the two arms, β-sheet like.[80] The bonds holding the hairpins in shape can be seen in Figure 1.5. As β-hairpins begin folding, two hairpins stack to protect the hydrophobic valines, creating bi-layer nanofibrils. The fibrils are held in shape by the interactions of neighboring lysines and hydrophobic valines between hairpins[53] As fibrils form and elongate, natural branch points form from kinetics while the fibrils entangle with itself to create a physically cross-linked hydrogel network.

While MAX1 self-assembles at physiological conditions (pH 7.4, 37°C, biological salts and concentrations), the overall gelation time is not fast enough to combat the effects of gravity when cells are encapsulated. MAX8 is a derivative of MAX1, which replaces the 15th reside (lysine, K) with glutamic acid(K). This substitution reduces the overall charge of the sequence from +9 to +7, reducing the electrostatic repulsion between lysines. This change greatly reduces overall gelation time in physiological conditions (37°C, pH 7.4, naturally found salt concentrations), from an hour to 20 minutes, allowing a homogenous distribution of cells to retain the distribution during encapsulation.[49] Figure 1.10 demonstrates the importance in the difference of gelation times. Because of its gelation time at physiological conditions, MAX8 is the hydrogel

that is used throughout the rest of this dissertation.

Besides quick gelation at physiological conditions, the MAX hydrogels are ideal candidates for many applications because of their shear-thinning and re-healing behavior. The shear-thinning and re-healing properties of the MAX family of peptides comes from its physically cross-linked network. Yan et al.[111] investigated and explained this phenomenon using rheological-SANS. Yan discovered that when a shear force is applied to the hydrogel, the hydrogel breaks up into smaller domains that are able to slide past each other. When shear forces cease, the fibril ends are able to quickly repercolate, re-forming bonds, re-creating a the overall physically cross-linked network. Figure 1.12 shows how the domains break down, roll past each other, and re-form. Understanding why the MAX hydrogels behave this way supports the hydrogels as ideal candidates for delivery applications. Additionally, it explains the hydrogel's ability to fully recover the original hydrogel stiffness as seen in Figure 1.10. The MAX hydrogels also retain their physical properties when encapsulating various payloads. This has been demonstrated with encapsulation of cells[48,49], neutral probes[96], and hydrophobic compounds.[130]

Compared to the examples of hydrogel drug delivery discussed at the beginning of the chapter, MAX8's advantages include its assembly technique, shear-thinning behavior, and cytocompatibility. Currently, many injectable hydrogels are designed as precursor, low viscosity solutions *ex vivo* that then assemble in vivo when exposed to environmental triggers such as temperature[135,145], ions[31,146], pH[35,54], or ultraviolet (UV) radiation.[31,35,36,71–74,108] External triggers such as UV radiation may damage nearby tissue, whereas introduction of non-physiological materials like iron oxide may lead to long term effects that greatly influence the body.[147–151] MAX8 can begin self-assembly and finish solid gel formation within a syringe, after which injection and deposition can occur without the need for further external interactions. After deposition, no further interactions are needed, due to the injectable solid hydrogel properties of MAX8 immediately recovering its hydrogel properties.

Once deposited, MAX8 is a model candidate as a payload delivery vehicle. MAX8 has been studied for in vitro and in vivo studies because it self-assembles at

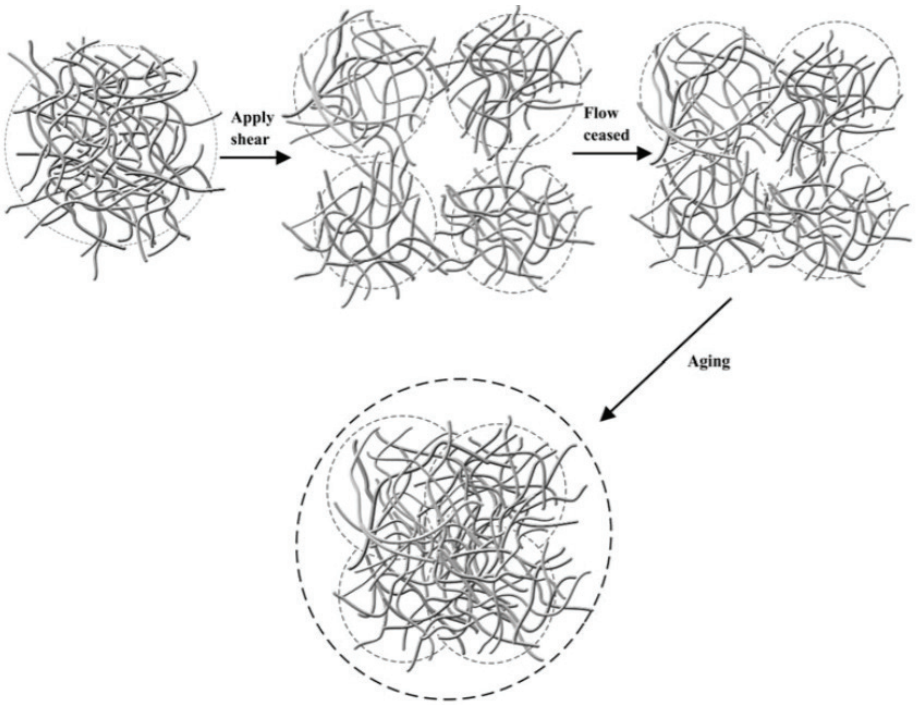

Figure 1.12: Because of the physical crosslinks within the network, the MAX family of hydrogels breaks into smaller domains when sheared. The small domains roll past one another, leading to a shear-thinning behavior. When shear is stopped, the sticky ends of the small domains repercolate and reform the original hydrogel network structure.[111]

physiological conditions. The overall physiological conditions of the MAX8 gel is important for its cytocompatibility, as cells are entering a more native environment. Stem cells, liver cells, chondrocytes are all cell lines that have had successful interactions with MAX8 without inducing cell death.[48,49,53,152,153] When using MAX8 in the future for depositions, the MAX8 hydrogel itself should not induce an immune response. Not only is MAX8 cytocompatible, it can successfully encapsulate many different types of payloads, necessary as a drug delivery vehicle. This combination of properties, gelation time, gelation conditions, shear-thinning, re-healing, and cytocompatibility make MAX8 a powerful candidate for various applications in payload delivery.

1.4.2 Past Applications

The injectable solid hydrogel properties allow solid gel formation within a syringe, after which injection and deposition can occur without the need for further external interactions. From this family of β-hairpin peptides, MAX8 is a model candidate as a payload delivery vehicle. MAX8 has been studied for in vitro and in vivo studies because it self-assembles at physiological conditions and can successfully encapsulate many different types of payloads. Previous studies using MAX8 have shown successful, homogenous encapsulation of various particles[96], drugs[130], and cell lines.[48,49,53,153] Branco et al. encapsulated dextran probes of neutral charge and varying sizes to better understand MAX8 network characteristics.[96] The probes showed the pore sizes of the overall networks and diffusion profiles for a neutral molecule from the hydrogel. Haines-Butterick et al and Yan et al. have both encapsulated mesenchymal stem cells (MSC) in MAX8 successfully.[48,49] Yan's goal was to better understand effects of shear on the overall hydrogel system and subsequent effects on encapsulated cells.

Additionally, smaller molecule encapsulation has also been studied. For example, MAX8 hydrogels have been utilized to encapsulate curcumin, a hydrophobic chemotherapeutic agent.[130] Curcumin degrades after 8 hours in water.[154] Altunbas et al. successfully encapsulated and released curcumin from MAX8. Despite the high water content of the MAX8 hydrogel, the continuously-released curcumin remained

active and effective even after 14 days of encapsulation. This experiment is important for the basis of the release of encapsulated hydrophobic chemothereapuetic from MAX8 in Chapter 3.

1.5 Organization

Having introduced the background and importance of peptide hydrogels, with a specific examination of the MAX family peptides, the rest of this dissertation will focus on the applications and characterization of MAX8 peptide hydrogels.In addition, the history and significance of previous encapsulation studies will be discussed to motivate the experimental investigations contained in the remainder of this thesis.

Chapter 2 examines the release of an encapsulated payload over a month's time. The chapter contains a detailed description of how MAX8 is synthesized and purified, as well as the techniques employed to encapsulate the various payloads, drugs and cells. The resultant methods of measuring release and response (cellular and structural) are also described in full. Vincristine, the encapsulated drug, is a commonly used chemotherapeutic currently prescribed for many cancer treatments. The hydrophobic drug encapsulated within the aqueous MAX8 hydrogel environment shows a slow, sustained release over the course of a month. More importantly, the concentrations being released are still significant and remain active despite the environment, able to target and attack the cancer cell line.

Chapter 3 uses the technique of small-angle neutron scattering to further examine gel structures of MAX8 and an additional gel system. Small-angle neutron scattering (SANS) is a powerful technique to measure structure in soft matter systems. Here, it is used to understand the effect of vincristine on the structure of the MAX8 hydrogel. The data indicates the vincristine location in relation to the fibrillar network is important in its continued effectiveness after long term encapsulation. Continuing understanding of gel structures using SANS, a poly(ethylene glycol) and palladium gel system is examined. The experiments and subsequent fits give features that agree well

with previous data, helping to form a more solid understanding of the fundamental structures of the gels.

Finally, all the work that has been done is summarized in Chapter 4‘, while also looking towards future work.

REFERENCES

[1] N A Peppas, J Z Hilt, A Khademhosseini, and Robert Langer. Hydrogels in Biology and Medicine: From Molecular Principles to Bionanotechnology. *Advanced Materials*, 18(11):1345–1360, June 2006.

[2] A K Bajpai, Sandeep K Shukla, Smitha Bhanu, and Sanjana Kankane. Responsive polymers in controlled drug delivery. *Progress In Polymer Science*, 33(11):1088–1118, November 2008.

[3] Nasim Annabi, Ali Tamayol, Jorge Alfredo Uquillas, Mohsen Akbari, Luiz E Bertassoni, Chaenyung Cha, Gulden Camci Unal, Mehmet R Dokmeci, Nicholas A Peppas, and Ali Khademhosseini. 25th Anniversary Article: Rational Design and Applications of Hydrogels in Regenerative Medicine. *Advanced Materials*, 26(1):85–124, January 2014.

[4] Penny J Martens, Stephanie J Bryant, and Kristi S Anseth. Tailoring the Degradation of Hydrogels Formed from Multivinyl Poly(ethylene glycol) and Poly(vinyl alcohol) Macromers for Cartilage Tissue Engineering. *Biomacromolecules*, 4(2):283–292, March 2003.

[5] Jia Kui Li, Nuo Wang, and Xue Shen Wu. Poly(vinyl alcohol) nanoparticles prepared by freezing–thawing process for protein/peptide drug delivery. *Journal of Controlled Release*, 56(1-3):117–126, December 1998.

[6] Parisa Ebrahimi Sadr, Fatemeh Ghaffarifar, Zuhir Mohammad Hassan, Mohammad Sirousazar, and Fatemeh Mohammadnejad. Effect of Polyvinyl Alcohol (PVA) Containing Artemether in Treatment of Cutaneous Leishmaniasis Caused by Leishmania major in BALB/c Mice. *Jundishapur Journal of Microbiology*, 7(5):e9696, May 2014.

[7] Robert Langer and NA Peppas. Advances in biomaterials, drug delivery, and bionanotechnology. *Aiche Journal*, 49(12):2990–3006, 2003.

[8] Yan Chen, Xue-Lian Zheng, Dai-Long Fang, Yang Yang, Jin-Kun Zhang, Hui-Li Li, Bei Xu, Yi Lei, Ke Ren, and Xiang-Rong Song. Dual Agent Loaded PLGA Nanoparticles Enhanced Antitumor Activity in a Multidrug-Resistant Breast Tumor Eenograft Model. *International Journal of Molecular Sciences*, 15(2):2761–2772, February 2014.

[9] Ida Berts, Yuri Gerelli, Jöns Hilborn, and Adrian R Rennie. Structure of polymer and particle aggregates in hydrogel composites. *Journal of Polymer Science Part B: Polymer Physics*, 51(6):421–429, March 2013.

[10] Roger Michel, Stephanie Pasche, Marcus Textor, and David G Castner. Influence of PEG architecture on protein adsorption and conformation. *Langmuir*, 21(26):12327–12332, December 2005.

[11] Kevin L Prime and George M Whitesides. Adsorption of proteins onto surfaces containing end-attached oligo(ethylene oxide): a model system using self-assembled monolayers. *Journal Of The American Chemical Society*, 115(23):10714–10721, November 1993.

[12] George M Whitesides, Emanuele Ostuni, Shuichi Takayama, Xingyu Jiang, and Donald E Ingber. Soft Lithography in Biology and Biochemistry. *dx.doi.org*, 3(1):335–373, November 2003.

[13] Brandon V Slaughter, Shahana S Khurshid, Omar Z Fisher, Ali Khademhosseini, and Nicholas A Peppas. Hydrogels in regenerative medicine. *Advanced Materials*, 21(32-33):3307–3329, 2009.

[14] Todd R Hoare and Daniel S Kohane. Hydrogels in drug delivery: Progress and challenges. *Polymer*, 49(8):1993–2007, 2008.

[15] Yong Qiu and Kinam Park. Environment-sensitive hydrogels for drug delivery. *Advanced Drug Delivery Reviews*, 64:49–60, December 2012.

[16] Jianjun Cheng, Benjamin A Teply, Ines Sherifi, Josephine Sung, Gaurav Luther, Frank X Gu, Etgar Levy-Nissenbaum, Aleksandar F Radovic-Moreno, Robert Langer, and Omid C Farokhzad. Formulation of functionalized PLGA–PEG nanoparticles for in vivo targeted drug delivery. *Biomaterials*, 28(5):869–876, February 2007.

[17] L Bromberg. Temperature-responsive gels and thermogelling polymer matrices for protein and peptide delivery. *Advanced Drug Delivery Reviews*, 31(3):197–221, May 1998.

[18] Sanal Payyappilly, Santanu Dhara, and Santanu Chattopadhyay. Thermoresponsive biodegradable PEG-PCL-PEG based injectable hydrogel for pulsatile insulin delivery. *Journal of Biomedical Materials Research Part A*, 102(5):1500–1509, May 2014.

[19] D Zhang, P Sun, P Li, A Xue, X Zhang, H Zhang, and X Jin. A magnetic chitosan hydrogel for sustained and prolonged delivery of Bacillus Calmette–Guérin in the treatment of bladder cancer. *Biomaterials*, 2013.

[20] Eve Ruel-Gariépy, Matthew Shive, Ali Bichara, Mohammed Berrada, Dorothée Le Garrec, Abdellatif Chenite, and Jean-Christophe Leroux. A thermosensitive chitosan-based hydrogel for the local delivery of paclitaxel. *European Journal of Pharmaceutics and Biopharmaceutics*, 57(1):53–63, January 2004.

[21] Sungwoo Kim, Satoru K Nishimoto, Joel D Bumgardner, Warren O Haggard, M Waleed Gaber, and Yunzhi Yang. A chitosan/beta-glycerophosphate thermosensitive gel for the delivery of ellagic acid for the treatment of brain cancer. *Biomaterials*, 31(14):4157–4166, May 2010.

[22] J Berger, M Reist, J M Mayer, O Felt, N A Peppas, and R Gurny. Structure and interactions in covalently and ionically crosslinked chitosan hydrogels for biomedical applications. *European Journal of Pharmaceutics and Biopharmaceutics*, 57(1):19–34, January 2004.

[23] Roberto Elia, Danny R Newhide, Paul D Pedevillano, G Russell Reiss, Matthew A Firpo, Edward W Hsu, David L Kaplan, Glenn D Prestwich, and Robert A Peattie. Silk–hyaluronan-based composite hydrogels: A novel, securable vehicle for drug delivery. *Journal of biomaterials applications*, 27(6):749–762, 2013.

[24] Joshua S Boateng, Kerr H Matthews, Howard N E Stevens, and Gillian M Eccleston. Wound healing dressings and drug delivery systems: A review. *Journal of Pharmaceutical Sciences*, 97(8):2892–2923, August 2008.

[25] Yash M Kolambkar, Kenneth M Dupont, Joel D Boerckel, Nathaniel Huebsch, David J Mooney, Dietmar W Hutmacher, and Robert E Guldberg. An alginate-based hybrid system for growth factor delivery in the functional repair of large bone defects. *Biomaterials*, 32(1):65–74, January 2011.

[26] Kuen Yong Lee and David J Mooney. Alginate: Properties and biomedical applications. *Progress In Polymer Science*, 37(1):106–126, January 2012.

[27] Kerstin M Galler, Jeffrey D Hartgerink, Adriana C Cavender, Gottfried Schmalz, and Rena N D'Souza. A Customized Self-Assembling Peptide Hydrogel for Dental Pulp Tissue Engineering. *Tissue Engineering Part A*, 18(1-2):176–184, January 2012.

[28] Minkyu Kim, Shengchang Tang, and Bradley D Olsen. Physics of engineered protein hydrogels. *Journal of Polymer Science Part B: Polymer Physics*, 51(7):587–601, February 2013.

[29] Matthew J Glassman, Jacqueline Chan, and Bradley D Olsen. Reinforcement of Shear Thinning Protein Hydrogels by Responsive Block Copolymer Self-Assembly. *Advanced Functional Materials*, 23(9):1182–1193, October 2012.

[30] W A Petka. Reversible Hydrogels from Self-Assembling Artificial Proteins. *Science*, 281(5375):389–392, July 1998.

[31] Rein V Ulijn and Andrew M Smith. Designing peptide based nanomaterials. *Chemical Society Reviews*, 37(4):664–675, 2008.

[32] Erkki Ruoslahti. RGD AND OTHER RECOGNITION SEQUENCES FOR INTEGRINS. *Annual Review of Cell and Developmental Biology*, 12(1):697–715, November 1996.

[33] Murat Guvendiren, Hoang D Lu, and Jason A Burdick. Shear-thinning hydrogels for biomedical applications. *Soft Matter*, 8(2):260–272, 2011.

[34] Ulrich Hersel, Claudia Dahmen, and Horst Kessler. RGD modified polymers: biomaterials for stimulated cell adhesion and beyond. *Biomaterials*, 24(24):4385–4415, 2003.

[35] Derek N Woolfson. Building fibrous biomaterials from alpha-helical and collagen-like coiled-coil peptides. *Biopolymers*, 94(1):118–127, 2010.

[36] Joel H Collier and Tatiana Segura. Evolving the use of peptides as components of biomaterials. *Biomaterials*, 32(18):4198–4204, June 2011.

[37] C Yan and D J Pochan. Rheological properties of peptide-based hydrogels for biomedical and other applications. *Chemical Society Reviews*, 39(9):3528–3540, 2010.

[38] E Ruoslahti. Integrins. *Journal of Clinical Investigation*, 87(1):1–5, January 1991.

[39] Elizabeth H C Bromley, Kevin J Channon, Patrick J S King, Zahra N Mahmoud, Eleanor F Banwell, Michael F Butler, Matthew P Crump, Timothy R Dafforn, Matthew R Hicks, Jonathan D Hirst, Alison Rodger, and Derek N Woolfson. Assembly Pathway of a Designed α-Helical Protein Fiber. *Biophysical Journal*, 98(8):1668–1676, April 2010.

[40] Bradley D Olsen, Julia A Kornfield, and David A Tirrell. Yielding Behavior in Injectable Hydrogels from Telechelic Proteins. *Macromolecules*, 43(21):9094–9099, November 2010.

[41] Erica L Bakota, Yin Wang, Farhad R Danesh, and Jeffrey D Hartgerink. Injectable multidomain peptide nanofiber hydrogel as a delivery agent for stem cell secretome. *Biomacromolecules*, 12(5):1651–1657, 2011.

[42] A Saiani, A Mohammed, H Frielinghaus, R Collins, N Hodson, C M Kielty, M J Sherratt, and A F Miller. Self-assembly and gelation properties of α-helix versusβ-sheet forming peptides. *Soft Matter*, 5(1):193, 2008.

[43] D Macaya and M Spector. Injectable hydrogel materials for spinal cord regeneration: a review. *Biomedical Materials*, 7(1):012001, January 2012.

[44] Yingkai Liang and Kristi L Kiick. Heparin-functionalized polymeric biomaterials in tissue engineering and drug delivery applications. *Acta Biomaterialia*, 10(4):1588–1600, April 2014.

[45] Aaron D Baldwin, Karyn G Robinson, Jaimee L Militar, Christopher D Derby, Kristi L Kiick, and Robert E Akins. In situ crosslinkable heparin-containing poly(ethylene glycol) hydrogels for sustained anticoagulant release. *Journal of Biomedical Materials Research Part A*, 100A(8):2106–2118, August 2012.

[46] Danielle S W Benoit and Kristi S Anseth. Heparin functionalized PEG gels that modulate protein adsorption for hMSC adhesion and differentiation. *Acta Biomaterialia*, 1(4):461–470, July 2005.

[47] Sarah B Anderson, Chien-Chi Lin, Donna V Kuntzler, and Kristi S Anseth. The performance of human mesenchymal stem cells encapsulated in cell-degradable polymer-peptide hydrogels. *Biomaterials*, 32(14):3564–3574, 2011.

[48] Congqi Yan, Michael E Mackay, Kirk Czymmek, Radhika P Nagarkar, Joel P Schneider, and Darrin J Pochan. Injectable Solid Peptide Hydrogel as a Cell Carrier: Effects of Shear Flow on Hydrogels and Cell Payload. *Langmuir*, 28(14):6076–6087, 2012.

[49] Lisa Haines-Butterick, Karthikan Rajagopal, Monica Branco, Daphne A Salick, Ronak Rughani, Matthew Pilarz, Matthew S Lamm, Darrin J Pochan, and Joel P Schneider. Controlling hydrogelation kinetics by peptide design for three-dimensional encapsulation and injectable delivery of cells. *Proceedings Of The National Academy Of Sciences Of The United States Of America*, 104(19):7791–7796, 2007.

[50] Jangwook P Jung, Joshua Z Gasiorowski, and Joel H Collier. Fibrillar peptide gels in biotechnology and biomedicine. *Biopolymers*, 94(1):49–59, January 2010.

[51] Ye F Tian, Jason M Devgun, and Joel H Collier. Fibrillized peptide microgels for cell encapsulation and 3D cell culture. *Soft Matter*, 7(13):6005–6011, 2011.

[52] Esmaiel Jabbari. Bioconjugation of hydrogels for tissue engineering. *Current opinion in biotechnology*, 22(5):655–660, 2011.

[53] Lisa A Haines-Butterick, Daphne A Salick, Darrin J Pochan, and Joel P Schneider. In vitro assessment of the pro-inflammatory potential of β-hairpin peptide hydrogels. *Biomaterials*, 29(31):4164–4169, November 2008.

[54] Jindrich Kopecek and Jiyuan Yang. Peptide-directed self-assembly of hydrogels. *Acta Biomaterialia*, 5(3):805–816, March 2009.

[55] Shani Eliyahu-Gross and Ronit Bitton. Environmentally responsive hydrogels with dynamically tunable properties as extracellular matrix mimetic. *Reviews in Chemical Engineering*, 29(3):159–168, 2013.

[56] I W Hamley. Self-assembly of amphiphilic peptides. *Soft Matter*, 7(9):4122, 2011.

[57] Charlotte A E Hauser and Shuguang Zhang. Designer self-assembling peptide nanofiber biological materials. *Chemical Society Reviews*, 39(8):2780, 2010.

[58] Yulin Li, João Rodrigues, and Helena Tomás. Injectable and biodegradable hydrogels: gelation, biodegradation and biomedical applications. *Chemical Society Reviews*, 41(6):2193, 2012.

[59] John T Ngo and David A Tirrell. Noncanonical Amino Acids in the Interrogation of Cellular Protein Synthesis. *Accounts of Chemical Research*, 44(9):677–685, September 2011.

[60] Apurba K Das, Richard Collins, and Rein V Ulijn. Exploiting Enzymatic (Reversed) Hydrolysis in Directed Self-Assembly of Peptide Nanostructures. *Small*, 4(2):279–287, 2008.

[61] Z Yang, H Gu, D Fu, P Gao, J K Lam, and B Xu. Enzymatic Formation of Supramolecular Hydrogels. *Advanced Materials*, 16(16):1440–1444, August 2004.

[62] Michael C Giano, Darrin J Pochan, and Joel P Schneider. Controlled biodegradation of Self-assembling β-hairpin Peptide hydrogels by proteolysis with matrix metalloproteinase-13. *Biomaterials*, 32(27):6471–6477, September 2011.

[63] Bradley L Nilsson, Matthew B Soellner, and Ronald T Raines. Chemical synthesis of proteins. *Annual review of biophysics and biomolecular structure*, 34:91, 2005.

[64] Rhiannon K Iha, Karen L Wooley, Andreas M Nyström, Daniel J Burke, Matthew J Kade, and Craig J Hawker. Applications of orthogonal "click"

chemistries in the synthesis of functional soft materials. *Chemical Reviews*, 109(11):5620–5686, 2009.

[65] Cole A DeForest, Evan A Sims, and Kristi S Anseth. Peptide-Functionalized Click Hydrogels with Independently Tunable Mechanics and Chemical Functionality for 3D Cell Culture. *Chemistry of Materials*, 22(16):4783–4790, August 2010.

[66] Cole A DeForest, Brian D Polizzotti, and Kristi S Anseth. Sequential click reactions for synthesizing and patterning three-dimensional cell microenvironments. *Nature Materials*, 8(8):659–664, June 2009.

[67] Stuart Kyle, Amalia Aggeli, Eileen Ingham, and Michael J McPherson. Production of self-assembling biomaterials for tissue engineering. *Trends in Biotechnology*, 27(7):423–433, July 2009.

[68] Derek N Woolfson and Zahra N Mahmoud. More than just bare scaffolds: towards multi-component and decorated fibrous biomaterials. *Chemical Society Reviews*, 39(9):3464, 2010.

[69] Andrew M Smith, Eleanor F Banwell, Wayne R Edwards, Maya J Pandya, and Derek N Woolfson. Engineering Increased Stability into Self-Assembled Protein Fibers. *Advanced Functional Materials*, 16(8):1022–1030, May 2006.

[70] JP Schneider, DJ Pochan, Bulent Ozbas, Karthikan Rajagopal, L Pakstis, and Juliana Kretsinger. Responsive hydrogels from the intramolecular folding and self-assembly of a designed peptide. *Journal Of The American Chemical Society*, 124(50):15030–15037, 2002.

[71] Charles J Bowerman and Bradley L Nilsson. A Reductive Trigger for Peptide Self-Assembly and Hydrogelation. *Journal Of The American Chemical Society*, 132(28):9526–9527, 2010.

[72] Jindrich Kopecek and Jiyuan Yang. Smart Self-Assembled Hybrid Hydrogel Biomaterials. *Angewandte Chemie International Edition*, 51(30):7396–7417, 2012.

[73] Derek M Ryan and Bradley L Nilsson. Self-assembled amino acids and dipeptides as noncovalent hydrogels for tissue engineering. *Self-assembled amino acids and dipeptides as noncovalent hydrogels for tissue engineering*, 3(1):18, 2011.

[74] Taco Nicolai and Dominique Durand. Controlled food protein aggregation for new functionality. *Current Opinion in Colloid & Interface Science*, 18(4):249–256, 2013.

[75] Yan Zhang, Hongwei Gu, Zhimou Yang, and Bing Xu. Supramolecular Hydrogels Respond to Ligand–Receptor Interaction. *Journal Of The American Chemical Society*, 125(45):13680–13681, November 2003.

[76] Jessica Y Shu, Brian Panganiban, and Ting Xu. Peptide-Polymer Conjugates: From Fundamental Science to Application. *Annual review of physical chemistry*, 64:631–657, 2013.

[77] Charles J Bowerman, Wathsala Liyanage, Alexander J Federation, and Bradley L Nilsson. Tuning β-Sheet Peptide Self-Assembly and Hydrogelation Behavior by Modification of Sequence Hydrophobicity and Aromaticity. *Biomacromolecules*, 12(7):2735–2745, July 2011.

[78] Jiayang Li, Yuan Gao, Yi Kuang, Junfeng Shi, Xuewen Du, Jie Zhou, Huaimin Wang, Zhimou Yang, and Bing Xu. Dephosphorylation of d-Peptide Derivatives to Form Biofunctional, Supramolecular Nanofibers/Hydrogels and Their Potential Applications for Intracellular Imaging and Intratumoral Chemotherapy. *Journal Of The American Chemical Society*, 135(26):9907–9914, July 2013.

[79] Omid Khakshoor and James S Nowick. Artificial β-sheets: chemical models of β-sheets. *Current opinion in chemical biology*, 12(6):722–729, December 2008.

[80] Bulent Ozbas, Karthikan Rajagopal, Joel Schneider, and Darrin Pochan. Semiflexible Chain Networks Formed via Self-Assembly of β-Hairpin Molecules. *Physical review letters*, 93(26):268106, December 2004.

[81] Bulent Ozbas, Juliana Kretsinger, Karthikan Rajagopal, Joel P Schneider, and Darrin J Pochan. Salt-triggered peptide folding and consequent self-assembly into hydrogels with tunable modulus. ..., 2004.

[82] Erica L Bakota, Lorenzo Aulisa, Kerstin M Galler, and Jeffrey D Hartgerink. Enzymatic Cross-Linking of a Nanofibrous Peptide Hydrogel. *Biomacromolecules*, 12(1):82–87, January 2011.

[83] Bradley D Olsen. Engineering materials from proteins. *Aiche Journal*, 59(10):3558–3568, September 2013.

[84] Jangwook P Jung, Arun K Nagaraj, Emily K Fox, Jai S Rudra, Jason M Devgun, and Joel H Collier. Co-assembling peptides as defined matrices for endothelial cells. *Biomaterials*, 30(12):2400–2410, 2009.

[85] Rebecca L DiMarco and Sarah C Heilshorn. Multifunctional Materials through Modular Protein Engineering. *Advanced Materials*, 24(29):3923–3940, June 2012.

[86] Lara A Estroff and Andrew D Hamilton. Water gelation by small organic molecules. *Chemical Reviews*, 104(3):1201–1218, 2004.

[87] Elizabeth H C Bromley, Kevin Channon, Efrosini Moutevelis, and Derek N Woolfson. Peptide and Protein Building Blocks for Synthetic Biology: From Programming Biomolecules to Self-Organized Biomolecular Systems. *ACS Chemical Biology*, 3(1):38–50, January 2008.

[88] Wei Seong Toh, Eng Hin Lee, Xi-Min Guo, Jerry K Y Chan, Chen Hua Yeow, Andre B Choo, and Tong Cao. Recombinant self-assembling peptides as biomaterials for tissue engineering. *Biomaterials*, 31(36):9395–9405, 2010.

[89] T J Smith, J Khatcheressian, G H Lyman, H Ozer, J O Armitage, L Balducci, C L Bennett, S B Cantor, J Crawford, and S J Cross. 2006 update of recommendations for the use of white blood cell growth factors: an evidence-based clinical practice guideline. *Journal of Clinical Oncology*, 24(19):3187–3205, 2006.

[90] Vineetha Jayawarna, Stephen M Richardson, Andrew R Hirst, Nigel W Hodson, Alberto Saiani, Julie E Gough, and Rein V Ulijn. Introducing chemical functionality in Fmoc-peptide gels for cell culture. *Acta Biomaterialia*, 5(3):934–943, March 2009.

[91] Dave J Adams, Michael F Butler, William J Frith, Mark Kirkland, Leanne Mullen, and Paul Sanderson. A new method for maintaining homogeneity during liquid–hydrogel transitions using low molecular weight hydrogelators. *Soft Matter*, 5(9):1856, 2009.

[92] S Doose, H Neuweiler, H Barsch, and M Sauer. Probing polyproline structure and dynamics by photoinduced electron transfer provides evidence for deviations from a regular polyproline type II helix. *Proceedings of the National Academy of Sciences*, 104(44):17400–17405, October 2007.

[93] Jaclyn Raeburn, Andre Zamith Cardoso, and Dave J Adams. The importance of the self-assembly process to control mechanical properties of low molecular weight hydrogels. *Chemical Society Reviews*, 42(12):5143–5156, 2013.

[94] Tuna Yucel, Chris M Micklitsch, Joel P Schneider, and Darrin J Pochan. Direct Observation of Early-Time Hydrogelation in β-Hairpin Peptide Self-Assembly. *Macromolecules*, 41(15):5763–5772, August 2008.

[95] Lorenzo Aulisa, He Dong, and Jeffrey D Hartgerink. Self-Assembly of Multidomain Peptides: Sequence Variation Allows Control over Cross-Linking and Viscoelasticity. *Biomacromolecules*, 10(9):2694–2698, September 2009.

[96] M C Branco, D J Pochan, N J Wagner, and J P Schneider. Macromolecular diffusion and release from self-assembled β-hairpin peptide hydrogels. *Biomaterials*, 2009.

[97] Brian F Lin, Katie A Megley, Nickesh Viswanathan, Daniel V Krogstad, Laurie B Drews, Matthew J Kade, Yichun Qian, and Matthew V Tirrell. pH-responsive

branched peptide amphiphile hydrogel designed for applications in regenerative medicine with potential as injectable tissue scaffolds. *Journal of Materials Chemistry*, 22(37):19447, 2012.

[98] Aristides D Tagalakis, Luisa Saraiva, David McCarthy, Kenth T Gustafsson, and Stephen L Hart. Comparison of Nanocomplexes with Branched and Linear Peptides for SiRNA Delivery. *Biomacromolecules*, 14(3):761–770, 2013.

[99] He Dong, Nikhil Dube, Jessica Y Shu, Jai W Seo, Lisa M Mahakian, Katherine W Ferrara, and Ting Xu. Long-Circulating 15 nm Micelles Based on Amphiphilic 3-Helix Peptide–PEG Conjugates. *Acs Nano*, 6(6):5320–5329, June 2012.

[100] Honggang Cui, Matthew J Webber, and Samuel I Stupp. Self-assembly of peptide amphiphiles: From molecules to nanostructures to biomaterials. *Biopolymers*, 94(1):1–18, January 2010.

[101] Walraj S Gosal, Allan H Clark, and Simon B Ross-Murphy. Fibrillar β-Lactoglobulin Gels: Part 1. Fibril Formation and Structure. *Biomacromolecules*, 5(6):2408–2419, November 2004.

[102] Tzu-Yu Liu, Waleed M Hussein, Zhongfan Jia, Zyta M Ziora, Nigel A J McMillan, Michael J Monteiro, Istvan Toth, and Mariusz Skwarczynski. Self-Adjuvanting Polymer–Peptide Conjugates As Therapeutic Vaccine Candidates against Cervical Cancer. *Biomacromolecules*, 14(8):2798–2806, August 2013.

[103] Walraj S Gosal, Allan H Clark, Paul DA Pudney, and Simon B Ross-Murphy. Novel amyloid fibrillar networks derived from a globular protein: β-lactoglobulin. *Langmuir*, 18(19):7174–7181, 2002.

[104] Yi-An Lin, Yu-Chuan Ou, Andrew G Cheetham, and Honggang Cui. Supramolecular Polymers Formed by ABC Miktoarm Star Peptides. *Acs Macro Letters*, 2(12):1088–1094, December 2013.

[105] Gaynor M Kavanagh, Allan H Clark, and Simon B Ross-Murphy. Heat-induced gelation of globular proteins. Part 5. Creep behaviour of β-lactoglobulin gels. *Rheologica Acta*, 41(3):276–284, April 2002.

[106] Ardy Kroes-Nijboer, Paul Venema, and Erik van der Linden. Fibrillar structures in food. *Food & Function*, 3(3):221–227, 2012.

[107] Kuen Yong Lee and David J Mooney. Hydrogels for Tissue Engineering. *Chemical Reviews*, 101(7):1869–1880, July 2001.

[108] Charles J Bowerman and Bradley L Nilsson. Review self-assembly of amphipathic β-sheet peptides: Insights and applications. *Biopolymers*, 98(3):169–184, May 2012.

[109] Richard P Cheng, Samuel H Gellman, and William F DeGrado. β-Peptides: from structure to function. *Chemical Reviews*, 101(10):3219–3232, 2001.

[110] Marc A Gauthier and Harm-Anton Klok. Peptide/protein–polymer conjugates: synthetic strategies and design concepts. *Chemical Communications*, (23):2591–2611, 2008.

[111] Congqi Yan, Aysegul Altunbas, Tuna Yucel, Radhika P Nagarkar, Joel P Schneider, and Darrin J Pochan. Injectable solid hydrogel: mechanism of shear-thinning and immediate recovery of injectable β-hairpin peptide hydrogels. *Soft Matter*, 6(20):5143–5156, October 2010.

[112] Jason A Moss. Guide for Resin and Linker Selection in Solid-Phase Peptide Synthesis. *Current Protocols in Protein Science*, pages 18.7. 1–18.7. 19, 2005.

[113] George Barany and Fernando Albericio. Three-dimensional orthogonal protection scheme for solid-phase peptide synthesis under mild conditions. *Journal Of The American Chemical Society*, 107(17):4936–4942, 1985.

[114] Wilda Helen, Piero de Leonardis, Rein V Ulijn, Julie Gough, and Nicola Tirelli. Mechanosensitive peptide gelation: mode of agitation controls mechanical properties and nano-scale morphology. *Soft Matter*, 7(5):1732, 2011.

[115] Kyle L Morris, Lin Chen, Jaclyn Raeburn, Owen R Sellick, Pepa Cotanda, Alison Paul, Peter C Griffiths, Stephen M King, Rachel K O'Reilly, Louise C Serpell, and Dave J Adams. Chemically programmed self-sorting of gelator networks. *Nature communications*, 4:1480, 2013.

[116] Sivakumar Ramachandran, Marc B Taraban, Jill Trewhella, Ignacy Gryczynski, Zygmunt Gryczynski, and Yihua Bruce Yu. Effect of Temperature During Assembly on the Structure and Mechanical Properties of Peptide-Based Materials. *Biomacromolecules*, 11(6):1502–1506, June 2010.

[117] Yue Feng, Marc Taraban, and Y Bruce Yu. The effect of ionic strength on the mechanical, structural and transport properties of peptide hydrogels. *Soft Matter*, 8(46):11723–11731, 2012.

[118] Chongwoo A Kim and Jeremy M Berg. Thermodynamic β -sheet propensities measured using a zinc-finger host peptide. *Nature*, 362(6417):267–270, March 1993.

[119] Katelyn J Nagy, Michael C Giano, Albert Jin, Darrin J Pochan, and Joel P Schneider. Enhanced Mechanical Rigidity of Hydrogels Formed from Enantiomeric Peptide Assemblies. *Journal Of The American Chemical Society*, 133(38):14975–14977, September 2011.

[120] James C Whisstock and Stephen P Bottomley. Molecular gymnastics: serpin structure, folding and misfolding. *Current opinion in structural biology*, 16(6):761–768, December 2006.

[121] Radhika P Nagarkar, Rohan A Hule, Darrin J Pochan, and Joel P Schneider. Domain swapping in materials design. *Biopolymers*, 94(1):141–155, January 2010.

[122] Karthikan Rajagopal, Matthew S Lamm, Lisa A Haines-Butterick, Darrin J Pochan, and Joel P Schneider. Tuning the pH Responsiveness of beta-Hairpin Peptide Folding, Self-Assembly, and Hydrogel Material Formation. *Biomacromolecules*, 10(9):2619–2625, 2009.

[123] Felix Freire, Aaron M Almeida, John D Fisk, Jay D Steinkruger, and Samuel H Gellman. Impact of Strand Length on the Stability of Parallel-β-Sheet Secondary Structure. *Angewandte Chemie International Edition*, 50(37):8735–8738, August 2011.

[124] Bojana Apostolovic, Maarten Danial, and Harm-Anton Klok. Coiled coils: attractive protein folding motifs for the fabrication of self-assembled, responsive and bioactive materials. *Chemical Society Reviews*, 39(9):3541, 2010.

[125] Efrosini Moutevelis and Derek N Woolfson. A Periodic Table of Coiled-Coil Protein Structures. *Journal Of Molecular Biology*, 385(3):726–732, January 2009.

[126] Hana Robson Marsden and Alexander Kros. Self-Assembly of Coiled Coils in Synthetic Biology: Inspiration and Progress. *Angewandte Chemie International Edition*, 49(17):2988–3005, April 2010.

[127] Peng Jing, Jai S Rudra, Andrew B Herr, and Joel H Collier. Self-assembling peptide-polymer hydrogels designed from the coiled coil region of fibrin. *Biomacromolecules*, 9(9):2438–2446, 2008.

[128] Rohan A Hule, Radhika P Nagarkar, Aysegul Altunbas, Hassna R Ramay, Monica C Branco, Joel P Schneider, and Darrin J Pochan. Correlations between structure, material properties and bioproperties in self-assembled β-hairpin peptide hydrogels. *Faraday Discuss.*, 139(0):251–264, August 2008.

[129] Monica C Branco, Florian Nettesheim, Darrin J Pochan, Joel P Schneider, and Norman J Wagner. Fast dynamics of semiflexible chain networks of self-assembled peptides. *Biomacromolecules*, 10(6):1374–1380, 2009.

[130] Aysegul Altunbas, Seung J Lee, Sigrid A Rajasekaran, Joel P Schneider, and Darrin J Pochan. Encapsulation of curcumin in self-assembling peptide hydrogels as injectable drug delivery vehicles. *Biomaterials*, 32(25):5906–5914, 2011.

[131] Sotirios Koutsopoulos, Larry D Unsworth, Yusuke Nagai, and Shuguang Zhang. Controlled release of functional proteins through designer self-assembling peptide nanofiber hydrogel scaffold. *Proceedings Of The National Academy Of Sciences Of The United States Of America*, 106(12):4623–4628, March 2009.

[132] Laney M Weber, Christina G Lopez, and Kristi S Anseth. Effects of PEG hydrogel crosslinking density on protein diffusion and encapsulated islet survival and function. *Journal Of Biomedical Materials Research*, 90A(3):720–729, September 2009.

[133] Jason A Burdick and Kristi S Anseth. Photoencapsulation of osteoblasts in injectable RGD-modified PEG hydrogels for bone tissue engineering. *Biomaterials*, 23(22):4315–4323, 2002.

[134] Sophie R Van Tomme, Gert Storm, and Wim E Hennink. In situ gelling hydrogels for pharmaceutical and biomedical applications. *International journal of pharmaceutics*, 355(1):1–18, 2008.

[135] Joel H Collier, Bi Huang Hu, Jeffrey W Ruberti, Jerry Zhang, Pochi Shum, David H Thompson, and Phillip B Messersmith. Thermally and Photochemically Triggered Self-Assembly of Peptide Hydrogels. *Journal Of The American Chemical Society*, 123(38):9463–9464, September 2001.

[136] Joel H Collier and Phillip B Messersmith. Enzymatic Modification of Self-Assembled Peptide Structures with Tissue Transglutaminase. *Bioconjugate Chemistry*, 14(4):748–755, July 2003.

[137] Adam J Engler, Shamik Sen, H Lee Sweeney, and Dennis E Discher. Matrix elasticity directs stem cell lineage specification. *Cell*, 126(4):677–689, August 2006.

[138] Iris L Kim, Robert L Mauck, and Jason A Burdick. Hydrogel design for cartilage tissue engineering: a case study with hyaluronic acid. *Biomaterials*, 32(34):8771–8782, 2011.

[139] Diego Silva, Antonino Natalello, Babak Sanii, Rajesh Vasita, Gloria Saracino, Ronald N Zuckermann, Silvia Maria Doglia, and Fabrizio Gelain. Synthesis and characterization of designed BMHP1-derived self-assembling peptides for tissue engineering applications. *Nanoscale*, 5(2):704–718, 2013.

[140] Matthew J Webber, Jörn Tongers, Marie-Ange Renault, Jerome G Roncalli, Douglas W Losordo, and Samuel I Stupp. Development of bioactive peptide amphiphiles for therapeutic cell delivery. *Acta Biomaterialia*, 6(1):3–11, January 2010.

[141] Joel H Collier, Jai S Rudra, Joshua Z Gasiorowski, and Jangwook P Jung. Multi-component extracellular matrices based on peptide self-assembly. *Chemical Society Reviews*, 39(9):3413, 2010.

[142] Nicole H Romano, Debanti Sengupta, Cindy Chung, and Sarah C Heilshorn. Protein-engineered biomaterials: Nanoscale mimics of the extracellular matrix. *Biochimica et Biophysica Acta (BBA) - General Subjects*, 1810(3):339–349, March 2011.

[143] John B Matson and Samuel I Stupp. Self-assembling peptide scaffolds for regenerative medicine. *Chemical Communications*, 48(1):26, 2011.

[144] V Jayawarna, A Smith, J E Gough, and R V Ulijn. Three-dimensional cell culture of chondrocytes on modified di-phenylalanine scaffolds. *Biochemical Society Transactions*, 35(3):535–537, 2007.

[145] DJ Pochan, JP Schneider, Juliana Kretsinger, Bulent Ozbas, Karthikan Rajagopal, and L Haines. Thermally reversible hydrogels via intramolecular folding and consequent self-assembly of a de Novo designed peptide. *Journal Of The American Chemical Society*, 125(39):11802–11803, 2003.

[146] J H Collier and P B Messersmith. Self-Assembling Polymer–Peptide Conjugates: Nanostructural Tailoring. *Advanced Materials*, 16(11):907–910, June 2004.

[147] Ananth K Vellimana, Violette Renard Recinos, Lee Hwang, Kirk D Fowers, Khan W Li, Yonggang Zhang, Saint Okonma, Charles G Eberhart, Henry Brem, and Betty M Tyler. Combination of paclitaxel thermal gel depot with temozolomide and radiotherapy significantly prolongs survival in an experimental rodent glioma model. *Journal of neuro-oncology*, 111(3):229–236, December 2012.

[148] Nipun Babu Varukattu and Soundarapandian Kannan. Enhanced Delivery of baisalein using cinnamaldehyde cross-linked chitosan nanoparticle inducing apoptosis. *International Journal of Biological Macromolecules*, 2012.

[149] Nancy L Elstad and Kirk D Fowers. OncoGel (ReGel/paclitaxel) — Clinical applications for a novel paclitaxel delivery system. *Advanced Drug Delivery Reviews*, 61(10):785–794, August 2009.

[150] Lorena Tavano, Marco Vivacqua, Valentina Carito, Rita Muzzalupo, Maria Cristina Caroleo, and Fiore Nicoletta. Doxorubicin loaded magnetoniosomes for targeted drug delivery. *Colloids And Surfaces B-Biointerfaces*, 102:803–807, February 2013.

[151] Cyril Lorenzato, Alexandru Cernicanu, Marie Edith Meyre, Matthieu Germain, Agnès Pottier, Laurent Levy, Baudouin Denis Senneville, Clemens Bos, Chrit Moonen, and Pierre Smirnov. MRI contrast variation of thermosensitive magnetoliposomes triggered by focused ultrasound: a tool for image-guided local drug delivery. *Contrast Media & Molecular Imaging*, 8(2):185–192, March 2013.

[152] L A Butterick. *Design of self-assembling beta-hairpin pepide-based hydrogels for tissue engineering applications*. PhD thesis, 2008.

[153] J K Kretsinger, L A Haines, Bulent Ozbas, and D J Pochan. Cytocompatibility of self-assembled β-hairpin peptide hydrogel surfaces. *Biomaterials*, 2005.

[154] V Basile, E Ferrari, S Lazzari, S Belluti, F Pignedoli, and C Imbriano. Curcumin derivatives: molecular basis of their anti-cancer activity. *Biochemical pharmacology*, 78(10):1305–1315, 2009.

Chapter 2

LONG TERM RELEASE OF HYDROPHOBIC PAYLOAD FROM MAX8 HYDROGELS

MAX8 is a peptidic hydrogel that folds and intramolecularly assembles into fibrils.When assembling, the peptide forms a β-hairpin that goes on to form bilayer fibrils with natural entanglements and branch points. The physically, cross-linked network of MAX8 can shear-thin and re-heal, and is also cytocompatible.[1] The previous applications of MAX peptides for cell and drug encapsulation are important pre-cursors for the bulk of this chapter.[1–6] This chapter builds upon these previous investigations to explore the encapsulation and release of hydrophobic vincristine from the aqueous network of MAX8 over the course of a month.

2.1 Release of Encapsulated Vincristine from MAX8

A current strategy for chemotherapeutic delivery vehicles is to use injectable delivery vehicles that can directly deliver chemotherapeutics or other drug therapies. Injectable vehicles include nanoparticles[7,8], polymer gels[9–11], or micelles loaded with chemotherapeutics.[12,13] Many of these vehicles are surface modified or functionalized with ligands or protein sequences for better targeting.[14,15] Presently, there are two types of injectable vehicles, those introduced intravenously and those introduced through site-specific local delivery. Intravenous delivery typically introduces a particle into the body, with modifiable targeting, drug encapsulation, and drug release methods.[16,17] While useful for broad targets easily reached by the blood stream, in some cases the vehicles coalesce in the kidney or liver permanently.[18,19] Site-specific, local delivery vehicles can be useful, reducing the exposure of healthy tissue to potentially toxic

drugs. Once administered, the drug-encapsulated vehicles can continuously administer active drugs through controlled release.

One family of drug delivery vehicles with potential for effective,sustained release is the hydrogel. Hydrogels are water-based three-dimensional solid networks composed of polymer chains. One use of hydrogels is as platforms for local, injectable applications, with the capability to encapsulate and distribute a wide range of materials such as drugs[3,20], large proteins[21], and even cells.[22–24] After injection for deposition, the hydrogel continues to release chemotherapeutics while remaining in the desired location for a prolonged, desired period of time, reducing the need for more surgeries and invasive procedures. Ideally, hydrogels also possess shear-thinning and self-healing capabilities that allow for more specific injectable locations and fewer needs for additional surgeries for continuous care, carrying fewer risks for complications.[25]

As discussed in Chapter 1, the Pochan and Schneider groups have extensively investigated extensively various β-hairpin forming peptide hydrogels that are able to intermolecularly self-assemble into nanofibrillar, physical hydrogels as a result of an intramolecular folding response.[6,27,43–46] These β-hairpin peptide hydrogels display injectable-solid properties; solid hydrogels that exhibit shear-thinning flow during syringe injection but also exhibit immediate solid recovery after cessation of shear. In addition, the hydrogel material properties such as gelation time, stiffness, and network mesh size are tunable via molecule design as well as solution conditions that control the intermolecular self-assembly into a hydrogel network. MAX8 has been studied for in vitro and in vivo studies because it self-assembles at physiological conditions and can successfully encapsulate many different types of payloads.

Vincristine, the target drug, is a long accepted, intravenously delivered, and commonly used clinical chemotherapeutic.[47] Vincristine alone, or in a combination, is usually administered to treat many types of cancers, including lymphoma (Hodgkin's and Non-Hodgkin's)[48–50], leukemia[51,52], glioma[53,54], embryoma[55], lung cancer[56], and neuroblastoma.[57] Vincristine disrupts cell division by binding to tubulin, poisoning the tubulin heterodimer, then incorporating itself into microtubule bundles to prevent

further growth.[58,59] However, the effectiveness of vincristine also leads to many adverse side effects such as organ toxicity, nausea/vomiting, and hair loss.[48,49] Vincristine is unable to differentiate healthy cells from cancerous cells and will target any dividing cell indiscriminately.[58,59] Several rounds of treatments are required in order to provide constant exposure of the cancerous cells to vincristine. Naturally, this prolonged exposure to the drug leads to an increase in detrimental side effects in patients.

In this chapter, vincristine is encapsulated within MAX8 hydrogel to show that the drug-hydrogel construct is a promising candidate as a site specific local delivery vehicle, with the potential to minimize overall invasiveness and damage to healthy tissue through the local, continuous release of the chemotherapeutic from the hydrogel. Importantly, the hydrogel provides a protective environment for the hydrophobic drug in the deposited area, so that released drug could continue to be effective at killing cancer cells at month-long time scales. We first demonstrate, using oscillatory rheometry, that the presence of vincristine within the MAX8 network does not alter the general viscoelastic properties, and specific shear-thinning and self-healing properties, that make it attractive as a drug delivery vehicle. In addition, small-angle neutron scattering (SANS) measurements find that the structure of the MAX8 network (e.g., fibrillar character, porous network) is not altered significantly by the presence of vincristine and that the drug appears to be closely associated with the fibrillar nanostructure and not relegated to separate domains of drug within the fibrillar network. Viscristine release from the hydrogel was quantified using tritium-labeled vincristine, and release profiles confirm that vincristine is released continuously from the material for up to 28 days from encapsulation. Furthermore, in vitro studies demonstrate that vincristine remains biologically active after 28 days — over 20 times longer than its half-life in bulk water. The present work shows that in contrast to the current intravenous vincristine delivery method vincristine-loaded MAX8 hydrogels provide sustained, low, but effective release to a specific target and may be excellent candidates as drug delivery vehicles that exhibit minimal side effects and damage to healthy tissue.

2.2 Materials, Methods and Characterizations

2.2.1 MAX8 Peptide

MAX8 peptide was synthesized on rink amide resin employing Fmoc-protocol and HCTU activation on one of three peptide synthesizers, the ABI 433A, the SONOTA, or the AAPPTEC Focus XC, using automated processes. Once synthesized, the peptides are cleaved and side-chain deprotected with a cleavage cocktail of trifluoroacetic acid (TFA), thioanisole, ethanedithiol and anisole – volume ratio of 90:5:3:2 – for two hours under an N_2 atmosphere. Next, the crude peptides are precipitated in ether and filtered. Purification through HPLC used solvents A (0.1%TFA in DI water) and B (90% acetonitrile with 0.1% TFA in 10% DI water). First, the crude peptide was dissolved at 5mg/mL in solvent A, then injected into a Vydac C18 column, previously washed by 100% of solvent B. The gradient, at a flow rate of 8mL/min, used 0% solvent B for 2 minutes, then ramped linearly to 21% solvent B over 4 minutes, finally to 100%B until all of MAX8 eluted out. Afterwards, eluted MAX8 was lyophilized, then dissolved in DI water to lyophilize a second time before use in hydrogels.

2.2.2 Vincristine and Curcumin

Vincristine sulfate salt was purchased from Sigma-Aldrich, Inc. Due to the limited solubilities of vincristine and curcumin, both were created into stock solutions and frozen at -20 °C. When using the vincristine or curcumin stock solution, it was diluted to the desired concentration by addition of Dulbecco's Modified Eagle's Medium (DMEM) without any additional fetal bovine serum (FBS) or penicillin streptomycin (Pen Strep). DMEM, FBS, Pen Strep were all purchased from Corning Cellgro.

Tritium (^{3}H) labeled vincristine was purchased from American Radiolabeled Chemicals, Inc at an activity of 15 Ci in 50 μL volumes. Cytoscint scintillation cocktail, a universal liquid scintillation counter cocktail fluid, was used for measuring tritium levels was purchased from Fisher Scientific, Inc. Tritium labeled vincristine was stored at -20 °C within several secondary safety containers.

2.2.3 Cell Lines

The DAOY cell line was used in the study of chemotherapeutic release. The DAOY cells come from American Type Culture Collection Cell lines are cultured in 75 cm^2 flasks using DMEM with 10% FBS and 1% Pen Strep added. Flasks are left in a 37 °C, humidified environment with 5% CO_2.

2.2.4 Miscellaneous

Transwell inserts for release and efficacy studies contain a 0.4 μm mesh (Corning). Lactate dehydrogenase (LDH) assays for cell vitality were obtained from Promega and used according to manufacturer instructions. Cy5.5 NHS Ester dye was purchased from Lumiprobe Corp. and dissolved into a stock solution of 10mmol/L in DMSO and stored frozen at -20 °C.

2.2.5 Assembly of MAX8

To prepare a 100mL 0.5wt% peptide hydrogel, 0.5mg of MAX8 was first dissolved in 50 μL of 4 °C DI water. Separately, an equal volume of approximately 37 °C DMEM containing 50mmol/L HEPES salt was prepared and then added to the MAX8 solution. Mixing the MAX8 solution with the buffer solution triggers intramolecular folding of the peptides and subsequent self-assembly into a hydrogel. Note that the presence of phenol red in DMEM may interfere with fluorescence measurements and, therefore, was omitted. To create higher weight percent hydrogels, the initial mass of dissolved MAX8 is increased appropriately — 1mg MAX8 in 50 μL of DI water for 100 μL of 1wt% hydrogel.

When encapsulating chemotherapeutic payloads, drugs were mixed with the cell medium before being added to MAX8/DI water solution. For encapsulation of vincristine, twice the final drug concentration desired was dissolved in cell medium before being added to the MAX8/DI water solution. For example, 100 μL of 0.5wt%

MAX8 hydrogel with 500 μmol/L encapsulated vincristine was prepared by dissolving 0.5mg MAX8 peptide in 50 μL of DI water and added to 50 μL of cell medium containing 1 mmol/L of vincristine.

2.2.6 Rheometry

Oscillatory rheology measurements were performed on a TA Instruments AR2000 stress-controlled rheometer with 20 mm-diameter acrylic, cross-hatched, parallel plate geometry. The parallel plate geometry was then lowered to a desired gap height of 0.5mm. Mineral oil was placed around the edge of the plate to prevent sample drying. 400 μL of each sample was prepared as described previously, combining 200 μL of peptide dissolved in DI water with 200 μL of desired vincristine concentration in DMEM. The samples were loaded immediately onto the rheometer and data collection was initiated. The rheometer maintained a constant temperature of 37°C through all sample loading and time or frequency sweeps. For dynamic frequency sweep measurements, 0.5 wt% MAX8 hydrogels were prepared with or without 500 μmol/L of vincristine encapsulated. To investigate gel stiffness, a frequency sweep of 0.1-100 rad/s with 0.2% strain was performed, measuring the storage (G$'$) and loss (G$''$) moduli.

500 μmol/L vincristine encapsulated in 0.5 wt% MAX8 was prepared for the shear-thinning experiment. The shear-thinning experiment was subjected to a time sweep at a frequency of 6 rad/s with 0.2% strain as the hydrogel assembled after mixing. Next, the hydrogel was subjected to a steady-state shear at 1000 s^{-1} for 30 seconds. After 30 seconds, the rheometer returned to a dynamic sweep oscillatory measurement, and the hydrogel was monitored for 90 minutes.

2.2.7 Release In Vitro Setup

MAX8 hydrogels (0.5 wt%) were prepared with a final concentration of 1.6 nmol/L, 8 nmol/L, and 40 nmol/L vincristine. Additionally, a hydrogel without any vincristine was prepared as a control. For the in vitro studies, vincristine applied directly to cells in culture was compared to the vincristine that was released into the

culture medium after encapsulation in the hydrogel. DAOY cells were plated in a 24-well plate and incubated overnight in DMEM. For hydrogel drug delivery, 100 μL of MAX8-vincristine gel-drug construct was pipetted into a polyester membrane insert and allowed an additional 20 minutes to complete assembly/rehealing after injection. After the initial wait, each transwell was inserted into a well of 2 mL of DMEM to remove unencapsulated vincristine. The transwell inserts were left in the wash for 20 minutes before being added subsequently to the DAOY cell plates. For experiments with direct treatment of vincristine, 100 μL of vincristine at the desired concentration was added directly into wells with 2 mL of DMEM and plated DAOY cells. Each measurement was measured three times and averaged. The direct treatment cell wells had 8 pmol/L, 40 pmol/L, and 200 pmol/L vincristine concentrations directly in contact with the cultured cells.

To measure cell death, released LDH from dead cells was isolated through centrifugation from the supernatant medium of the cells at desired time points. To measure LDH within live cells, the cells were lysed and crushed after freeze-thawing. Cytotoxcity was then determined on the basis of the ratio of LDH released into the medium to the sum of medium LDH and viable cell LDH.

2.2.8 Vincristine Release Setup

For release studies, three samples of 100 μL of 0.5wt% MAX8 hydrogel were prepared with 500 μmol/L encapsulated vincristine for the UV-Vis spectroscopy studies and 10 μmol/L encapsulated tritiated vincristine for the liquid scintillation counter studies (LSC). Each hydrogel was deposited into a transwell, and, as with the in vitro studies, the hydrogels were set aside to allow for complete healing after pipetting. Next, the hydrogels were washed for 20 minutes in 2 mL of phosphate buffered saline (PBS) for UV-vis or DMEM for the LSC studies, to remove any unencapuslated vincristine. After the wash, how often the insert was moved to each new well was dependent on the method of detection.

The first measurements of released concentrations of vincristine were performed using UV-Vis spectroscopy on a UV-Vis spectrophotometer (Agilent 8453 Uv-Visible Spectrophotometer). In order to accurately measure the amounts of vincristine released at every measurement, a master curve and known concentration of 100uM to standardize the measurements at that light intensity were used. The UV-Vis spectroscopy experiments used a concentration gradient of 2 μmol/L, 5 μmol/L, 10 μmol/L, 20 μmol/L, 30 μmol/L, 40 μmol/L, 50 μmol/L, 60 μmol/L, 70 μmol/L, 100 μmol/L, and 500 μmol/L. Each concentration was measured with three different samples. The release was measured per 10 minutes for the first hour, then at 1.5 hours, 2 hours, 2.5 hours, 3 hours, 6 hours, 12 hours, and 24 hours. To measure the release of vincristine into the PBS, three 100 μL aliquots were pulled from the supernatant and measured. After each measurement, fresh 300 μL of PBS was added to maintain constant osmotic pressure for sustained release of vincristine. The excitation wavelength to measure the samples was set at 297nm.

Unlike the UV-vis spectroscopy experiments, the transwell insert was left undisturbed in a 2 mL well for one hour then was moved to a new well once per hour for the first 6 hours then moved again to a new well of fresh medium at 24 hours. With the tritiated vincristine samples, the short exposure time for the first few time points ensured accurate measurement of the relatively high drug concentrations released at early time points because of the concentration limitation of the LSC (Beckman Coulter LS6500). Due to LSC counter sensitivity, concentrations greater than 1mM were unable to be measured because of over counting by the detector, causing the concentration limitation. After the first 24 hours, the insert was then moved to a new well of fresh medium on day 3, 7, 10, 14, 17, 21, 24, and 28. To measure the release of vincristine into each well, three 100 μL aliquots were removed from the supernatant in each well and measured by scintillation counting. Each 100 μL of supernatant was added to 3 mL of scintillation fluid and counted for 5 min on the LSC. Points measured are averages of nine total measurements, three from each sample for three different samples, with uncertainty measured as standard deviation.

To correlate scintillation counts with vincristine concentration, a calibration curve was created for each day of measurements at five known concentrations of 10 pmol/L, 100 pmol/L, 1 nmol/L, 10 nmol/L, and 100 nmol/L. 100 μL of each known concentrations was added to 3 mL of scintillation fluid and measured for 5 minutes on the LSC. The calibration was performed separately for each day of measurement in order to account for fluctuations in sample radioactivity and background radiation.

2.2.9 Sustained Drug Potency Setup

To best measure vincristine's efficacy in inducing cell death after release from MAX8 encapsulation, a sustained drug potency study was designed to match the conditions of the release study and to observe cytotoxicity effects of drug concentrations observed from hydrogel release. DAOY cells were cultured in 24-well plates as with the in vitro studies described above. Three concentrations of vincristine were utilized for the efficacy study in three sets each of 100 μL of 0.5wt% MAX8 hydrogels: 0 μmol/L, 10 μmol/L, and 500 μmol/L. 10 μmol/L matched the concentration used for the release study and 500 μmol/L is the highest possible concentration that can be encapsulated due to solubility. After mixing the 50 μL of DMEM with the 50 μL of MAX8 solution, the entire drug-gel construct was pipetted into a transwell insert, allowed to complete hydrogelation for 20 minutes and then placed in a wash of 2 mL fresh medium for 20 minutes, same as the release study setup. In order to match the release study's time course setup, the insert was moved into a new well of 2mL fresh medium at the same time intervals (once per hour for the first 6 hours, at 24 hours, then days 3, 7, 10, 14, 17, 21, 24, 28). Rather than measure' the vincristine's potency at every well change during the time course, the potency was measured at weekly intervals. To measure the potency at the end of each week, wells for days 3 to 7, 10 to 14, 17 to 21, and 24 to 28 were plated with DAOY cells. Additionally, to measure initial release efficacy, the well used for the first hour of drug release had plated DAOY cells. Using an LDH assay from Promega and used according to manufacturer instructions, cell deaths were measured in the newly vacated wells containing DAOY cells having been exposed to vincristine

release over desired time intervals, for all time points except for those exposed in the first hour of release. The first set of treated cells were incubated for 2 days after the initial hour of treatment so that a full cell cycle occurred, allowing for full drug effects, and then measured with an LDH assay. Points measured are averages of across the three samples at each condition with uncertainty measured as standard deviation.

2.2.10 Statistics

Data for all LDH assays are presented as mean ± standard deviation. Data was obtained across 3 separate samples. Statistical significance was determined using Student's T-test to compare data sets, where $p<0.05$ considered significant.

2.2.11 Fluorescence Recovery After Photobleaching

For the Fluorescence Recovery After Photobleaching (FRAP) experiments. 100 mL of MAX8 hydrogels were prepared using previously described methods for 0.5wt%, 1wt%, and 2wt% hydrogels with 4 mmol/L, 2 mmol/L, 400 μmol/L, and 80 μmol/L concentrations of vincristine encapsualted. Each of the twelve hydrogels were added to Lab-Tek II Chamber, 8 well plates.

FRAP measurements were taken using laser scanning confocal microscopy on a Zeiss 510 LCM Confocal Mircroscope with a 20 times magnification objective. Each measurement, regardless of curcumin concentration or hydrogel weight percentage used an argon ion laser set at 50% power. All experiments were performed at 25 °C. The microscope scans each image along the xy plane of the sample, with a circle diameter of 100 pixels or 90 μm for the bleaching area. Before bleaching, 12 images (about 5 seconds each image) are taken at lower laser intensity (5% power), then 10 seconds of 100% laser intensity for bleaching occurs. The fluorescence recovery detection then collects images every 5 seconds at lower laser intensity for the next 240 seconds, for a total of 60 images.

2.3 Results

2.3.1 Rheometry

The injectable solid properties of MAX8, or shear thinning and immediate solidification, make the material a desirable injection delivery vehicle. To ensure that the hydrogel retains these properties with drug included, the storage (G′) and loss (G″) moduli of the system were measured with a frequency sweep for 0.5 wt% MAX8 hydrogel with or without 500 μmol/L vincristine. The storage and loss moduli characterize the elastic and viscous behavior of the material.[6,60,61] The thesis work of Sameer Sathaye investigates MAX hydrogel rheological properties further.[62] As shown in Figure 2.1a, there is a negligible difference between G′ and G′ with and without vincristine for the MAX8 hydrogel showing that the presence of the drug does not alter the material properties of the hydrogel. Moreover, these data show that once deposited, the drug-gel construct will retain all the desirable gel physical properties of MAX8.

Previous studies have shown that when a constant shear force is applied on the hydrogel, the material flows with properties of a low viscosity material.[6,61] Once shear forces cease, the hydrogel has been shown to immediately recover solid gel properties, reaching pre-shear peak G′ and G″values quickly after shearing. Figure 2.1b demonstrates the same shear-thinning and re-healing properties of MAX8 with 500 μmol/L of vincristine encapsulated. Thus, after gelation the drug-loaded hydrogel flows easily when sheared and recovers original properties of the presheared gel after shear cessation. This ability is critical for delivery applications, allowing the hydrogel to be injected into a specific site and trusted to recover to a gel state with known properties and to stay in place at the injection site.

2.3.2 In Vitro Studies

In order to show MAX8 would be an effective delivery vehicle, releasing vincristine to induce cell death, a series of in vitro studies were performed. In order to show the IC_{50} value, the concentration of vincristine directly applied for treatment was in the picomolar range. These picomolar concentrations agreed with previous *in*

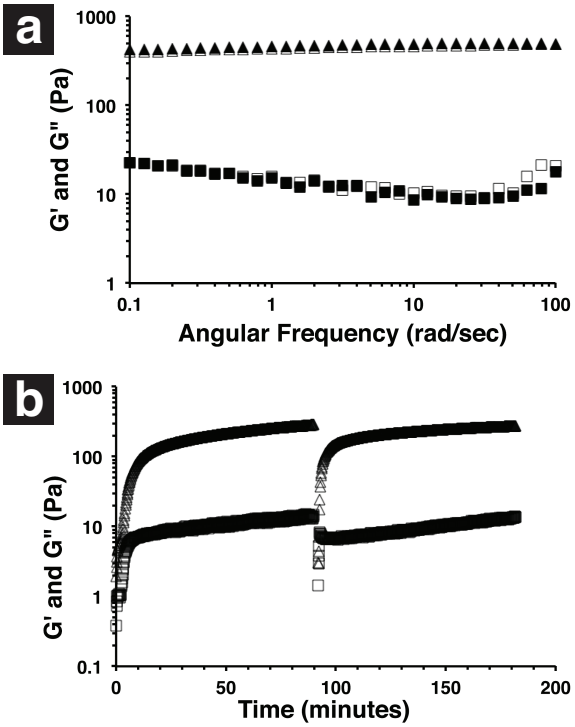

Figure 2.1: Triangles correspond to G′ (storage modulus), and squares correspond to G″ (loss modulus). **a.**) A frequency sweep from 0.1-100rad/s with 0.2% strain was run for 0.5 wt% MAX8 hydrogels with 500 μM vincristine (filled symbols) and without vincristine (open symbols). No difference is observed in the viscoelastic properties of the hydrogel with and without vincristine encapsulated. **b.**) A time sweep at a frequency of 6rad/s with a 0.2% strain was run on a 0.5wt% MAX8 hydrogel with 500 μM vincristine encapsulated. Early time shows the initial gelation within 10 minutes. A constant shear at a steady-state shear of 1000/s is applied for 30 seconds at 90 minutes. As soon as the large shear ceases, the time sweep data shows the hydrogel immediately as a solid material and quickly recovering original gel properties.

vitro studies, consistent with the potency of vincristine.[51] In order to measure the IC_{50} for cells being treated either directly with vincristine, or by vincristine released from a MAX8 gel, a series of decreasing concentrations for both directly applied and hydrogel-released vincristine were prepared. An LDH assay was performed for both models to find the IC_{50} as presented in Figure 2.2. Figure 2.2a and Figure 2.2b both show that cell death increases as the concentration of vincristine increases. For direct treatment, the IC_{50} was determined to be between 5 nmol/L and 25 nmol/L, after showing a clear trend of cell death with increasing drug concentration of treatment. For the encapsulated vincristine the IC_{50} is reached when 8 nmol/L of vincristine is encapsulated into a hydrogel and then exposed to cells. It should be noted that the released drug concentration for the direct applied treatment are extremely low.

Determining the IC_{50} concentrations was important in ensuring that vincristine encapsulated in MAX8 would still induce cell death, and drug concentration affected cell death percentage. When beginning the in vitro experiments, 500 μmol/L was first attempted. This first concentration was chosen since it is the highest concentration that could be encapsulated due to the limited solubility in aqueous solution of hydrophobic vincristine. But the potency of vincristine quickly showed that μmol/L was too high of a concentration, killing cell populations completely. Nevertheless, the result clearly shows that the concentrations of drug required for original encapsulation prior to release can be very low and still effective/useful for local delivery. These low values demonstrate that lower vincristine doses are still effective and would minimize the amount of undesirable side effects and healthy cell death during local delivery. Figure 3c to Figure 3f shows light microscope images of the cells treated with the corresponding concentrations of vincristine encapsulated in the hydrogel to confirm the presence of the drug is responsible for cell death. The 0 nM sample consisted of pure MAX8 hydrogel without any vincristine. The presence of the MAX8 does not result in significant cell death, indicating any cell death with vincristine is a result of the drug, while at 40 nM, the cells are almost all round and opaque, showing clear signs of cell death.

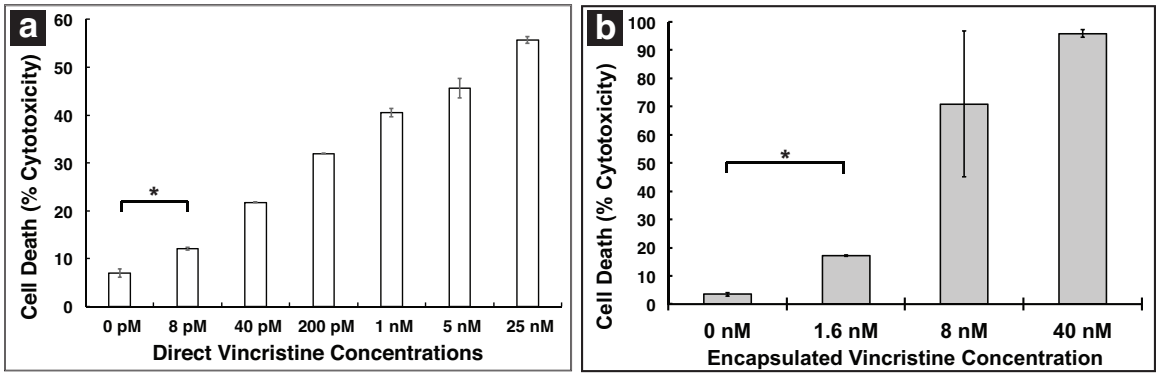

Figure 2.2: Cell death measured using LDH assays, show percent cell death of DAOY cells **a.**) after direct treatment with vincristine and **b.**) vincristine encapsulated and released from a 0.5wt% MAX8 hydrogel. All measurements are taken after 2 days of cell incubation with each listed concentration. * indicates noted concentrations are significantly different ($p<0.05$).

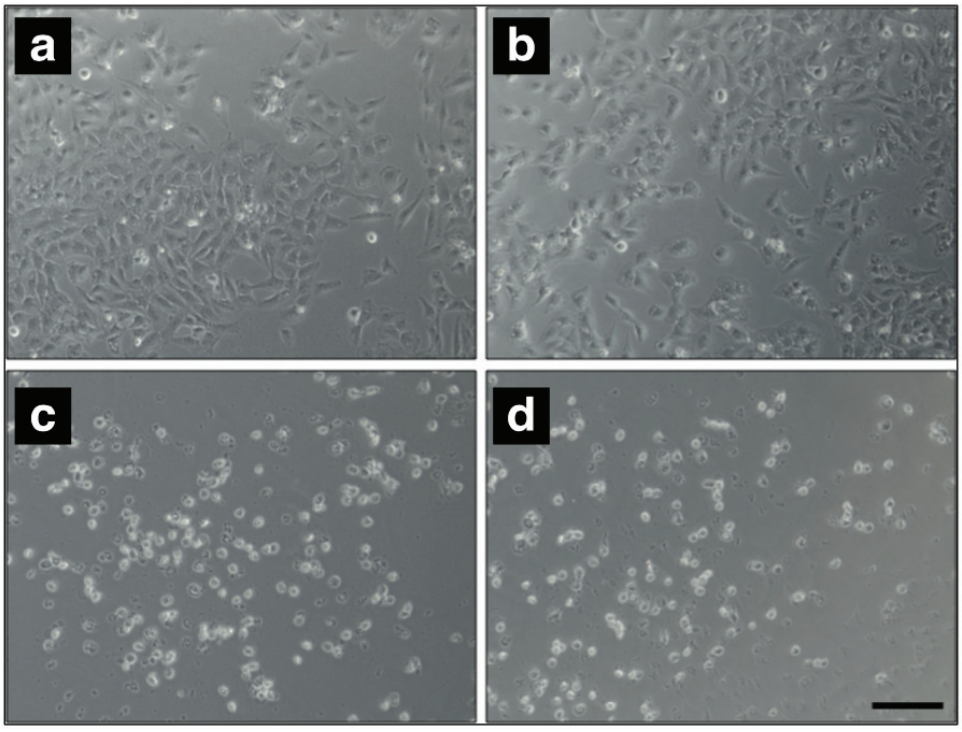

Figure 2.3: Optical micrographs of DAOY cells treated with **a.**) 0 nmol/L **b.**) 1.6 nmol/L **c.**) 8 nmol/L and **d.**) 40 nmol/L of vincristine encapsulated in a MAX8 hydrogel. Live cells appear elongated and transparent, dead cells are rounded and opaque. The scale bar is 200 μm.

2.3.3 Initial Release Study

UV-Vis spectroscopy was originally used to measure the released drug from MAX8 into an infinite sink environment. 500 μmol/L of vincristine was encapsulated in 0.5wt% MAX8 hydrogel. Table 2.1 shows the measured absorption of the concentration gradient. The absorption intensities are low at 500 μmol/L but more importantly, after 10 μmol/L, the values are close to zero and difficult to detect.

After measuring the intensities of the concentration gradient, the 500 μmol/L vincristine encapsulated MAX8 hydrogel was set up for a day long release. The concentrations released decrease with time, as seen in Figure 2.4. However, after a day of release, the measured concentrations near 5 μmol/L, the detector resolution limit for when the detector could not reliably measure released drug amount. Based on the gradient, the estimated released concentration at 24 hours was around 5 μmol/L. The limitation of only accurately measuring one day of release, when the goal is for long-term release, lead to the use of tritium-labled vincristine.

2.3.4 Release and Sustained Potency

The LSC was chosen for its capabilities to detect lower concentrations. Tritium (^{3}H) labeled vincristine had to be ordered and used in release studies to be able to use the LSC. Due to the concentration and volume of the obtained tritium-labeled vincristine, 10 μmol/L was the highest concentration that could be encapsulated.A month long time release of vincristine from a 0.5 wt% MAX8 hydrogel containing 10 μmol/L tritiated vincristine encapsulated in 0.5wt% is shown in Figure 2.5. The time points are of concentrations measured at days 1 (accumulated from measurements between hours 1 through 6, and 24 hours), 3, 7, 10, 14, 17, 21, 24, and 28 in the release. The inset of Figure 2.5 highlights days 14, 17, 21, 24, and 28 to show that the released concentrations are non-zero, and these concentrations can be found in Table 2.2 at these long time points of release. In particular, note that after 28 days, approximately 2 nM concentration vincristine is still released from the gel. This concentration, while low, is still a viable concentration that can induce cell death as shown in Figure 2.2a, where

Table 2.1: Absorption measured via UV-Vis spectroscopy is a function of concentration, the lower concentrations made it difficult for detctor resolution and could no longer accurately measure the drug amount.

Concentration	Absorption (297nm)
2 μmol/L	0.0047
5 μmol/L	0.043
10 μmol/L	0.12
20 μmol/L	0.32
30 μmol/L	0.53
40 μmol/L	0.73
50 μmol/L	0.87
60 μmol/L	1.11
70 μmol/L	1.2
100 μmol/L	2.2
500 μmol/L	3.7

picomol/L are effective concentrations. This measurement shows that the continu ously released concentrations are not irrelevant.

In order to ensure the vincristine released from the hydrogel is still biologically active after prolonged hydrogel encapsulation we determined the efficacy of vincris tine to induce cell death in DAOY cells at extended time points The experimental set up mimicked the release study but with an additional interaction step with fresh DAOY cells after long time points of drug release. A negative control of 0.5wt% MAX8 hydrogel without vincristine was run at the same time to establish that the cells were dying from the presence of the drug and not the hydrogel or environment.

Two encapsulated drug concentrations were used to test the sustained drug potency. The first experiment used 10 μmol/L concentration of encapsulated vincris tine to match the concentration used to measure release. This concentration was chosen to match the concentration that was used for the release study in Figure 2.5. The second second experiment used a higher concentration of 500 μmol/L to show a difference in release amounts at the highest possible initial drug concentration due to the limited solubility of vincristine. Figure 2.6 shows a clear increase in cell death for

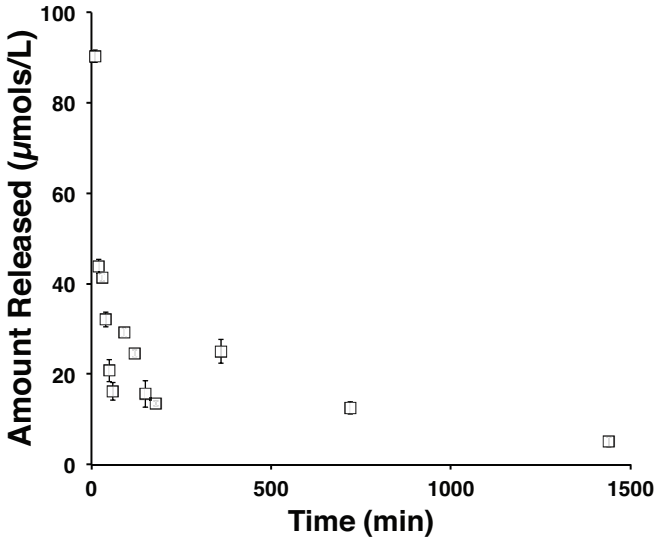

Figure 2.4: UV-Vis Spectroscopy data showing one day of release of 500 μmol/L of vincristine encapsulated in 0.5wt% MAX8 hydrogel using a UV-Vis spectrophotometer. The concentrations measured at the one day time point are hard to resolve by the detctor.

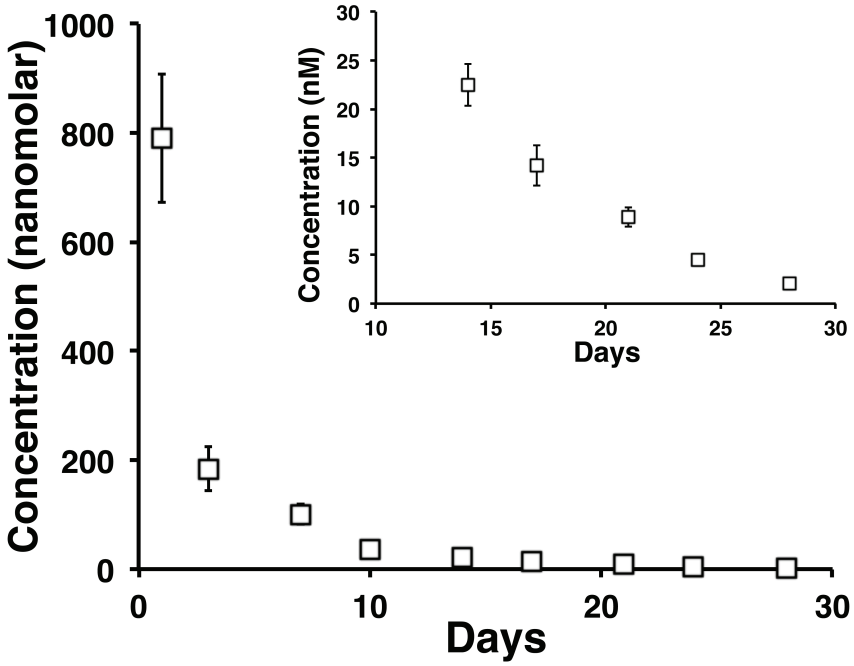

Figure 2.5: 28 day release profile of tritiated vincristine from a 0.5wt% MAX8 peptide hydrogel, using a Liqud Scintillation Counter (LSC), which initially encapsulated 10 μM of tritium (^{3}H) labeled vincristine vincristine. After 28 days of release, the amount of drug being released was still in nanomolar quantities, as seen in the inset which highlights days 14 through 28 of the release study.

Table 2.2: The concentrations of released vincristine for the last two weeks of a month long encapsulation in 0.5wt% MAX8 hydrogel. These time points accompany the inset of Figure 2.5. Even after a month of encapsulation, vincristine continues to be released at effective concentrations.

Time of Release	Concentration (nmol/L)
14 Days	22.5 ± 2.13
17 Days	14.2 ± 2.08
21 Days	8.88 ± 0.980
24 Days	4.48 ± 0.480
28 Days	2.04 ± 0.308

the higher vincristine concentration, confirming that the cell death is a result of the encapsulated vincristine. At first glance, it may seem contrary that the encapsulated vincristine experiment in Figure 2.2b showed higher percentage cell death at 8nmol/L and 40nmol/L, both lower than 10 μmol/L, than in the efficacy study in Figure 2.6. However, the experimental for the two are greatly different. The cell death measured for time 0 in Figure 2.6 is after only an hour of cell exposure to the drug-gel construct, as opposed to Figure 2.2, where the cells were exposed for two days, until the LDH assay was performed. The two days of exposure meant there was an accumulation of released drug that remain within the wells. The later release and efficacy studies were modified to simulate a more realistic environment, closer to an infinite sink.

In Figure 2.6, for both concentrations, cell death is greater in vincristine encapsulated MAX8 than hydrogels without vincristine, even after a month of continuous release in an aqueous environment. The concentration of 2.04 nmol/L ± 0.31 nmol/L released after 28 previous days of release for the 10 μmol/L vincristine encapsulated hydrogel should be sufficient to kill almost half the population of cells according to Figure 2.2a containing direct treatment data. However, as seen in Figure 2.6, the cells dying due to the presence of vincristine is to a lower extent than predicted by Figure 2.2a, implying the vincristine is slightly less effective after 28 days begin encapsulated inside the hydrogel. This indicates that there is a percentage of vincristine that deteriorates

in the aqueous environment, but, more importantly, that there is also a significant percentage of vincristine that remains effective after 28 days of encapsulation. Figure 2.6 shows that the percentage of effective vincristine also increases with increased initial encapsulated drug concentration.

Previous studies of vincristine have shown that very low amounts of vincristine are extremely effective. Tsuruo et al. showed IC_{50} values of less than 2 nmol/L for direct treatment of leukemia cells.[51] However, much higher concentrations, ranging from 1 μmol/L to 100 μmol/L, are used for intravenous treatments because of the poor target specificity of the drug.[50,63,64] Vincristine has a bulk solution half life range of 164 minutes to 32 hours[65,66] within the body due to its hydrophobicity and functionality. These studies have shown these cytotoxic effectiveness of released drug has been protected by the MAX8 hydrogel for longer than what has been measured in the body. In usage, once injected, the vincristine-loaded hydrogel can be relied on to continuously release low but effective concentrations of vincristine to the intended site to treat cancers and other diseases. Chapter 3 uses SANS data to examine overall structure and vincristine location to help in understanding the mechanics of the encapsulation and ultimately, the release from the hydrogel. The efficacy study suggests the vincristine's location within the fibrils. This possible configuration is discussed further in chapter 3. There is clearly some delay of drug exposure to a degrading environment, shielding the vincristine from its surroundings to achieve the high half-life, similar to pro-drugs or time-release drugs.

Attempts to prolong hydrophobic drug half-life in aqueous environments do so by isolating the drug from the environment in a separate hydrophobic area through encapsulation.[67,68] The difference with the MAX8 hydrogel is that there is no distinctly hydrophobic cavity that would offer overall obvious protection. As mentioned earlier, the vincristine is mostly likely shielded by the lysine side chains, providing long-time drug stability. This protection coupled with the continued release of vincristine from the 0.5wt% MAX8 hydrogel further support the use of the drug-hydrogel construct for local and targeted drug delivery to a tumor environment while decreasing the exposure

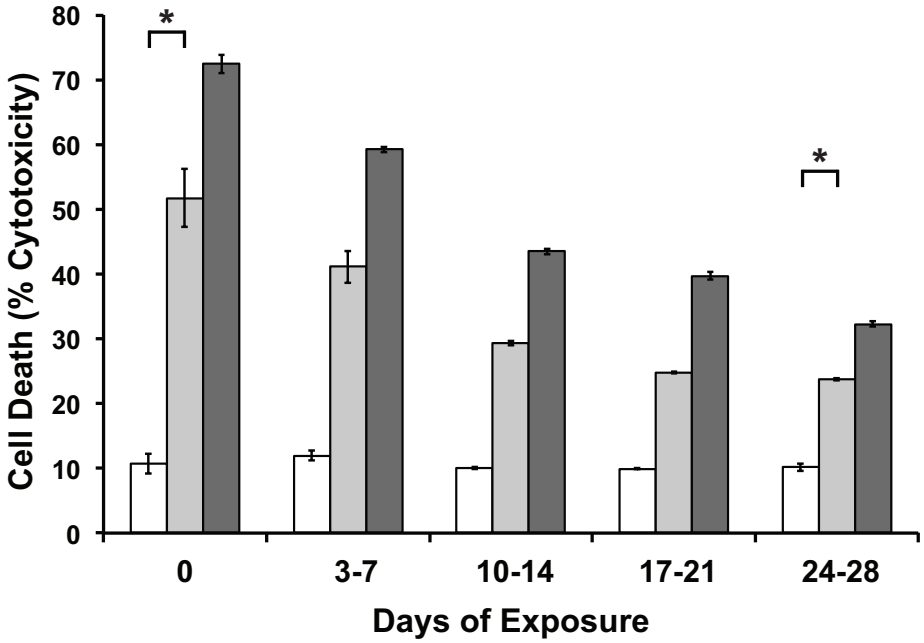

Figure 2.6: A measure of cytoxocity to assess efficacy of released vincristine from 0.5wt% MAX8 hydrogels over 28 days. To ensure efficacy of the drug released from they hydrogel, 0 μmol/L (empty bars), 10 μmol/L (lighter gray bars) and 500 μmol/L (darker gray bars) of vincristine were encapsulated in 0.5wt% MAX8 hydrogels. There is a noticeable difference in the effectiveness of the hydrophobic drug on cells despite encapsulation in an aqueous. DAOY cell death was measured using LDH assays after cells were exposed to the drug-gel constructs in the listed days of release. Day 0 cells were exposed for an hour to drug-gel transwells, then measured two days later. * indicates noted concentrations are significantly different ($p<0.05$).

and effects on healthy tissue.

While direct treatment of cells is prudent in an in vitro setting, during actual cancer treatment other non-cancer cells present in the environment should not be exposed to chemotherapeutics such as vincristine. Current methods of treating cancers with vincristine lead to negative side effects due to the large, systemic dosages required and healthy tissue exposed. These large dosages are needed because of the lack of specific drug targeting. In order to better treat specific regions of the body, such as the site of a newly resected tumor, a specific, local delivery with an injectable solid delivery system using a shear-thinning hydrogel is a viable strategy. This deposition of chemotherapeutic would minimize the need for repeated treatments or intrusions,

Encapsulated vincristine does not affect the shear-thinning and re-healing qualities of MAX8 hydrogel. The drug release and effectiveness of a vincristine-loaded hydrogel was examined. Over the course of one month, the vincristine-encapsulated MAX8 demonstrated continuous release of vincristine at low concentrations. The low, but effective, concentrations of drug release would limit exposure of healthy tissue to the potent drug. The released drug was shown to retain potency for up to one month, well beyond the typical hours-to-days time reported for the drug to degrade in vitro, indicating that the hydrogel encapsulation protects the drug from normal degradation mechanisms. Most importantly, the sustained, continuously released concentrations remained effective against cancer cells while in an aqueous environment during a month of release.

In practice, the sustained release will allow a targeted area to receive treatment continuously over long time periods that will alleviate problems seen in multiple, frequent chemotherapy treatments that are used for systemic treatment today. These multiple treatments expose healthy tissue to vincristine, leading to negative side effects. The shear thinning and immediate re-healing properties of MAX8 hydrogel allows the deposition of the drug-loaded, solid hydrogel directly to a desired injection site. Additionally, the injection would be ideal for post-operative treatment after tumor removal surgeries by depositing the drug-gel construct into the cancer's previous location. The

low dosage and continuous release of the vincristine can target any cancerous cells that may not have been resected as well as preventing the return of any cancer in that area.

2.4 Diffusion Coefficient of Curcumin

To better understand and quantify the release of vincristine from the MAX8 hydrogel, fluorescence recovery after photobleaching (FRAP) was used to measure vincristine's diffusion coefficient. FRAP bleaches a selected area and measures the fluorescence as the area recovers, allowing for brownian motion and diffusion of the targeted molecule to un-bleach the region of interest (ROI). The time taken to recover and the area of the ROI are accounted for in the overall calculation for diffusion coefficient. Before finding the diffusion coefficient of vincristine, FRAP was used to find the diffusion coefficient of curcumin.

While the focus on the chapter is on release of the drug vincristine, encapsulated curcumin was used as a model for setting up release experiments for hydrophobic payloads.[3] Curcumin is a hydrophobic, natural compound derived from the Indian spice turmeric and degrades after 8 hours in water.[69] Altunbas et al. successfully encapsulated and released curcumin from MAX8 over a course of two weeks. Despite the high water content of the MAX8 hydrogel, the continuously-released curcumin remained active and effective after 14 days of encapsulation. To quantify the behavior seen by Altunbas, et al, FRAP experiments were performed on MAX8, using a

Four concentrations of encapsulated curcumin, and three weight percents of MAX8 were used as seen in Table 2.3. Previously Branco et al, used FRAP to measure a neutral dextran probe in different weight percents of MAX1 and MAX8 hydrogels.[2] Because of curcumin's hydrophobic nature and the aqueous environment of the MAX8 hydrogel, the anticipated diffusion coefficients were expected to be much less than the dextran probes.

As seen in Figure 2.7, 80 μmol/L of curcumin was encapsulated in a 0.5wt% MAX8 hydrogel and bleached for FRAP. Here four time points are shown — 0 seconds, 75 seconds - right after bleaching the ROI, 100 seconds - bleached molecules continue

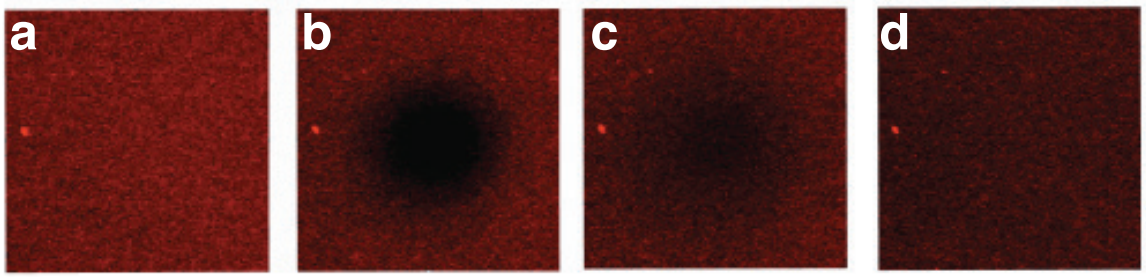

Figure 2.7: Lascer Scanning Confocal Microscopy images of FRAP on 80 μmol/L of curcumin encapsulated in 0.5wt%MAX8 hydrogel at times **a.**) 0 sec, **b.**) 75 sec - once the ROI has been bleached, **c.**) 100 sec, and **d.**) 300 sec - the ROI has recovered from original bleaching.

diffusing, and 300 seconds - when the ROI has recovered from bleaching and diffusion re-distributes the bleached and unbleached molecules. 75 seconds was the required amount of time to effectively photobleach the ROI as seen in Figure 2.7b, showing the clearly bleached ROI. 100 seconds, seen in Figure 2.7c shows the faint blurred outline of the ROI as the bleached molecules continue diffusing through the rest of the sample.In Figure 2.7d, the same ROI no longer is no longer distinguishable from its surrounding area. Noticeably, the fluorescence of the overall area in Figure 2.7d is less than that of Figure 2.7a. This decrease in fluorescence intensity over time comes from the re-distribution of the bleached molecules.

The diffusion coefficient (D) can be obtained from the intensities of the ROI's as seen below:

$$D = \frac{\omega^2}{4\tau_D} \tag{2.1}$$

where ω is the radius of the circular spot and τ_D is the characteristic diffusion time. τ_D is obtained from the normalized fractional fluorescence recovery function $f(t)$:[70]

$$f(t) = 1 - \left(\frac{\tau_D}{t}\right) exp\left(-\frac{2\tau_D}{t}\right)\left[I_0\left(\frac{2\tau_D}{t}\right) + I_1\left(\frac{2\tau_D}{t}\right)\right] + f_0 \tag{2.2}$$

where I_0 and I_2 are modified Bessel functions. The normalized fractional fluorescence

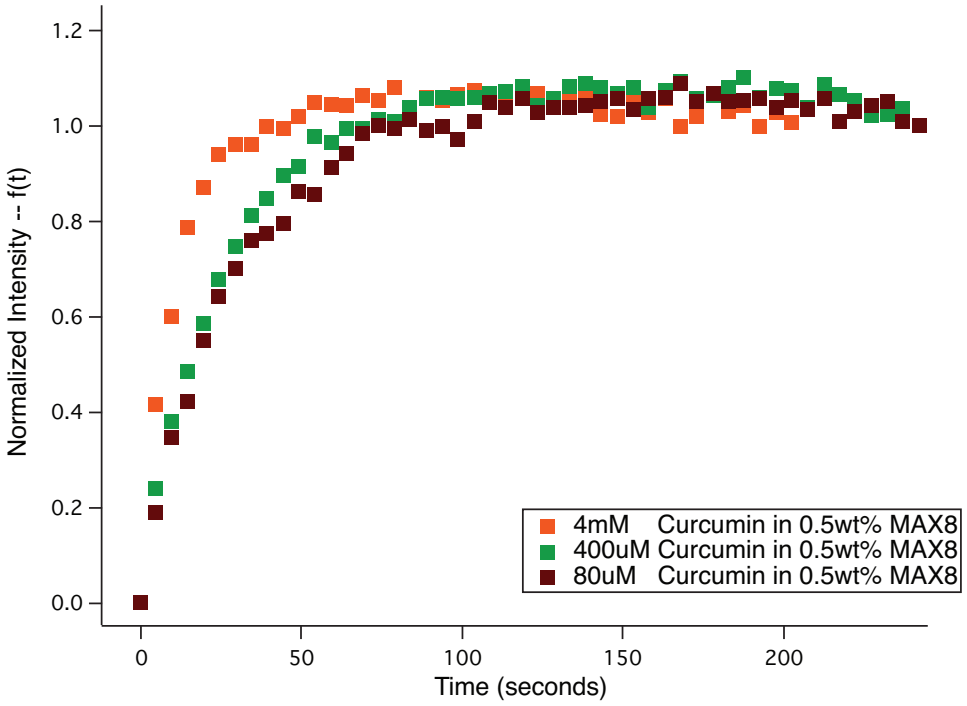

Figure 2.8: The normalized fluorescence recovery curves for three concentrations of curcumin 4mmol/L, 400 μmol/L, and 80 μmol/L encapsulated in 0.5wt% MAX8 hydrogel. These intensities were used to find the diffusion coefficient for each concnetration of curcumin.

function is related to the raw intensities through:

$$f(t) = \frac{F(t) - F_0(t)}{F_\infty - F_0} \tag{2.3}$$

where F_0 is 75 seconds after bleaching, like in Figure 2.7b, F_∞ is 300 seconds after bleaching, as seen in Figure 2.7d. The normalized intensity curves for each of the four concentrations of curcumin and three weight percents of MAX8 resemble those found for three concentrations of curcumin at 0.5wt% MAX8 as seen in Figure 2.8.

The calculated diffusion coefficients for the different weight percent hydrogels and concentrations of curcumin from using the normalized fractional fluorescence recovery are listed in Table 2.3.

The calculated diffusion coefficients show a clear decreasing trend for 4mmol/L and 2mmol/L as weight percent of MAX8 increases. As shown by Branco, the higher

Table 2.3: The diffusion coefficients, 10^{-8} cm^2/sec, show a clear decreasing trend for 4mmol/L and 2mmol/Las weight percent of MAX8 increases. For the more dilute amounts of curcumin, the data does not exhibit a clear trend.

MAX8	**Amount of Curcumin Encapsulated**			
	4 mmol/L	2 mmol/L	400 μmol/L	80 μmol/L
0.5wt%	3.10 ± 2	12.1 ± 7	1.82 ± 0.3	1.74 ± 0.2
1wt%	2.64 ± 0.3	2.29 ± 0.9	7.10 ± 0.5	7.22 ± 0.5
2wt%	—	1.88 ± 0.1	1.10 ± 0.09	7.41 ± 0.5

weight percentage of the hydrogel has smaller pores, due to the increased number of peptides forming branch points and entanglements. Due to the hydrophobic nature of the curcumin, the diffusion coefficients are lower than those of the neu tral dextran probes. This diffusion coefficient trend confirms and supports the diffusion of the cur- cumin molecule, supporting the continuous release observed by Altunbas. For the more dilute amounts of curcumin, the data does not exhibit a clear trend. Whereas FRAP measurements can be performed for curcumin encapsu lated hydrogels, the technique cannot be applied to vincristine encapsulated hydro gels because the fluorescence peak (λ) is outside the detection window of the instrument.

REFERENCES

[1] Lisa A Haines-Butterick, Daphne A Salick, Darrin J Pochan, and Joel P Schneider. In vitro assessment of the pro-inflammatory potential of β-hairpin peptide hydrogels. *Biomaterials*, 29(31):4164–4169, November 2008.

[2] M C Branco, D J Pochan, N J Wagner, and J P Schneider. Macromolecular diffusion and release from self-assembled β-hairpin peptide hydrogels. *Biomaterials*, 2009.

[3] Aysegul Altunbas, Seung J Lee, Sigrid A Rajasekaran, Joel P Schneider, and Darrin J Pochan. Encapsulation of curcumin in self-assembling peptide hydrogels as injectable drug delivery vehicles. *Biomaterials*, 32(25):5906–5914, 2011.

[4] J K Kretsinger, L A Haines, Bulent Ozbas, and D J Pochan. Cytocompatibility of self-assembled β-hairpin peptide hydrogel surfaces. *Biomaterials*, 2005.

[5] Congqi Yan, Michael E Mackay, Kirk Czymmek, Radhika P Nagarkar, Joel P Schneider, and Darrin J Pochan. Injectable Solid Peptide Hydrogel as a Cell Carrier: Effects of Shear Flow on Hydrogels and Cell Payload. *Langmuir*, 28(14):6076–6087, 2012.

[6] Lisa Haines-Butterick, Karthikan Rajagopal, Monica Branco, Daphne A Salick, Ronak Rughani, Matthew Pilarz, Matthew S Lamm, Darrin J Pochan, and Joel P Schneider. Controlling hydrogelation kinetics by peptide design for three-dimensional encapsulation and injectable delivery of cells. *Proceedings Of The National Academy Of Sciences Of The United States Of America*, 104(19):7791–7796, 2007.

[7] Forrest M Kievit and Miqin Zhang. Surface Engineering of Iron Oxide Nanoparticles for Targeted Cancer Therapy. *Accounts of Chemical Research*, 44(10):853–862, April 2011.

[8] Aysegul Altunbas, Nikhil Sharma, Matthew S Lamm, Congqi Yan, Radhika P Nagarkar, Joel P Schneider, and Darrin J Pochan. Peptide–Silica Hybrid Networks: Biomimetic Control of Network Mechanical Behavior. *Acs Nano*, 4(1):181–188, January 2010.

[9] Mahfoud Boustta, Pierre-Emmanuel Colombo, Sébastien Lenglet, Sylvain Poujol, and Michel Vert. Versatile UCST-based thermoresponsive hydrogels for locoregional sustained drug delivery. *Journal of Controlled Release*, 174:1–6, January 2014.

[10] D Zhang, P Sun, P Li, A Xue, X Zhang, H Zhang, and X Jin. A magnetic chitosan hydrogel for sustained and prolonged delivery of Bacillus Calmette–Guérin in the treatment of bladder cancer. *Biomaterials*, 2013.

[11] Jung-Kyo Cho, Ki-Yun Hong, Jung Won Park, Han-Kwang Yang, and Soo-Chang Song. Injectable delivery system of 2-methoxyestradiol for breast cancer therapy using biodegradable thermosensitive poly(organophosphazene) hydrogel. *Journal of Drug Targeting*, 19(4):270–280, May 2011.

[12] F Philipp Seib and David L Kaplan. Doxorubicin-loaded silk films: Drug-silk interactions and in vivo performance in human orthotopic breast cancer. *Biomaterials*, 33(33):8442–8450, 2012.

[13] Jianwei Guo, Xiaoling Gao, Lina Su, Huimin Xia, Guangzhi Gu, Zhiqing Pang, Xinguo Jiang, Lei Yao, Jun Chen, and Hongzhuan Chen. Aptamer-functionalized PEG-PLGA nanoparticles for enhanced anti-glioma drug delivery. *Biomaterials*, 32(31):8010–8020, November 2011.

[14] Rachael Mooney, Yiming Weng, Elizabeth Garcia, Sukhada Bhojane, Leslie Smith-Powell, Seung U Kim, Alexander J Annala, Karen S Aboody, and Jacob M Berlin. Conjugation of pH-responsive nanoparticles to neural stem cells improves intratumoral therapy. *Journal of Controlled Release*, 191:82–89, October 2014.

[15] Xiaoyong Wang and Zijian Guo. Targeting and delivery of platinum-based anticancer drugs. *Chemical Society Reviews*, 42(1):202–224, 2012.

[16] Alexandre Albanese, Peter S Tang, and Warren C W Chan. The Effect of Nanoparticle Size, Shape, and Surface Chemistry on Biological Systems. *Annual review of biomedical engineering*, 14(1):1–16, August 2012.

[17] Mark E Davis, Zhuo Georgia Chen, and Dong M Shin. Nanoparticle therapeutics: an emerging treatment modality for cancer. *Nature Reviews Drug Discovery*, 7(9):771–782, September 2008.

[18] EVAN S GLAZER, CIHUI ZHU, AMIR N HAMIR, AGATHA BORNE, Catherine Shea Thompson, and STEVEN A CURLEY. Biodistribution and acute toxicity of naked gold nanoparticles in a rabbit hepatic tumor model. *Nanotoxicology*, 5(4):459–468, December 2011.

[19] Frank Alexis, Eric Pridgen, Linda K Molnar, and Omid C Farokhzad. Factors Affecting the Clearance and Biodistribution of Polymeric Nanoparticles. *Molecular pharmaceutics*, 5(4):505–515, August 2008.

[20] E Fournier, C Passirani, C N Montero-Menei, and J P Benoit. Biocompatibility of implantable synthetic polymeric drug carriers: focus on brain biocompatibility. *Biomaterials*, 24(19):3311–3331, August 2003.

[21] William H Blackburn, Erin B Dickerson, Michael H Smith, John F McDonald, and L Andrew Lyon. Peptide-functionalized nanogels for targeted siRNA delivery. *Bioconjugate Chemistry*, 20(5):960–968, 2009.

[22] Brian A Aguado, Widya Mulyasasmita, James Su, Kyle J Lampe, and Sarah C Heilshorn. Improving Viability of Stem Cells During Syringe Needle Flow Through the Design of Hydrogel Cell Carriers. *Tissue Engineering Part A*, 18(7-8):806–815, April 2012.

[23] Kyle J Lampe and Sarah C Heilshorn. Building stem cell niches from the molecule up through engineered peptide materials. *Neuroscience letters*, 519(2):138–146, 2012.

[24] Jason A Burdick and Kristi S Anseth. Photoencapsulation of osteoblasts in injectable RGD-modified PEG hydrogels for bone tissue engineering. *Biomaterials*, 23(22):4315–4323, 2002.

[25] Murat Guvendiren, Hoang D Lu, and Jason A Burdick. Shear-thinning hydrogels for biomedical applications. *Soft Matter*, 8(2):260–272, 2011.

[26] Joel H Collier, Bi Huang Hu, Jeffrey W Ruberti, Jerry Zhang, Pochi Shum, David H Thompson, and Phillip B Messersmith. Thermally and Photochemically Triggered Self-Assembly of Peptide Hydrogels. *Journal Of The American Chemical Society*, 123(38):9463–9464, September 2001.

[27] DJ Pochan, JP Schneider, Juliana Kretsinger, Bulent Ozbas, Karthikan Rajagopal, and L Haines. Thermally reversible hydrogels via intramolecular folding and consequent self-assembly of a de Novo designed peptide. *Journal Of The American Chemical Society*, 125(39):11802–11803, 2003.

[28] J H Collier and P B Messersmith. Self-Assembling Polymer–Peptide Conjugates: Nanostructural Tailoring. *Advanced Materials*, 16(11):907–910, June 2004.

[29] Rein V Ulijn and Andrew M Smith. Designing peptide based nanomaterials. *Chemical Society Reviews*, 37(4):664–675, 2008.

[30] Jindrich Kopecek and Jiyuan Yang. Peptide-directed self-assembly of hydrogels. *Acta Biomaterialia*, 5(3):805–816, March 2009.

[31] Derek N Woolfson. Building fibrous biomaterials from alpha-helical and collagen-like coiled-coil peptides. *Biopolymers*, 94(1):118–127, 2010.

[32] Charles J Bowerman and Bradley L Nilsson. Review self-assembly of amphipathic β-sheet peptides: Insights and applications. *Biopolymers*, 98(3):169–184, May 2012.

[33] Charles J Bowerman and Bradley L Nilsson. A Reductive Trigger for Peptide Self-Assembly and Hydrogelation. *Journal Of The American Chemical Society*, 132(28):9526–9527, 2010.

[34] Joel H Collier and Tatiana Segura. Evolving the use of peptides as components of biomaterials. *Biomaterials*, 32(18):4198–4204, June 2011.

[35] Jindrich Kopecek and Jiyuan Yang. Smart Self-Assembled Hybrid Hydrogel Biomaterials. *Angewandte Chemie International Edition*, 51(30):7396–7417, 2012.

[36] Taco Nicolai and Dominique Durand. Controlled food protein aggregation for new functionality. *Current Opinion in Colloid & Interface Science*, 18(4):249–256, 2013.

[37] Derek M Ryan and Bradley L Nilsson. Self-assembled amino acids and dipeptides as noncovalent hydrogels for tissue engineering. *Self-assembled amino acids and dipeptides as noncovalent hydrogels for tissue engineering*, 3(1):18, 2011.

[38] Ananth K Vellimana, Violette Renard Recinos, Lee Hwang, Kirk D Fowers, Khan W Li, Yonggang Zhang, Saint Okonma, Charles G Eberhart, Henry Brem, and Betty M Tyler. Combination of paclitaxel thermal gel depot with temozolomide and radiotherapy significantly prolongs survival in an experimental rodent glioma model. *Journal of neuro-oncology*, 111(3):229–236, December 2012.

[39] Nipun Babu Varukattu and Soundarapandian Kannan. Enhanced Delivery of baisalein using cinnamaldehyde cross-linked chitosan nanoparticle inducing apoptosis. *International Journal of Biological Macromolecules*, 2012.

[40] Nancy L Elstad and Kirk D Fowers. OncoGel (ReGel/paclitaxel) — Clinical applications for a novel paclitaxel delivery system. *Advanced Drug Delivery Reviews*, 61(10):785–794, August 2009.

[41] Lorena Tavano, Marco Vivacqua, Valentina Carito, Rita Muzzalupo, Maria Cristina Caroleo, and Fiore Nicoletta. Doxorubicin loaded magnetoniosomes for targeted drug delivery. *Colloids And Surfaces B-Biointerfaces*, 102:803–807, February 2013.

[42] Cyril Lorenzato, Alexandru Cernicanu, Marie Edith Meyre, Matthieu Germain, Agnès Pottier, Laurent Levy, Baudouin Denis Senneville, Clemens Bos, Chrit Moonen, and Pierre Smirnov. MRI contrast variation of thermosensitive magnetoliposomes triggered by focused ultrasound: a tool for image-guided local drug delivery. *Contrast Media & Molecular Imaging*, 8(2):185–192, March 2013.

[43] Karthikan Rajagopal, Matthew S Lamm, Lisa A Haines-Butterick, Darrin J Pochan, and Joel P Schneider. Tuning the pH Responsiveness of beta-Hairpin Peptide Folding, Self-Assembly, and Hydrogel Material Formation. *Biomacromolecules*, 10(9):2619–2625, 2009.

[44] Bulent Ozbas, Juliana Kretsinger, Karthikan Rajagopal, Joel P Schneider, and Darrin J Pochan. Salt-triggered peptide folding and consequent self-assembly into hydrogels with tunable modulus. . . . , 2004.

[45] JP Schneider, DJ Pochan, Bulent Ozbas, Karthikan Rajagopal, L Pakstis, and Juliana Kretsinger. Responsive hydrogels from the intramolecular folding and self-assembly of a designed peptide. *Journal Of The American Chemical Society*, 124(50):15030–15037, 2002.

[46] Lisa A Haines, Karthikan Rajagopal, Bulent Ozbas, Daphne A Salick, Darrin J Pochan, and Joel P Schneider. Light-activated hydrogel formation via the triggered folding and self-assembly of a designed peptide. *Journal Of The American Chemical Society*, 127(48):17025–17029, 2005.

[47] T J Smith, J Khatcheressian, G H Lyman, H Ozer, J O Armitage, L Balducci, C L Bennett, S B Cantor, J Crawford, and S J Cross. 2006 update of recommendations for the use of white blood cell growth factors: an evidence-based clinical practice guideline. *Journal of Clinical Oncology*, 24(19):3187–3205, 2006.

[48] Paul P Carbone, Vincent Bono, Emil Frei, and Brindley Clyde O. Clinical studies with vincristine. *Blood*, 21(5):640–647, 1963.

[49] Bertrand Coiffier, Eric Lepage, Josette Brière, Raoul Herbrecht, Hervé Tilly, Reda Bouabdallah, Pierre Morel, Eric Van Den Neste, Gilles Salles, Philippe Gaulard, Felix Reyes, Pierre Lederlin, and Christian Gisselbrecht. CHOP Chemotherapy plus Rituximab Compared with CHOP Alone in Elderly Patients with Diffuse Large-B-Cell Lymphoma. *New England Journal of Medicine*, 346(4):235–242, January 2002.

[50] Marinus van Oers, Richard Klasa, Robert E Marcus, Max Wolf, Eva Kimby, Randy D Gascoyone, Andrew Jack, Mars van't Veer, Andrej Vranovsky, Harald Holte, Martine von Glabbeke, Ivana Teodorovic, Cynthia Rozewicz, and Anton Hagenbeek. Rituximab maintenance improves clinical outcome of relapsed/resistant follicular non-Hodgkin lymphoma in patients both with and without rituximab during induction: results of a prospective randomized phase 3 intergroup trial. *Blood*, 2006.

[51] T Tsuruo, H Iida, S Tsukagoshi, and Y Sakurai. Overcoming of vincristine resistance in P388 leukemia in vivo and in vitro through enhanced cytotoxicity of vincristine and vinblastine by verapamil. *Cancer research*, 41(5):1967–1972, May 1981.

[52] J P Fermand, P Ravaud, S Chevret, M Divine, V Leblond, C Belanger, M Macro, E Pertuiset, F Dreyfus, X Mariette, C Boccacio, and J C Brouet. High-dose therapy and autologous peripheral blood stem cell transplantation in multiple myeloma: up-front or rescue treatment? Results of a multicenter sequential randomized clinical trial. *Blood*, 92(9):3131–3136, November 1998.

[53] Ben Shofty, Michal Mauda Havakuk, Lior Weizman, Shlomi Constantini, Dafna Ben Bashat, Rina Dvir, Li Tal Pratt, Leo Joskowicz, Anat Kesler, Michal Yalon, Lior Ravid, and Liat Ben Sira. The effect of chemotherapy on optic pathway gliomas and their sub-components: A volumetric MR analysis study. *Pediatric Blood & Cancer*, 62(8):1353–1359, August 2015.

[54] Murali Chintagumpala, Sandrah P Eckel, Mark Krailo, Michael Morris, Adekunle Adesina, Roger Packer, Ching Lau, and Amar Gajjar. A pilot study using carboplatin, vincristine, and temozolomide in children with progressive/symptomatic low-grade glioma: a Children's Oncology Group study†. *Neuro-oncology*, 17(8):1132–1138, August 2015.

[55] Guilio J D'Angio, Norman Breslow, J Bruce Beckwith, Audrey Evans, Edward Baum, Alfred deLorimier, Donald Fernbach, Ellen Hrabovsky, Barabara Jones, Panayotis Kelalis, H Biemann Otherson, Melvin Tefft, and Patrick R M Thomas. Treatment of Wilms' tumor. Results of the Third National Wilms' Tumor Study. *Cancer*, 64(2):349–360, July 1989.

[56] Alastair Spira and David S Ettinger. Multidisciplinary Management of Lung Cancer. *New England Journal of Medicine*, 350(4):379–392, January 2004.

[57] Ehsan Aboutaleb, Fatemeh Atyabi, Mohammad Reza Khoshayand, Ali Reza Vatanara, Seyed Nasser Ostad, Farzad Kobarfard, and Rassoul Dinarvand. Improved brain delivery of vincristine using dextran sulfate complex solid lipid nanoparticles: Optimization and in vivo evaluation. *Journal of Biomedical Materials Research Part A*, 2013.

[58] A Jordan, J A Hadfield, N J Lawrence, and A T McGown. Tubulin as a target for anticancer drugs: agents which interact with the mitotic spindle. *Medicinal research reviews*, 18(4):259–296, 1998.

[59] Benoît Gigant, Chunguang Wang, Raimond B G Ravelli, Fanny Roussi, Michel O Steinmetz, Patrick A Curmi, André Sobel, and Marcel Knossow. Structural basis for the regulation of tubulin by vinblastine. *Nature*, 435(7041):519–522, May 2005.

[60] Francis G Mussatti and Christopher W Macosko. Rheology of network forming systems. *Polymer Engineering & Science*, 13(3):236–240, May 1973.

[61] Congqi Yan, Aysegul Altunbas, Tuna Yucel, Radhika P Nagarkar, Joel P Schneider, and Darrin J Pochan. Injectable solid hydrogel: mechanism of shear-thinning and immediate recovery of injectable β-hairpin peptide hydrogels. *Soft Matter*, 6(20):5143–5156, October 2010.

[62] Sameer Sathaye. *Multifunctional Hybrid Networks Based on Self Assembling Peptide Sequences*. PhD thesis, June 2014.

[63] Richard I Fisher, Ellen R Gaynor, Steve Dahlberg, Martin M Oken, Thomas M Grogan, Evonne M Mize, John H Glick, Charles A Coltman Jr., and Thomas P Miller. Comparison of a Standard Regimen (CHOP) with Three Intensive Chemotherapy Regimens for Advanced Non-Hodgkin's Lymphoma. *New England Journal of Medicine*, 328(14):1002–1006, April 1993.

[64] D L Longo, V T DeVita Jr, P L Duffey, M N Wesley, D C Ihde, S M Hubbard, M Gilliom, E S Jaffe, J Cossman, and R I Fisher. Superiority of ProMACE-CytaBOM over ProMACE-MOPP in the treatment of advanced diffuse aggressive lymphoma: results of a prospective randomized trial. *Journal of Clinical Oncology*, 9(1):25–38.

[65] V Sagar Sethi, Don V Jackson, Douglas R White, Frederick Richards, John J Stuart, Hyman B Muss, M Robert Cooper, and Charles L Spurr. Pharmacokinetics

of vincristine sulfate in adult cancer patients. *Cancer research*, 41(9 Part 1):3551–3555, 1981.

[66] V Sagar Sethi and Kuntebommanahalli N Thimmaiah. Structural studies on the degradation products of vincristine dihydrogen sulfate. *Cancer research*, 45(11 Part 1):5386–5389, 1985.

[67] Maria Coimbra, Benedetta Isacchi, Louis van Bloois, Javier Sastre Torano, Aldo Ket, Xiaojie Wu, Femke Broere, Josbert M Metselaar, Cristianne J F Rijcken, Gert Storm, Rita Bilia, and Raymond M Schiffelers. Improving solubility and chemical stability of natural compounds for medicinal use by incorporation into liposomes. *International journal of pharmaceutics*, 416(2):433–442, September 2011.

[68] Indrajit Ghosh and Werner M Nau. The strategic use of supramolecular pKa shifts to enhance the bioavailability of drugs. *Advanced Drug Delivery Reviews*, 64(9):764–783, June 2012.

[69] V Basile, E Ferrari, S Lazzari, S Belluti, F Pignedoli, and C Imbriano. Curcumin derivatives: molecular basis of their anti-cancer activity. *Biochemical pharmacology*, 78(10):1305–1315, 2009.

[70] D Axelrod, D E Koppel, J Schlessinger, E Elson, and W W Webb. Mobility Measurement by Analysis of Fluorescence Photobleaching Recovery Kinetics. *Biophysical Journal*, 16(9):1055–1069, 1976.

Chapter 3

STRUCTURAL CHARACTERIZATION OF MAX8 AND ADDITIONAL GELS

Chapter 2 examined the release of vincristine from the MAX8 hydrogel and the resultant drug characteristics within the hydrogel. Chapter 3 looks more closely at the relationship between vincristine and the peptide network through small-angle neutron scattering (SANS). Using SANS, Chapter 3 investigates the location of vincristine and how it is incorporated into the network structure. Understanding this relationship would explain how vincristine can retain its hydrophobic properties and remain active, despite the long term encapsulation in an aqueous environment. Finally, Chapter 3 concludes with an investigation of a separate class of gels through a collaborative project with the Johnson group using neutron scattering.

3.1 Small-Angle Neutron Scattering of Peptidic Hydrogels

SANS is a technique for structure characterization of materials that analyzes the coherent scattering cross section of a sample. The scattering of neutrons is due primarily to nuclear interactions between incident neutrons and nucleons within the material, though they can also interact with unpaired electrons. The sample itself can be a solid, crystal, powder, or solution.

SANS is non-invasive, unlike small-angle X-ray scattering (SAXS), and will not heat, burn, or ionize samples. This trait is particularly desirable for more carbon heavy systems such as polymers. Additionally, the range of SANS detection is from nanometers to hundreds of nanometers, relevant for many polymer systems, both from basic structure components to larger network structures.

While traditional transmission electron microscopy (TEM) can be useful for visualizing structure at the desired length scale, the sample preparation of drying out the sample can distort or cause artificial structures. Radii or fibril lengths found for a desiccated sample may be less than those in solution. Cryogenic TEM can sometimes alleviate these effects but it is not always suitable or feasible. Dynamic light scattering (DLS) can evaluate samples in solution, but DLS cannot examine structure below the surface. Also, DLS has difficulties with non-uniformly sized or shaped samples. For many polymer samples, SANS is the best technique candidate for quantifying and identifying nanoscale and mesoscopic structures.

Polymer samples of varying degrees of structural order or complexity have all benefitted from SANS for analysis. Starting with systems that exhibit more defined structures, block copolymers have been known to microphase separate into different ordered phases, depending on sample environment or preparation.[1] Using SANS, various groups have been able to accurately identify what phases or structures are formed by block copolymer systems (*e.g.* lamellae, cylinders, micelles).[2–7] SANS experiments were able to also quantify the phase characteristics, finding radius of gyration or fibril length.

Another advantage of SANS is the ability to contrast match features, isolating a desired scattering profile. Explained later on, hydrogen and deuterium have greatly different scattering length densities (SLD). By mixing water and deuterium oxide in different ratios, the scattering cross section of the mixture could match a feature so that it becomes part of the background, allowing any not matched structures to scatter and exhibit an intensity curve. For example, when using SANS for block copolymer micelles, to identify the core radius, the corona can be contrast matched so that it does not have a scattering profile, isolating the core.

Besides block copolymers, SANS is useful for many polymer systems, including those with distinct individual structures such as Tetra-Poly(ethylene gylcol)(Tetra-PEG)[8], monoclonal antibodies[9], or polypeptides[10]. SANS can also be used to better understand microstructure and greater network behavior. SANS is powerful enough to

calculate fibril definitions while also quantifying the mesh size of the overall network, structures often seen in polymeric or protein hydrogels.[11–20] Even for less organized systems, SANS is a powerful tool that provides important information, such as membranes whether from lipids[21,22] or ionomers[23]

Particularly for MAX8 and the MAX family of gels, the detectable size range of SANS is ideal for understanding the structure the encapsulated payload. Previously, Yucel[17], Yan[18], Hule[19], and Sathaye's thesis work[24] have all examined MAX1 or MAX8 peptides with SANS to determine the structure of the hydrogels. The model that best describes the MAX scattering patterns uses a combination of the cylinder fit and the power law. The cylinder model fits and quantifies the fibrils while the power law helps describe the greater fibrillar network.

3.2 Small-Angle Neutron Scattering Theory

Neutrons are highly penetrating and weakly interacting. While non-destructive, neutron measurements require a greater number of neutrons than x-rays due to the lower flux of neutrons compared to even laboratory x-ray sources. The scattering time is dependent on neutron flux, instrument configuration, and the mass of the sample being measured. Samples are typically loaded into cells with 1 mm thickness and 1 cm diameter.

Unlike small-angle x-ray scattering (SAXS), the scattering cross-section is not easily predictable based on the material used. X-ray scattering uses photons that interact with the electron cloud. The expected SAXS scattering cross-sections for materials can be predicted by atomic number of elements present, which dictates the size of the electron cloud. The larger the electron cloud, the larger the scattering cross-section.

Neutrons have a mass, spin, and magnetic moment, all of which contribute to the nuclear interaction between the directed neutron beam and the sample nuclei or magnetic momentum of unpaired electrons (for magnetic samples). Unlike electron clouds, which are predictable in size based on atomic number, the nucleus makeup of

a sample is dependent on isotope and is not easily predictable. Therefore, scattering cross-sections for SANS are not easily predicted on the basis of the elements present. One example of this major difference is the comparison of the scattering length densities (SLD) for elemental hydrogen (^{1}H) versus deuterium(^{2}H or D). The nuclei compositions of the two isotopes are different, but their electron clouds are not. In SAXS, this would result in the exact same scattering but in SANS the scattering lengths for hydrogen is -3.74$\times10^{-5}\mathring{A}$ and for deuterium is 6.67x$10^{-5}\mathring{A}$. Because of the variation of X-ray scattering cross sections, X-ray techniques are more informative or fitting for higher atomic number samples. SANS may be able to provide more information for samples with high hydrogen content as compared to SAXS. Additionally, the stark difference between the scattering lengths of hydrogen and deuterium can be used to adjust the SLD by combining deuterium and hydrogen, accentuating structure features of interest.

When scattering, the coherent macroscopic cross section or scattering intensity in absolute scale is:

$$I(q) = \frac{d\Sigma}{d\Omega}(q) = \frac{N}{V}(\rho_1 - \rho_1)^2 {V_p}^2 P(q) S(q) \tag{3.1}$$

where $S(q)$ is the inter-particle structure factor and $P(q)$ is the single particle form factor. Here, ρ_1 and ρ_2 are scattering length densities, $\frac{N}{V}$ is the number density of the sample and V_p is the sample particle volume. Additionally, the incoherent scattering cross section is Q-independent and therefore a constant background added to the coherent scattering. The incoherent scattering scattering profile comes mostly from hydrogen scattering in the sample.

If the solution is dilute and there are no inter-particle interactions, $S(q)$, is assumed to be one. Otherwise, the isotropic solution structure factor is seen as:

$$S(q) = 1 + 4\pi N_p \int_0^\infty [g(r) - 1] \frac{\sin(qr)}{qr} r^2 dr \tag{3.2}$$

where $g(r)$ is the pair correlation function for the interparticle scattering objects. The potential energy function describing the interparticle relationship is directly related to

$\ln g(r)$. In theory, using Fourier inversion on $S(q)$ should be able to calculate $g(r)$. In practice, there are are approximate forms of $S(q)$ developed for model fitting.

All SANS measurements were performed at the National Institute of Standards and Technology (NIST) Center for Neutron Research (NCNR) (Gaithersburg, MD, USA). Experiments were performed on the NGB 30m SANS instrument. All collected data were reduced and analyzed using the SANS macros package provided by the NCNR[25]. The scattered neutron intensity was measured as a function of scattering variable q, where q=$(4\pi/\lambda)$ $\sin(\theta/2)$ and θ is the scattering angle. The beam was monochromated to a wavelength, λ, of 6 $\mathring{A}$. Three sample-to-detector distances of 1m, 4m, and 13m were used to cover a total q range of 0.004 to 0.5 $\mathring{A}^{-1}$. Titanium sample cells with a 1 mm path length were loaded with 400μL of each sample. The resulting data were placed on an absolute scale and corrected for background electronic noise, detector inhomogeneity, and empty cell scattering using standard techniques.

3.3 MAX8 Hydrogels

3.3.1 MAX8 and Vincristine

Chapter 2 characterized the released vincristine, showing that the hydrophobic vincristine released is still active despite the aqueous environment. To better understand how vincristine interacts with the MAX8 hydrogel network, SANS experiments were performed so analyze the structures within the hydrogel.

During the vincristine release experiments in Chapter 2, the rheometry data shown in Figure 2.1 indicated there were no noticeable differences in hydrogelation behavior or overall stiffness. This implies that the vincristine's presence does not affect the overall hydrogel network itself. If the fibrils had more branching points or fewer entanglements from due to the presence of vincristine, it would impact hydrogelation kinetics and the complex modulus for the vincristine encapsulated hydrogels.

Because the rheometry measurements cannot determinethe location of the vincristine within the network, SANS measurements are necessary to probe the bulk nanostructure of the MAX8 hydrogels. In particular, SANS has the ability to determine if

vincristine alters the fibrillar nanostructure and clarify where the drug is located within the nanostructure of the network.

Figure 3.1 shows the scattering profile of 0.5wt% MAX8 hydrogel with 500 μM vincristine (shaded squares) and without (open squares). The scattering intensity, $I(q)$, as a function of scattering variable, q, gives information o the sample structure over hundreds of nanometers. measurement determines sample structure, giving information in the length scale of nanometers to hundreds of nanometers. The presence of the vincristine does not alter significantly the overall shape and intensity, implying that the hydrogel structure is practically identical in both cases. The SANS results reveal that when encapsulated, there are three configurations for the drug in the overall hydrogel network: a.) evenly integrated along the fibrils, b.) in aggregated vincristine clusters with as little exposure to the surrounding aqueous environment or c.) mostly uniformly distributed through the entire network unassociated with the network completely.

It is possible the vincristine domains would both scatter as individual particles of polydisperse size and shape due to the large hydrogen content within the drug molecules and could display interparticle correlations due to their presence throughout the gel network. Both of these effects would significantly increase intensity at lower q regions of the graph. The lack of a significant difference in overall curve shape for low and mid q scattering, in both intensity and slope, confirms that there are no size differences in the morphology of the hydrogel networks with or without vincristine. While not significant enough to change the curve shape, there is a definite, albeit slight, increase in intensity within the mid-q range, associated with the nanofibrillar characteristics of the overall hydrogel.In particular the similar slope of the two curves implies that the large fibrillar network has the same structure both with and without vincristine present. A slight increase in the scattering intensity is observed when vincristine is present in the system($q > 0.03$ Å^{-1}),however, this is likely due to an increase in the incoherent scattering cross section from the additional hydrogen atoms in the vincristine molecules.

The rheology shown in Figure 2.1 shows that the storage moduli are the same

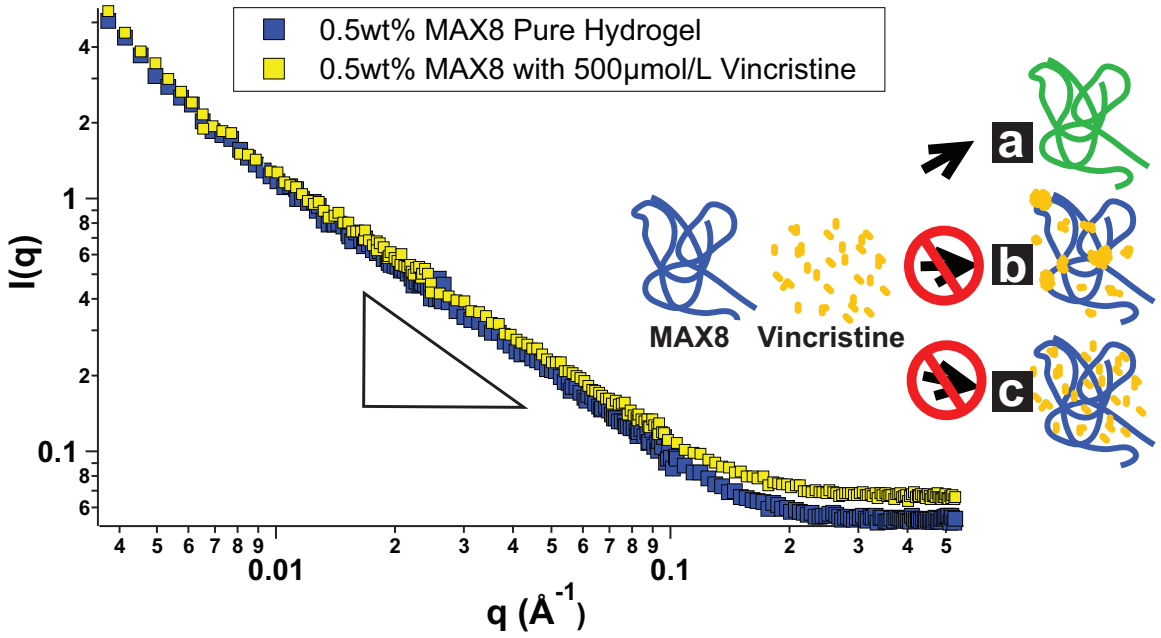

Figure 3.1: Small-angle neutron scattering from 0.5 wt% MAX8 hydrogels with 500μM vincristine (yellow) and without (blue) as a function of scattering variable q. Both lines have a similar overall shape and slope throughout the measured q range, implying that the presence of vincristine does not alter the structure of the MAX8 gel or the intramolecular folding of individual MAX8 chains. The measured slopes for the mid-q region are 0.922 and 0.948, for hydrogels with and without 500μM of vincristine respectively. The cartoon inset shows the possible drug-gel configurations, **a.)** green fibrils indicating the yellow vincristine bound to the blue MAX8 fibrils, **b.)** domains of yellow vincristine mostly at the branch and entanglement points, or **c.)** yellow vincristine evenly scattered throughout the MAX8 network. Only **(a.)** is supported by the scattering curve.

with or without drug, indicating no fibrillar disruption or gel network differences, suggesting that the vincristine is not within the fibrils. Another way of confirming the presence of fibrils, is to measure the slope in the mid-q range of a SANS scattering measurement. A slope around -1 in this range is indicative of nanofibrillar structure. In this case, as seen in Figure 3.1, the slope was measured in the q-range of 0.015 to 0.05. For hydrogels with and without 500μM of vincristine the slope was 0.922 and 0.948 respectively, both close to one, indicating preservation of nanofibrillar structure.

Most likely, the vincristine evenly incorporates itself around the outside of the fibrils, perhaps buried within the hydrophobic lysine side chains[26]. A third possibility of vincristine freely moving throughout the entire network is discounted because of the lack of change in intensity of the scattering. Furthermore, during the release studies shown in Figure 2.5, the infinite sink setup would cause a concentration gradient that would release most of the vincristine before the final time point. If vincristine was unassociated with the fibrillar network and freely soluble in the buffer background, the intensity of the hydrogel-drug sample curve would be less than the pure hydrogel at low and mid q due to the presence of the hydrogenated drug compounds floating freely in solution and lowering the contrast between the peptide fibrils and the deuterated solvent.

3.3.2 Vincristine Encapsulated MAX8 Over Time

As seen in Figure 3.1, the network structure of MAX8 with and without vincristine does not greatly change. The greatest difference is the noticeable increase in background is due to the increased hydrogen presence of vincristine. Rheometry and the similarity in scattering profile suggest the vincristine is not interfering with or located around branch points and entanglements. The slight difference in slope may imply that the vincristine is embedded uniformly along the fibrils. The presence of large domains, although dilute, may create enough contrast to influence the shape, not just the slope of the scattering curves. As vincristine is released from the hydrogel, if

the vincristine is incorporated with the fibers, the contrasting SLD of vincristine could show a change in the scattering curves.

The next experiment examines vincristine encapsulated MAX8 hydrogels remaining in the same environment for 10 days. There is no release of the vincristine into a sink or diffusion gradient. If in fact, the vincristine were in large domains, it would be protecting the hydrophobic drug by reducing overall surface area exposure to the aqueous environment. Over the course of 10 days, if there were large domains of vincristine, the domains would break and diffusion within the hydrogel, resulting in a change in the shape or intensity of the scattering curve. Similar to the samples of Figure 3.1, these long term hydrogels were immediately deposited into the titanium sample cells after self-assembly. As in Figure 3.1, the Day 0 samples were measured on the same day as assembly into the sample cells. Afterwards, the sample cells were placed aside and undisturbed for 10 days, where both samples were run again.

The 10 day time course can be seen in Figure 3.2, showing the scattering for the MAX8 hydrogels with and without vincristine at days 0 and 10. Unlike in Figure 3.1, there is a major difference in slope between hydrogels with and without vincristine. This is most likely an error from how the hydrogel was made, as a later set up with the same concentration of vincristine encapsulated (Figure 3.3) shows the curves with very similar slopes at the mid-q range. While the slopes are different, the overall shape of the curve still suggests a uniform fibrillar network.

The most important difference of the time course samples is the increase in background. The hydrogels were not disturbed over 10 days in a sealed sample cell. Most likely, the increase in background comes from an increase of hydrogen in the envrionment. The hydrogen exchanges with the deuterium, changing the overall scattering cross section, increasing the scattering intensity. The exchange occurs, despite the sealed environment, and happens for both samples. The average background (high q) $I(q)$ at Day 0 and Day 10 for both hydrogels and the intensity increase can be seen in Table 3.1. The increase in background for both samples were similar. While vincristine has the higher overall background for both time points due to the increased

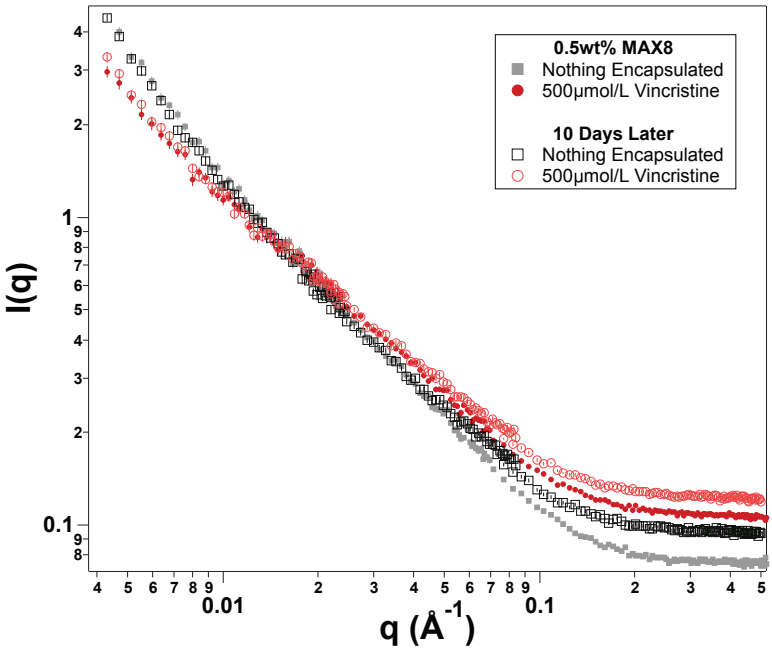

Figure 3.2: Comparison of 0.5wt% MAX8 hydrogels with and without 500μmol/L of vincristine at assembly and 10 days after sitting in the same sample cell, without release or change in environment.

hydrogen content of vincristine, MAX8 has a greater increase in hydrogen content over time.

Table 3.1: Average of background intensities for each 0.5wt% MAX8 hydrogel with and without vincristine at Day 0 and Day 10 and the resultant increase in background intensity from Day 0 to Day 10.

0.5wt% MAX8 Hydrogel	**Day 0** $I(q)$	**Day 10** $I(q)$	**Difference**
0μmol/L Vincristine	.0754	.0953	.0199
500μmol/L Vincristine	.106	.123	.0172

While between MAX8 hydrogels with and without vincristine, there is a difference in the scattering curve at a lower q range. For each individual hydrogel, there were no changes in low and mid-q regions between Day 0 and Day 10. This further supports vincristine is not in large domains, unattached to the fibrils. If vincristine were in clumps or domains, it would diffuse and decrease in size, changing the shape of the scattering curve.

3.3.3 Release of Vincristine from MAX8

The last SANS measurement conducted was a time course of vincristine release from the MAX8 hydrogel The hydrogel structure is examined at days 7 and 10 of release. As in Chapter 2, the vincristine encapsulated hydrogels are formed and placed in a transwell insert and moved to a fresh well at the same time points referenced in section 2.2.8. In order to have enough sample for SANS, four hydrogel setups were needed for each time point. When loading the sample cell, each hydrogel was collected from the insert and placed into the sample cell. After realizing the amount of hydrogen that is exchanged even in a sealed environment from the previous experiment, each 24 well plate was sealed with parafilm and packed into an airtight bag. The day 0 time point for the drug encapsulated hydrogel is not assembled and immediately added to a sample cell. To best mimic the release studies performed in Chapter 2, the day 0 time point also has four gels made and deposited into transwells. These four gels are washed to remove any unencapsulated drug, as described in chapter2, and then collected from each and placed into the sample cell.

Figure 3.3a shows the the scattering curves for the 10 days of vincristine release from the MAX8 hydrogel. Despite best efforts to prevent hydrogen exchange, the increase in background (high-q, $q > 0.3$-q) intensities are still noticeable for days 7 and 10. As background intensities increased, the overall intensity in lower q regions decreased over days of release. The decrease of intensity could be the result of an overall contrast change or a loss of material. While the scattering curve shapes for day 7 and day 10 are still indicative of fibrils present, the slopes of day 7 and day 10 at low-q are different than when vincristine is first encapsulated suggesting there may be a change in the greater overall network. This effect of release over time could be from vincristine's attachment to the MAX8 during encapsulation, supporting the hypothesis of vincristine uniformly associated along the hydrogel's fibrils.

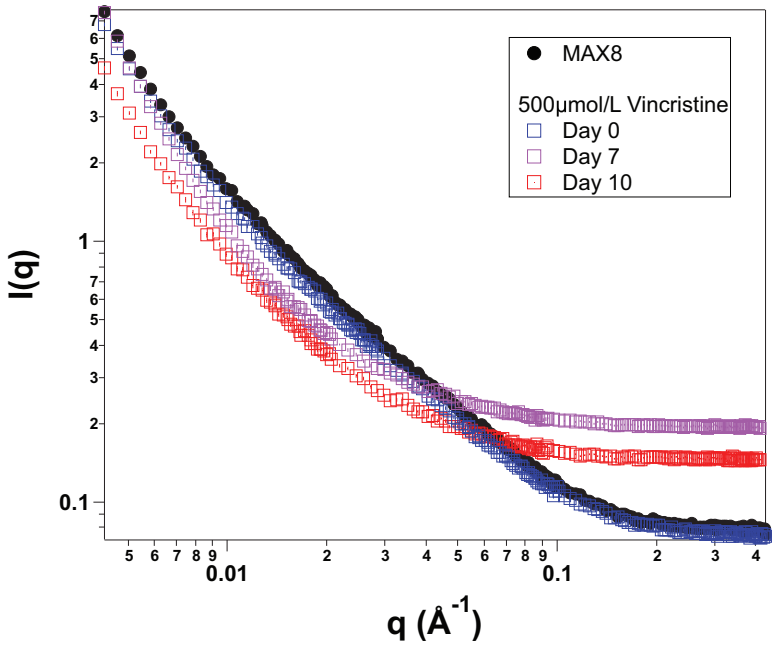

Figure 3.3: SANS of a 10 day release of 500μmol/L vincristine from 0.5wt% MAX8.

3.3.4 MAX8 and Cisplatin

Another approach to understanding how the payload interacts with the fibrillar network and where it is located, was to replace vincristine with a different drug, cisplatin. Cisplatin, another hydrophobic chemotherapeutic, was encapsulated in 0.5wt% MAX8 hydrogels. Three concentrations of cisplatin were encapsulated in 0.5wt%MAX8 as seen in Figure 3.4. The curves of the three concentrations of cisplatin encapsulated in MAX8 hydrogel have a similar shape as MAX8 hydrogel alone. Unlike the vincristine scattering, there is no increase in background intensity because cisplatin has 6 total hydrogens compared to vincristine's 56 hydrogens. The 500μmol/L cisplatin encapsulated hydrogel has the exact same slope as MAX8 alone, while the lowest encapsulated concentrations share similarities. This difference could be from how the hydrogels were assembled, and show that the fibrillar network of MAX8 is not disrupted by the presence of cisplatin.

Similar to the time course of Figure 3.2, 500μmol/L cisplatin encapsulated MAX8 hydrogel was set aside for 10 days to allow for diffusion of cisplatin within

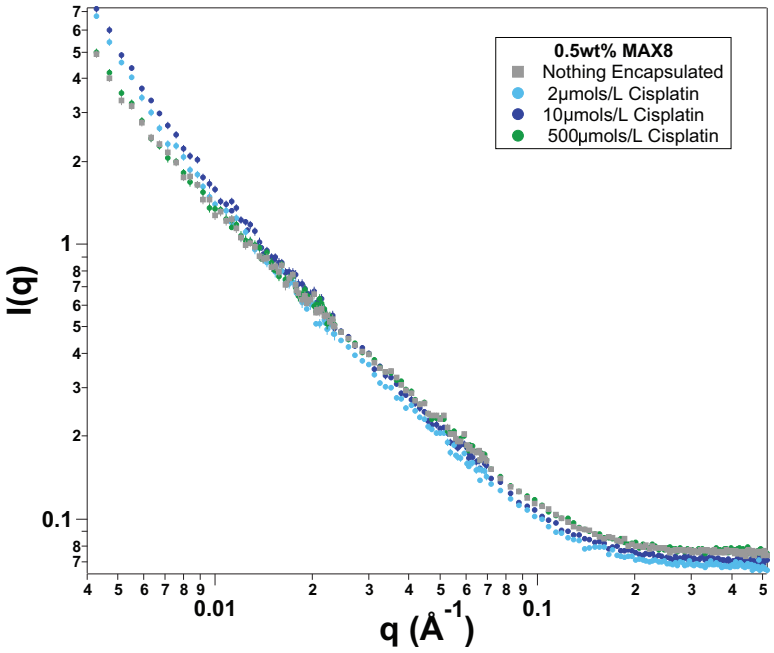

Figure 3.4: Three concentrations of cisplatin are encapsulated in MAX8, showing similar scattering patterns through most of mid–q and high-q. There is some difference in the low-q, indicating the presence of cisplatin may cause possible changes to the network.

the sample cell. SANS for 0.5wt% MAX8 hydrogel with and without 500μmol/L cisplatin was measured, set aside for 10 days and then measured again, as seen in Figure 3.5. The scattering curves show no change in slope or shape. Additionally, the same background intensity increase implies the same amount of hydrogen exchange for both samples, despite sealed sample cells. Figure 3.5 supports the possibility that cisplatin is distributed along the fibrillar network of MAX8. Cisplatin is much smaller in size than vincristine, and would explain why vincristine encapsulated hydrogels show a slight difference in slope where cisplatin hydrogels do not.

A 10 day cisplatin release experiment was arranged for one time point at day 10 the same way as the vincristine release SANS experiment seen in Figure 3.3. There is no change in mid-q slope and a slight change in low-q slope between the two time points. This further confirms the overall fibrillar network of MAX8 remains intact throughout release of the drug from the hydrogel. Cisplatin's smaller size could create

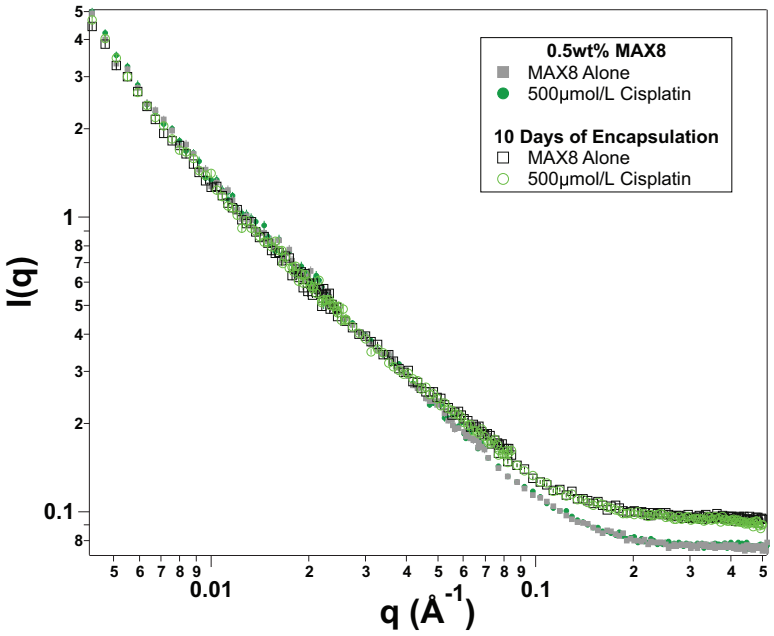

Figure 3.5: Comparison of 0.5wt% MAX8 hydrogels with and without 500μmol/L of cisplatin at assembly and 10 days after sitting in the same sample cell, without release or change in environment.

domains that would be harder to detect with SANS measurements, especially since cisplatin has less contrast than vincristine. Additionally, cisplatin has overall lesser hydrophobicity, this would allow cisplatin to diffuse through the aqueous environment of the MAX8 hydrogel more freely and uniformly than vincristine. These differences could explain the differences between the scattering of the two payloads during the time course.

The SANS data from the three different experimental setups examine the relationship of vincristine within the polymer fibrillar network. The results suggest the encapsulated vincristine cannot be in large domains or clumps, and is likely, distributed throughout the hydrogel network.

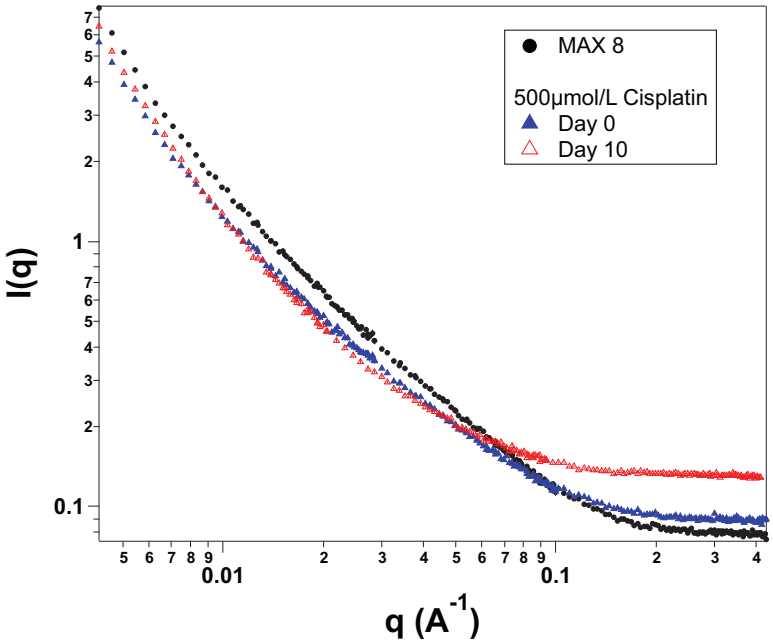

Figure 3.6: SANS of a 10 day release of 500μmol/L cisplatin from 0.5wt% MAX8.

3.4 Small-Angle Neutron Scattering on Supramolecular Assemblies

3.4.1 Poly(ethylene gylcol) and Palladium Gels

Poly(ethylene gylcol) (PEG) and palladium gels were synthesized and preared by the Johnson group at MIT. The gels are formed through multi-metal/ligand supramolecular assembly of metal cages held by a polymer network. The palladium atoms are held in place by bis-pyridine ligands attached to PEG chains. Two different ligands with different binding points were used, creating two different types of clusters a paddlewheel and a cage core. Nuclear magnetic resonance (NMR) and simulations of the two different gels were performed by the Johnson group. These characterizations did not quantify the cluster sizes of each gel. Using SANS, the remainder of this chapter determines the average radius of each cluster for both paddlewheel and cage gels. The proposed models of the two types of gels can be seen in Figure 3.7.

3.4.2 Core-Chain Model

When first fitting the data, sphere-based fits were used due to the nature of the palladium constructs. While using the sphere-based fits, there was a noticeable

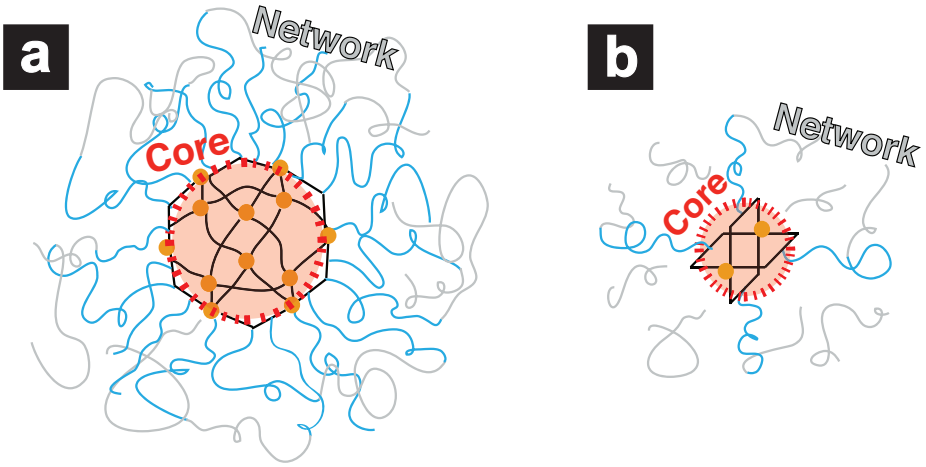

Figure 3.7: Models of the **a.)** paddlewheel gel and the **b.)** cage gel, where the red core and blue polymers are modeled by the core-chain model and the gray polymers are modeled by the power law for overall fit.

mismatch of the fit to the data. The fit overestimated the intensity for any q less than 0.035. Because it is in the nanometer range, the overestimation indicates the fit's interpretation of what was going on at the surface of the palladium construct, where the ligands connect. A different model was needed to best fit the data. Recently, Hore et al. created the Core Chain model to interpret the SANS data of polymer grafted iron oxide particles[27]. The model's interpretation of the interface difference between polymer and center reflected the Johnson group samples much more accurately than previously used sphere models provided by the NIST macros.

Scattering data for both samples were fit using a sum of two models, the power law model and the core chain model. The power law model is primarily used to show the presence of a larger entangled network, and describes the scattering intensity as

$$I(q) = Aq^{-n} \tag{3.3}$$

The core-chain model used here is a slightly modified version of the reported model[27] . The original Hore core-shell-chain model described an inorganic iron oxide core with a shell layer of dense polymer brush, surrounded by grafted polymer chains with excluded volume. Here, the shell layer element is omitted but the model remains intact

otherwise. In addition, the core in the present system is not inorganic entirely, but a mixed composition of Pd and poly(ethylene glycol).

The modified model examines the polymer surrounding the core, the interactions between polymers as well as between polymer and core. Most importantly, the model does not assume that the polymer chains are Gaussian, and allows the excluded volume of the chains to vary. For this reason, Debye functions are omitted in favor of a more detailed description of polymer chain scattering. The scattering intensity is calculated from the sum of the spherical core form factor, core-chain form factor correlations, chain-chain correlations, and the form factor of a polymer chain with excluded volume. The form factor amplitude of the spherical core is given by $F_A(q)$,

$$F_A(q) = \left[(\rho_{core} - \rho_{solvent})V_{core}\frac{3j_i(qr_{core})}{qr_{core}}\right] \tag{3.4}$$

where j_1 is a spherical Bessel function of order 1, r_{core} is the radius of the paddlewheel or cage, V_{core} is the volume of the paddlewheel or cage, core is the scattering length density (SLD) of the paddlewheel or cage, and solvent is the SLD of the solvent.

Scattering from polymer chains is described by the form factor amplitude and form factor of the polymer chains, $F_B(q)$ and$P_B(q)$, respectively. Note that because polymer chains are fractal in nature, the form factor is a separate function from the form factor amplitude. The functions are given by,

$$F_B(q) = \frac{1}{2\nu U^{1/2\nu}}\gamma\Big(\frac{1}{2\nu}, U\Big) \tag{3.5}$$

$$P_B(q) = \frac{1}{\nu U^{1/2\nu}}\gamma\Big(\frac{1}{2\nu}, U\Big) - \frac{1}{\nu U^{1/\nu}}\gamma\Big(\frac{1}{\nu}, U\Big) \tag{3.6}$$

where the lower incomplete gamma function reads

$$\gamma(d, U) = \int_0^U dt(e^{-t}t^{d-1}) \tag{3.7}$$

The parameter $U = q^2a^2N^{2\nu}/6$ contains the scattering variable q, the statistical segment length of the polymer chain (a), the degree of polymerization of the chain (N), and the excluded volume parameter ν.

The total macroscopic scattering cross section for N_p/V density of nanoparticles with N_g grafted polymer chains per particle, including the power law term, is then expressed as

$$\begin{aligned}\frac{d\Sigma(q)}{d\Omega} = Aq^{-n} + \frac{N_p}{V}\big[&F_A(q)^2 + N_g V_B(\rho_{chain} - \rho_{solvent})F_A(q)F_B(q) + \\ &N_g(N_g-1)V_B^2(\rho_{chain} - \rho_{solvent})^2 F_B(q)E_A(q)^2F_B(q) + \\ &N_g V_B^2(\rho_{chain} - \rho_{solvent})^2 P_B(q)\big]\, S_i(q) + B\end{aligned} \tag{3.8}$$

where $E_A = j_0(qr_{core})$ is a spherical Bessel function, and B is the constant incoherent background. The radius of gyration for the chains surrounding the paddlewheel or cage is calculated from the parameters of Eq. 3.8 as

$$R_g^2 = \frac{N^{2\nu}a^2}{(2\nu+1)(2\nu+2)} \tag{3.9}$$

This model is then summed with the power law seen in Equation 3.3. The core-chain model examines the core and the immediately surrounding polymer chains, in high and mid-q ranges. The power law examines length scales greater than 50nm in lower-q, examining the higher-order network of the polymer chains. The combination of the two models gives a complete picture of what is happening throughout the entire network and what is happening locally with each palladium core. Figure 3.7 shows what is considered the core for the paddlewheel sample and the cage sample, where blue polymers are those seen by the core-chain model. The gray polymers are part of the larger network and modeled by the power law. The fit for the paddlewheel gel is seen in Figure 3.8a, and the fit for the cage gel is seen in Figure 3.8b.

The SLDs for the core of each sample were calculated using an average of the PEG and palladiums SLD on the basis of the composition of the two components.

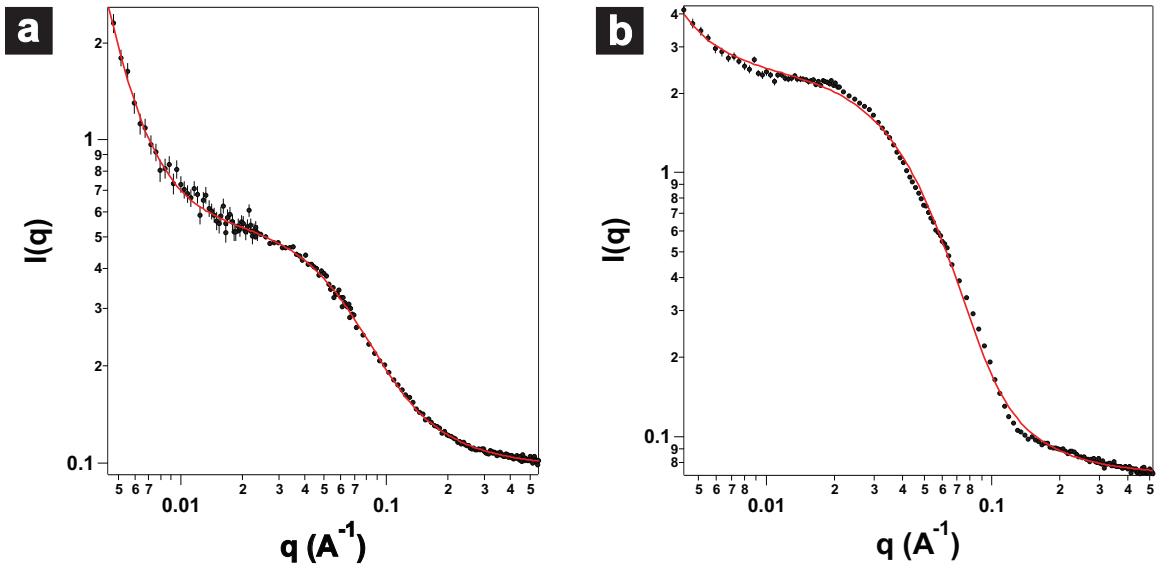

Figure 3.8: SANS scattering of the **a.)**paddlewheel gel with a calculated radius of 5.5nm with 4 chains surrounding the core and **b.)** cage gel with a calculated radius of 1.7 nm with 20 chains surrounding the core.

Using the NCNR SLD calculator, the bis-pyridine SLD was 1.98 x 10^{-6} / $\AA^2$, the Pd SLD was 4.02 x 10^{-6} / $\AA^2$, and DMSO-d6 had an SLD of 5.28 x 10^{-6} / $\AA^2$. The composition of the components, calculated on the basis of the density and mass for paddlewheel and cage gels, was 70% polymer and 30% Pd yielding an initial SLD of 2.59 x 10^{-6} / $\AA^2$. The initial SLD does not take into account the possible presence of PEG or DMSO within the core, and so is only an initial approximation. The calculated radii, resulting from the core-chain model fits, for the paddlewheel and cage structures were 0.55 $\pm$ 0.054 nm and 1.7 $\pm$ 0.25nm, respectively. The calculated number of ligands, also from the core-chain model fits, for the paddlewheel and cage structures, N_g, were approximately 4 and 20, respectively. The excluded volume parameter (ν), calculated from the core-chain model fit, for the paddlewheel gel and cage gel, were 0.574 and 0.595, respectively. A value of that is close to 0.6 is indicative of a swollen polymer chain (i.e., R_g ~ $N^{0.6}$).The radius of gyration (R_g), calculated using Eq. 3.9, with parameters obtained from the core-chain model fits, for paddlewheel and cage gel were, 0.493 nm and 0.456nm, respectively.

REFERENCES

[1] Frank S Bates and Glenn H Fredrickson. Block Copolymer Thermodynamics: Theory and Experiment. *dx.doi.org*, 41(1):525–557, November 2003.

[2] Kell Mortensen and Jan Skov Pedersen. Structural study on the micelle formation of poly(ethylene oxide)-poly(propylene oxide)-poly(ethylene oxide) triblock copolymer in aqueous solution. *Macromolecules*, 26(4):805–812, July 1993.

[3] Paul D T Huibers, Lev E Bromberg, Brian H Robinson, and T Alan Hatton. Reversible Gelation in Semidilute Aqueous Solutions of Associative Polymers: A Small-Angle Neutron Scattering Study. *Macromolecules*, 32(15):4889–4894, June 1999.

[4] Ian W Hamley, Kurt A Koppi, Jeffrey H Rosedale, Frank S Bates, Kristoffer Almdal, and Kell Mortensen. Hexagonal mesophases between lamellae and cylinders in a diblock copolymer melt. *Macromolecules*, 26(22):5959–5970, May 2002.

[5] Stefan Reinicke, Joachim Schmelz, Alain Lapp, Matthias Karg, Thomas Hellweg, and Holger Schmalz. Smart hydrogels based on double responsive triblock terpolymers. *Soft Matter*, 5(13):2648–2657, June 2009.

[6] Isabella Goldmints, Friedrich K von Gottberg, Kenneth A Smith, and T Alan Hatton. Small-Angle Neutron Scattering Study of PEO—PPO—PEO Micelle Structure in the Unimer-to-Micelle Transition Region. *Langmuir*, 13(14):3659–3664, July 1997.

[7] Wayne W Maurer, Frank S Bates, Timothy P Lodge, Kristofer Almdal, Kell Mortensen, and Glenn H Frederickson. Can a single function for χ account for block copolymer and homopolymer blend phase behavior? *The Journal of ...*, 108(7):2989, 1998.

[8] Takuro Matsunaga, Takamas Sakai, Yuki Akagi, Ung-il Chung, and Mitsuhrio Shibayama. Structure characterization of tetra-PEG gel by small-angle neutron scattering. . . . , 2009.

[9] Eric J Yearley, Isidro E Zarraga, Steven J Shire, Thomas M Scherer, Yatin Gokarn, Norman J Wagner, and Yun Liu. Small-Angle Neutron Scattering Characterization of Monoclonal Antibody Conformations and Interactions at High Concentrations. *Biophysical Journal*, 105(3):720–731, August 2013.

[10] Ayben Top, Sheng Zhong, Congqi Yan, Christopher J Roberts, Darrin J Pochan, and Kristi L Kiick. Controlling assembly of helical polypeptidesvia PEGylation strategies. *Soft Matter*, 7(20):9758–9766, October 2011.

[11] Ian W Hamley, Marta J Krysmann, Antonios Kelarakis, Valeria Castelletto, Laurence Noirez, Rohan A Hule, and Darrin J Pochan. Nematic and Columnar Ordering of a PEG–Peptide Conjugate in Aqueous Solution. *Chemistry-A European Journal*, 14(36):11369–11375, December 2008.

[12] Annette Meister, Martin Bastrop, Sven Koschoreck, Vasil M Garamus, Thomas Sinemus, Günter Hempel, Simon Drescher, Bodo Dobner, Walter Richtering, Klaus Huber, and Alfred Blume. Structure—Property Relationship in Stimulus-Responsive Bolaamphiphile Hydrogels. *Langmuir*, 23(14):7715–7723, July 2007.

[13] Beth A Schubert, Eric W Kaler, and Norman J Wagner. The Microstructure and Rheology of Mixed Cationic/Anionic Wormlike Micelles. *Langmuir*, 19(10):4079–4089, May 2003.

[14] Hui Yan, Alberto Saiani, Julie E Gough, and Aline F Miller. Thermoreversible Protein Hydrogel as Cell Scaffold. *Biomacromolecules*, 7(10):2776–2782, October 2006.

[15] A Saiani, A Mohammed, H Frielinghaus, R Collins, N Hodson, C M Kielty, M J Sherratt, and A F Miller. Self-assembly and gelation properties of α-helix versusβ-sheet forming peptides. *Soft Matter*, 5(1):193, 2008.

[16] Asish Pal, Hajra Basit, Saikat Sen, Vinod K Aswal, and Santanu Bhattacharya. Structure and properties of two component hydrogels comprising lithocholic acid and organic amines. *Journal of Materials Chemistry*, 19(25):4325–4334, June 2009.

[17] Tuna Yucel, Chris M Micklitsch, Joel P Schneider, and Darrin J Pochan. Direct Observation of Early-Time Hydrogelation in β-Hairpin Peptide Self-Assembly. *Macromolecules*, 41(15):5763–5772, August 2008.

[18] Congqi Yan, Aysegul Altunbas, Tuna Yucel, Radhika P Nagarkar, Joel P Schneider, and Darrin J Pochan. Injectable solid hydrogel: mechanism of shear-thinning and immediate recovery of injectable β-hairpin peptide hydrogels. *Soft Matter*, 6(20):5143–5156, October 2010.

[19] Rohan A Hule, Radhika P Nagarkar, Aysegul Altunbas, Hassna R Ramay, Monica C Branco, Joel P Schneider, and Darrin J Pochan. Correlations between structure, material properties and bioproperties in self-assembled β-hairpin peptide hydrogels. *Faraday Discuss.*, 139(0):251–264, August 2008.

[20] Rosa Ricciardi, Gaetano Mangiapia, Fabrizio Lo Celso, Luigi Paduano, Roberto Triolo, Finizia Auriemma, Claudio De Rosa, and Françoise Lauprêtre. Structural Organization of Poly(vinyl alcohol) Hydrogels Obtained by Freezing and Thawing Techniques: A SANS Study. *Chemistry of Materials*, 17(5):1183–1189, February 2005.

[21] Roland Winter. Synchrotron X-ray and neutron small-angle scattering of lyotropic lipid mesophases, model biomembranes and proteins in solution at high pressure. *Biochimica et Biophysica Acta (BBA) - Protein Structure and Molecular Enzymology*, 1595(1-2):160–184, March 2002.

[22] Mu-Ping Nieh, Charles J Glinka, Susan Krueger, R Scott Prosser, and John Katsaras. SANS Study of the Structural Phases of Magnetically Alignable Lanthanide-Doped Phospholipid Mixtures. *Langmuir*, 17(9):2629–2638, May 2001.

[23] G Gebel and O Diat. Neutron and X-ray Scattering: Suitable Tools for Studying Ionomer Membranes. *Fuel Cells*, 2005.

[24] Sameer Sathaye. *Multifunctional Hybrid Networks Based on Self Assembling Peptide Sequences*. PhD thesis, June 2014.

[25] S R Kline. Reduction and analysis of SANS and USANS data using IGOR Pro. *Journal of Applied Crystallography*, 39(6):895–900, 2006.

[26] Lisa A Haines-Butterick, Daphne A Salick, Darrin J Pochan, and Joel P Schneider. In vitro assessment of the pro-inflammatory potential of β-hairpin peptide hydrogels. *Biomaterials*, 29(31):4164–4169, November 2008.

[27] Michael J A Hore, Jamie Ford, Kohji Ohno, Russell J Composto, and Boualem Hammouda. Direct Measurements of Polymer Brush Conformation Using Small-Angle Neutron Scattering (SANS) from Highly Grafted Iron Oxide Nanoparticles in Homopolymer Melts. *Macromolecules*, 46(23):9341–9348, November 2013.

Chapter 4

SUMMARY AND FUTURE WORK

4.1 Summary

Peptide hydrogels are gaining attention for biomedical applications. The different assemblies structures of peptides and the resultant properties have many advantages. Chapter 1 explores the chemistry and characteristics of peptide hydrogels. In particular, peptide hydrogels are useful for drug delivery applications. The ability to self-assemble at physiological conditions, cytocompatibility, and physical characteristics of shear-thinning are all advantages for the hydrogel. In this thesis, the focus has been on on peptide hydrogel in particular, MAX8 from the MAX family of peptides. MAX8 self-assembles at physiological conditions into β-hairpin based fibrillar network that is physically cross-linked. Previous work encapsulated and characterized many different payloads including cells, drugs, probes. Using this previous experience, Chapter 2 focuses on encapsulating vincristine, a very hydrophobic chemotherapeutic in 0.5wt% MA8 hydrogels, as a future drug delivery. Vincristine is an often used chemotherapeutic that require very low concentrations (nmol/L) to be effective at killing cells. Vincristine attacks any cell, cancerous or not, causing many of the side effects (*e.g.* hair lossor stomach irritation)associated with chemotherapy. To measure Vincristine's IC_{50}, DAOY cells, a model for medullablastoma—pediatric brain cancer, were used. For direct application of vincristine and vincristine encapsulated in MAX8, the IC_{50} was found to be in the nmol/L range.

Vincristine's presence does not alter the MAX8 shear-thinning or assembly properties, characteristics important for MAX8 as a drug delivery vehicle. As a drug delivery vehicle, MAX8 loaded with vincristine would be deposited and remain in the

targeted area. After deposition, the MAX8 would release vincristine continuously to the surrounding area.

Measurements of released vincristine from MAX8 were first performed with UV-Vis spectroscopy. The released concentrations were too low after a day for the detector resolution. Instead of UV-Vis spectroscopy, release studies were measured using a liquid scintillation counter and tritium (^{3}H) labeled vincristine. Over the course of a month of encapsulation, the drug encapsulated hydrogels showed continuous release. Vincristine's hydrophobic nature and subsequent deactivation were a concern, since the encapsulation over the month was in an aqueous environment. An efficacy test to measure if released vincristine still killed DAOY cells, shows that even after the month long encapsulation, vincristine was still active. Additionally, of the two concentrations encapsulated, the higher concentration killed a greater number of cells continuously through all time points. This trend confirms the cell death measured is a result of the vincristine itself. Through all cell death experiments, MAX8 without vincristine was also placed in the presence of cells and shown that the peptide hydrogel by itself odes not kill or affect cells.

To better characterize vincristine, an attempt to calculate the diffusion coefficient by FRAP proved unsuccessful. Vincristine has an excitation peak not visible on the confocal microscope. FRAP is a useful technique used to calculate the diffusion coefficient of curcumin, a hydrophobic derivative of turmeric with medicinal properties. The FRAP measurements show the more dilute concentrations of encapsulated curcumin had less predictable trends. The lack of trend most likely is a result of curcumin not being a dye and not meant to stay stable under long periods of exposure or bleaching.

The results of chapter 2 support MAX8 hydrogels as potential vincristine carrying drug delivery vehicles. Vincristine is hydrophobic, with a half life at most of 32 hours as a bulk material in clinical studies. With the MAX8 encapsulation, this half life can be extended, prolonging the usefulness and exposure of vincristine to cancerous tissue. The targeted deposition of the drug-hydrogel construct would provide

local, continuous release of the vincristine. The local delivery would reduce exposure of healthy tissue to vincristine, minimizing harmful and uncomfortable side effects.

Chapter 2 characterized vincristine and its release from MAX8 while chapter 3 used SANS to exam the relationship of vincristine with the MAX8 network itself. Based on rheometry data from chapter 2, the vincristine does not disturb the gelation, shear-thinning or re-healing properties, indicating the branch points and entanglements of the fibrillar network are not disturbed. If vincristine is not at the branch points or entanglements, vincristine with in MAX8 could exist as A.) evenly distributed areas attached or associated along the fibrils, B.) large domains or clumps that minimize surface area exposure of vincristine, or C.) uniformly distributed smaller domains unattached to the fibrils.

Using SANS, a powerful structure characterization technique, to investigate the vincristine encapsulated hydrogel network, three experiments across several time points were performed. The first compares MAX8 with or without vincristine The overall slope and shape of the scattering curve were very similar with a slight change in slope. This change is seen at mid-q, implying there might be a difference between fibril characteristics.

The next experiment examines diffusion of vincristine within the hydrogel. After assembly, the MAX8 hydrogels with and without vincristine are left for ten days within a sealed sample cell environment. Between time points, each hydrogel's scattering curves showed almost no change, except in the background (high-q, $q > 0.3$) intensities. The increase for MAX8 with and without vincristine are very similar, and an indication of hydrogen exchange, despite the sealed samples. The lack of change in scattering curve for each sample, indicates there are not structural changes for either the MAX8 or the vincristine. If the vincristine were in large clumps, there would be inner-gel diffusion or change in aggregation size over the course of 10 days, resulting in a change in the shape or intensity of the scattering curve.

Finally, the structures of the hydrogel as the vincristine is released for 10 days is examined. Most noticeably, there is a decrease in intensity as the hydrogel releases over

time. A decrease in intensity can be from a hang in contrast or a decreased amount of material to scatter. In this case, it is possible the intensity decrease could be vincristine leaving the hydrogel environment and altering the contrast of the fibrillar network

While the work with vincristine was telling, another drug was also encapsulated to better understand the relationship of an encapsulated payload and the MAX8 hydrogel. The second drug used was cisplatin, another, slightly less hydrophobic chemotherapeutic that is much smaller than vincristine with fewer hydrogens throughout. As with vincristine, three experimental setups, two of which involve a time course, were used to characterize the hydrogel structure with cisplatin encapsulated.

First, three concentrations of cisplatin were encapsulated in 0.5wt% MAX8 hydrogels. Despite the orders of magnitude in difference of concentration, the scattering curves did not show a comprehendible trend. The lowest and highest concentrations of cisplatin shared the same scattering curve shape while the middle concentration shared the same scattering curve as MAX8 without anything encapsulated. Most noticeable here, because of the decrease in hydrogen as compared to vincristine, the high-q background intensities between MAX8 hydrogels with and without cisplatin does not create a huge difference.

The next scattering experiment looked at MAX8 hydrogels with and without 500μmol/L cisplatin at two different time points for the same environment. Once assembled and measured in the neutron beam, the hydrogels remained in the sample cell for ten days and were measured again. The only changes seen were like the vincristine experiment, an increase in background indicating an increase in hydrogen content. There are no changes in the shapes or slopes of the scattering curves.

Finally, the scattering to examine the structure of the hydrogel after cisplatin is released over 10 days. There is a slight decrease in intensity, most likely from a slight loss in material when combining the four gels in transwells into one sample. This same decrease in seen after 10 days of release. The two curves show no major difference in scattering curve shape, or decrease in intensity, unlike the vincristine experiment. These major differences could stem from the difference in drug itself.

The lowered contrast of cisplatin may not have as big of an effect on overall hydrogel intensity scattering and therefore less noticeable when the drug is released and removed from the system. The lesser hydrophobicity may mean the cisplatin is not as tightly associated with the fibrils, creating less of an effect after release into each well.

The last part of Chapter 3 uses SANS to better characterize a PEG-Palladium gel system. The multi-metal/ligand assembly is synthesized by the Johnson group at MIT. While NMR and simulations were used to characterize the gels, other methods of quantifying size of each gel were more difficult. Using SANS and the excluded volume core-chain model, radii sizes for the metallic core of each chain and the number of attached polymer chains were quantified.

4.2 Future Work

4.2.1 Vincristine and Release

Having effectively shown encapsulated vincristine can be released at continuous effective amounts from MAX8 hydrogels creates many other potential application possibilities. These possibilities include changing the drug encapsulated or creating combinations of drugs to be encapsulated, more realistically like current cancer treatments. Changing the hydrogel itself or having different concentrations of drug encapsulated could result in better control in the rate of encapsulated drug release over time. Showing the effectiveness of the vincristine release from MAX8 *in vitro*, there are also obvious next steps towards *in vivo* work.

4.2.1.1 Addition of Payloads or Concentrations

The most obvious potential for future work with vincristine encapsulated hydrogels, would be to change the drug or payload encapsulated. The models for measuring cell death and release are already configured and understood, reducing the difficulty in characterizing new drugs of varying hydrophobicity or size encapsulated in the MAX8 hydrogels. The change in hydrophobicity or size would also change the released concentrations and time of release, leading to new applications with MAX8 as a delivery

vehicle, not just aimed at cancer treatment. A different payload could also be easier to characterize within the MAX8 hydrogel, showing excitation peaks that are detectable with the confocal microscope. With a detectable peak, FRAP and other fluorescence methods could obtain diffusion coefficients for the payload, further quantifying the relationship of payload and MAX8.

Thinking larger scale, MAX8 could deliver multiple payloads and not be limited to one drug. In reality, chemotherapy is often a combination of drugs to be most effective. While encapsulating two payloads into one hydrogel may not seem the most practical, since the release of both payloads cannot be guaranteed to be uniform, two different drugs in two different hydrogels can be feasibly combined.

MAX8 hydrogels carrying different encapsulated payloads can be loaded into the same syringe and then deposited. Because of the solid behavior of the hydrogels, the physical barrier between different hydrogels would be maintained. This can be seen in Figure 4.2. First, two separate 0.5wt% MAX8 hydrogels were assembled, one with phenol red in DMEM as the assembly triggering buffer and the other with NaCl solution as the assembly triggering buffer. The phenol red containing hydrogel is assembled and deposited first in the vial. After gelation, the second hydrogel is deposited on top. Figure 4.2b.) shows a 0.75wt% MAX8 hydrogel, encapsulating trypan blue deposited into different columns within the bilayer hydrogel via 26-gauge needle and syringe. As the blue hydrogel was deposited, the more quickly the needle was pulled upwards, the thinner the column. The bilayers and columns did not run or mix after deposition, maintaining a clear interface.

The clear interface and ability to combine MAX8 hydrogel with several payloads would provide a way of administering or depositing several drugs at once. Faster releasing or a higher concentration payload could be created and deposited farther away from the surface like the trypan blue hydrogel. The slower releasing or lower concentration payload could surround the first drug. For different payloads, this could create more uniform release across the entire hydrogel. By encapsulating payloads of varying concentration, release could be sustained for a longer time, as the lower

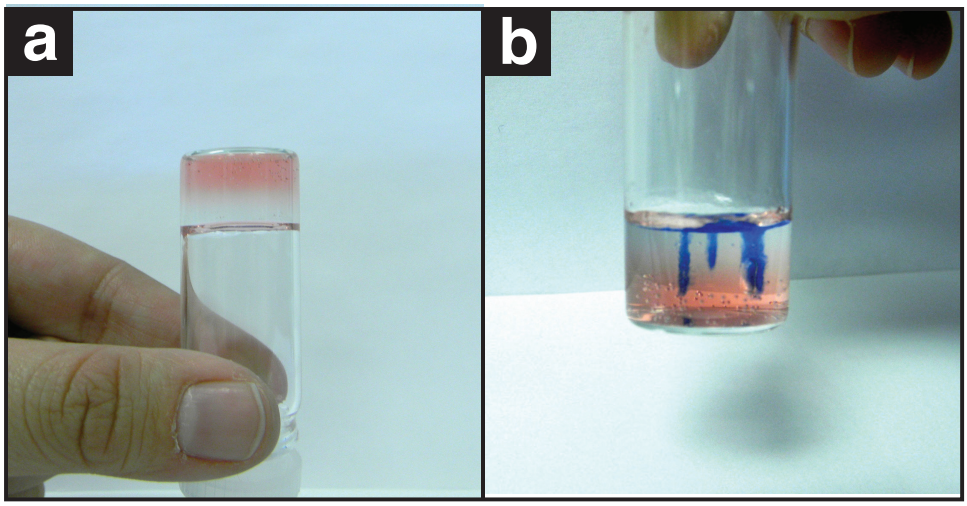

Figure 4.1: a.) An upside down vial of two layers of 0.5wt% MAX8 hydrogels, one assembled with phenol red present and one assembled without phenol red layered on top. **b.)** Trypan blue in 0.5wt% MAX8 hydrogels are inserted into the bilayer gel and show clear interfaces within the hydrogel.

concentration releases initially, the higher concentration of drug would diffuse into the lower concentration hydrogel, then release.

4.2.1.2 *In vivo* Work

Having shown success in killing cells *in vitro*, *in vivo* work could come next. Medullablastoma was the potential cancer focused on throughout chapter 2. It is a pediatric brain cancer. The next *in vivo* experiment would focus on injecting MAX8 hydrogel into the brain, specifically mice brains. Because of the delicate nature of the brain and the smaller volume of a mouse brain, very low volumes would have to be injected to ensure the presence and pressure of MAX8 do not cause undue side effects.

A major question *in vivo* work could address would be whether or not MAX8 peptide hydrogel stays put and remains in the deposition location within the brain. One way of visualizing this would be to attach a near-infrared (NIR) dye to MAX8. An NIR dye is necessary because the living body of the mouse fluoresces more in the infrared (IR) spectrum and the dye would be detectable if the mouse were imaged while still alive. Once the hydrogel is deposited, the MAX8 within the brain can easily be

monitored for a long period of time.

Another *in vivo* experiment could use brain tumor expressing mice to see if vincristine encapsulated MAX8 could shrink or affect the tumor. Two experiment conditions for the tumor expressing mice would show if MAX8 would really be an ideal drug delivery candidate. The first condition, deposits the vincristine loaded MAX8 hydrogel near/around the tumor. Monitoring the tumor size could show the effectiveness of the released vincristine from the MAX8 hydrogel. The second experiment would first remove the tumor. After the tumor is resected, the hydrogel would be deposited in the cavity. The tumor site would be monitored for tumor reappearance and local tissue reactions or sensitivities.

4.2.2 SANS

4.2.2.1 Vincristine and Other Drugs

At first glance, the SANS data of chapter 3 could not conclusively state that the vincristine was distributed along the fibrillar surfaces of MAX8. The data shown did not quantify the radii or length of the fibrils before or after release of vincristine from the overall system. Previous work used a summed model of the cylinder model and the power law model to determine the radii for MAX hydrogels.

Using the summed model, fitting for the vincristine and cisplatin encapsulated hydrogels would show if the encapsulated drug changes the fibril size. A change in fibrillar size would be calculated and confirm the current idea that the vincristine resides along the surface of the fibrils, evenly. These calculations would also quantify the hydrogel network over time of encapsulation, an area that has not received attention before.

While previous Pochan group members have fit MAX peptide hydrogel scattering data before, the MAX peptide does not have the presence of other payloads. In these experiments, the presence and constantly changing surrounding concentration of vincristine have to be taken into account. The presence of vincristine clearly affects intensity, meaning its SLD will have an effect on fit calculations.

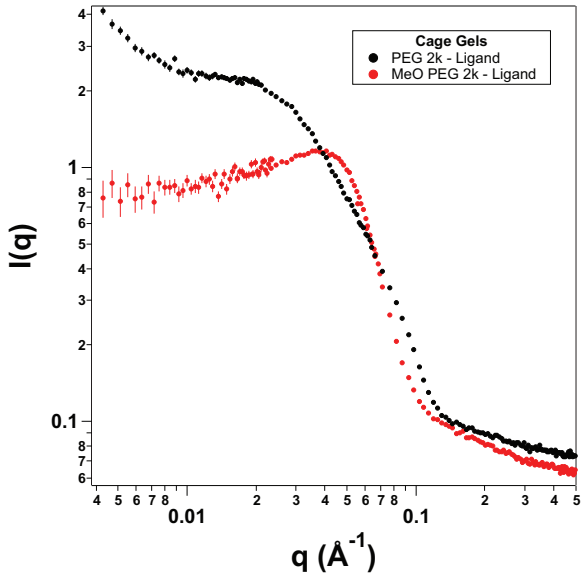

Figure 4.2: While the two ligand configurations are the same, the PEG 2k ligand is biarmed and the MeO PEG 2k ligand is only one armed. While both form cage cores, only the linked, bi-armed ligand creates a network.

Taking the time to fit each time point and variation of drug encapsulated MAX8 is important, since each scattering curve had slightly different features than MAX8 hydrogel without drug. This work is an obvious next step, and could pave the road for a better understanding of how payloads interact within the hydrogel and its effects.

4.2.2.2 PEG-Palladium Gels

The supramolecular gels created by the Johnson group used two-arm ligands. The ligand at each end of a PEG molecule helped create a larger overall network with the entanglements. Among the Johnson group samples examined with SANS, one armed ligands that formed gels were also measured. These samples create a drastically different low-q profile as seen in Figure 4.2. Here, the PEG chain and ligand configuration are exactly the same, creating a cage gel. The greatest difference is the lack of a network throughout the hydrogel. Next steps would characterize these one armed ligand supramolecular gels to create a more complete story for the PEG-Palladium systems.

4.2.3 Cell Encapsulation in MAX8 Hydrogels

The focus of chapters two and three have been on the encapsulation of vincristine in MAX8. During the vincristine project, there was also experiment optimizations and characterizations for encapsulating chondrocytes in MAX8 for eventual, clinical, delivery vehicle purposes. The goal of the project aimed to reduce the effects of shear on chondrocytes during injection. After injection the cells would be able to take advantage of the 3D hydrogel environment, growing and proliferating as needed to eventually rebuild cartilage.

The ATDC5 cell line used to develop the assays needed was an acceptable chondrocyte model. Cells were encapsulated in the same manner as other payloads, added to DMEM then mixed with MAX8 peptide solution dissolved in water. When first encapsulating the cells in 0.5wt% MAX8 hydrogels, there was an issue with unexpected cell death at the bottom of the hydrogels. After several different hydrogel formation conditions as well as many different cell concentrations, the best conditions for cell encapsulated MAX8 were found. First, the hydrogel is created with a 1 million cell/mL density and deposited in a well. After gelation, ensuring the hydrogel has formed properly, the hydrogels are removed from the first well and transferred into the final desired well. To emulate more realistic conditions, the samples were all injected by hand at speeds of 10mL/min, 50mL/min, and 200mL/min from 1mL syringe with an 18G needle.

Once injected and settled, each sample was is then covered in 2mL of DMEM, which is changed every three days. On the desired day of the time course, samples containing hydrogel for RNA extraction are aspirated, then covered and incubated in liquid nitrogen for 10 minutes. After being flash frozen, the samples are treated with a TRIzol reagent to isolate RNA. Using Qiagen kits and primers, the desired RNA sequences are replicated for polymerase chain reaction (PCR) and marker concentrations are compared.

Cell filled hydrogels were also stained with Alcian blue, another assay used to

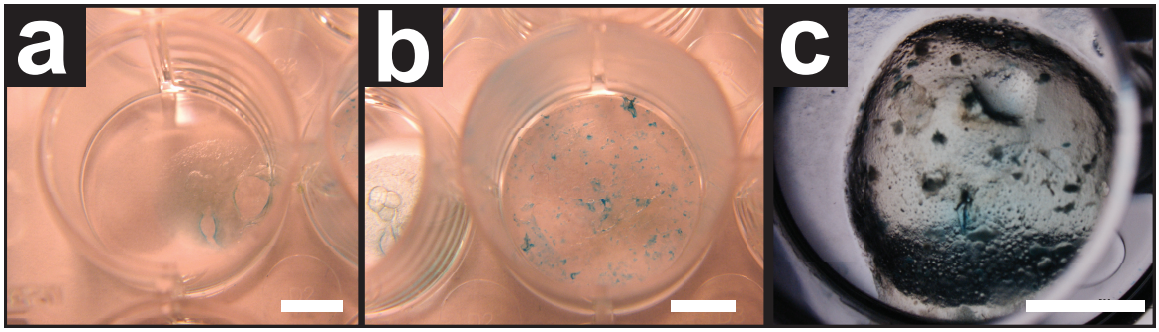

Figure 4.3: Light micrographs showing Alcian blue staining on one week time course 0.5wt% MAX8 hydrogels containing **a.)** no cells after the hydrogel has dried, **b.)** ATDC5 cells after the hydrogel has dried, **c.)** ATDC5 cells, while still hydrated. Scale bar represents 5mm.

detect extracellular matrix (ECM) related proteins in the cell-gel constructs. Traditional Alcian blue methods cannot be followed for the hydrogel, because of Alcian blue's charged dye and the 3D nature of the hydrogel, false positives from dye retention is an issue. A protocol requiring many more wash steps and a negative control of plain MAX8 hydrogel are needed to properly assess the results of Alcian blue staining. Figure 4.3a shows the light, but still noticeable blue stain for the negative control hydrogel with no cells. Figure 4.3b and 4.3c show the obvious darker blue stained areas where the ATDC5 cells grew, a week after injection.

All of the major sticking points and issues that naturally occur from creating new protocols have been ironed out. Having fine-tuned the many details required for understanding and quantifying the benefits of chondrocytes encapsulated in MAX8 hydrogels, the next step would be just to run the experiment as a whole. Several time points would be run to show if there are any major differences in cell markers between injecting chondrocytes suspended in DMEM or injecting chondrocytes encapsulated in MAX8 hydrogels. Cell death and apoptosis markers would be of importance for immediately after injection, while markers for ECM growth and development would be important for weeks after injection.

Appendix

FIGURE PERMISSIONS

NATURE PUBLISHING GROUP LICENSE TERMS AND CONDITIONS

Aug 13, 2015

This is a License Agreement between Jessie Sun ("You") and Nature Publishing Group ("Nature Publishing Group") provided by Copyright Clearance Center ("CCC"). The license consists of your order details, the terms and conditions provided by Nature Publishing Group, and the payment terms and conditions.

All payments must be made in full to CCC. For payment instructions, please see information listed at the bottom of this form.

License Number	3687260443345
License date	Aug 13, 2015
Licensed content publisher	Nature Publishing Group
Licensed content publication	Nature Communications
Licensed content title	Chemically programmed self-sorting of gelator networks
Licensed content author	Kyle L. Morris, Lin Chen, Jaclyn Raeburn, Owen R. Sellick, Pepa Cotanda, Alison Paul
Licensed content date	Feb 12, 2013
Volume number	4
Type of Use	reuse in a dissertation / thesis
Requestor type	academic/educational
Format	print and electronic
Portion	figures/tables/illustrations
Number of figures/tables/illustrations	2
High-res required	no
Figures	Figure 2.a, Figure 4
Author of this NPG article	no
Your reference number	None
Title of your thesis / dissertation	Hydrophobic Payload Encapsulation and Release Effects on Self-Assembling Hydrogel
Expected completion date	Sep 2015
Estimated size (number of pages)	130
Total	0.00 USD

Title: Self-Assembly of Multidomain Peptides: Sequence Variation Allows Control over Cross-Linking and Viscoelasticity

Author: Lorenzo Aulisa, He Dong, Jeffrey D. Hartgerink

Publication: Biomacromolecules

Publisher: American Chemical Society

Date: Sep 1, 2009

PERMISSION/LICENSE IS GRANTED FOR YOUR ORDER AT NO CHARGE

This type of permission/license, instead of the standard Terms & Conditions, is sent to you because no fee is being charged for your order. Please note the following:

- Permission is granted for your request in both print and electronic formats, and translations.
- If figures and/or tables were requested, they may be adapted or used in part.
- Please print this page for your records and send a copy of it to your publisher/graduate school.
- Appropriate credit for the requested material should be given as follows: "Reprinted (adapted) with permission from (COMPLETE REFERENCE CITATION). Copyright (YEAR) American Chemical Society." Insert appropriate information in place of the capitalized words.
- One-time permission is granted only for the use specified in your request. No additional uses are granted (such as derivative works or other editions). For any other uses, please submit a new request.

If credit is given to another source for the material you requested, permission must be obtained from that source.

JOHN WILEY AND SONS LICENSE TERMS AND CONDITIONS

Aug 13, 2015

This Agreement between Jessie Sun ("You") and John Wiley and Sons ("John Wiley and Sons") consists of your license details and the terms and conditions provided by John Wiley and Sons and Copyright Clearance Center.

License Number	3687260830497
License date	Aug 13, 2015
Licensed Content Publisher	John Wiley and Sons
Licensed Content Publication	Biopolymers
Licensed Content Title	Building fibrous biomaterials from α-helical and collagen-like coiled-coil peptides
Licensed Content Author	Derek N. Woolfson
Licensed Content Date	Jan 20, 2010
Pages	10
Type of use	Dissertation/Thesis
Requestor type	Author of this Wiley article
Format	Print and electronic
Portion	Figure/table
Number of figures/tables	1
Original Wiley figure/table number(s)	Figure 1
Will you be translating?	No
Title of your thesis / dissertation	Hydrophobic Payload Encapsulation and Release Effects on Self-Assembling Hydrogel
Expected completion date	Sep 2015
Expected size (number of pages)	130
Requestor Location	Jessie Sun 201 DuPont Hall NEWARK, DE 19711 United States Attn: Jessie Sun
Billing Type	Invoice

JOHN WILEY AND SONS LICENSE TERMS AND CONDITIONS

Aug 13, 2015

This Agreement between Jessie Sun ("You") and John Wiley and Sons ("John Wiley and Sons") consists of your license details and the terms and conditions provided by John Wiley and Sons and Copyright Clearance Center.

License Number	3687261047471
License date	Aug 13, 2015
Licensed Content Publisher	John Wiley and Sons
Licensed Content Publication	Advanced Functional Materials
Licensed Content Title	Engineering Increased Stability into Self-Assembled Protein Fibers
Licensed Content Author	A. M. Smith,E. F. Banwell,W. R. Edwards,M. J. Pandya,D. N. Woolfson
Licensed Content Date	Apr 10, 2006
Pages	9
Type of use	Dissertation/Thesis
Requestor type	University/Academic
Format	Print and electronic
Portion	Figure/table
Number of figures/tables	2
Original Wiley figure/table number(s)	Figure 1, Figure 7
Will you be translating?	No
Title of your thesis / dissertation	Hydrophobic Payload Encapsulation and Release Effects on Self-Assembling Hydrogel
Expected completion date	Sep 2015
Expected size (number of pages)	130
Requestor Location	Jessie Sun 201 DuPont Hall NEWARK, DE 19711 United States Attn: Jessie Sun
Billing Type	Invoice

Title: Salt-Triggered Peptide Folding and Consequent Self-Assembly into Hydrogels with Tunable Modulus

Author: Bulent Ozbas, Juliana Kretsinger, Karthikan Rajagopal, et al

Publication: Macromolecules

Publisher: American Chemical Society

Date: Sep 1, 2004

PERMISSION/LICENSE IS GRANTED FOR YOUR ORDER AT NO CHARGE

This type of permission/license, instead of the standard Terms & Conditions, is sent to you because no fee is being charged for your order. Please note the following:

- Permission is granted for your request in both print and electronic formats, and translations.
- If figures and/or tables were requested, they may be adapted or used in part.
- Please print this page for your records and send a copy of it to your publisher/graduate school.
- Appropriate credit for the requested material should be given as follows: "Reprinted (adapted) with permission from (COMPLETE REFERENCE CITATION). Copyright (YEAR) American Chemical Society." Insert appropriate information in place of the capitalized words.
- One-time permission is granted only for the use specified in your request. No additional uses are granted (such as derivative works or other editions). For any other uses, please submit a new request.

If credit is given to another source for the material you requested, permission must be obtained from that source.

Title: Direct Observation of Early-Time Hydrogelation in β-Hairpin Peptide Self-Assembly

Author: Tuna Yucel, Chris M. Micklitsch, Joel P. Schneider, et al

Publication: Macromolecules

Publisher: American Chemical Society

Date: Aug 1, 2008

PERMISSION/LICENSE IS GRANTED FOR YOUR ORDER AT NO CHARGE

This type of permission/license, instead of the standard Terms & Conditions, is sent to you because no fee is being charged for your order. Please note the following:

- Permission is granted for your request in both print and electronic formats, and translations.
- If figures and/or tables were requested, they may be adapted or used in part.
- Please print this page for your records and send a copy of it to your publisher/graduate school.
- Appropriate credit for the requested material should be given as follows: "Reprinted (adapted) with permission from (COMPLETE REFERENCE CITATION). Copyright (YEAR) American Chemical Society." Insert appropriate information in place of the capitalized words.
- One-time permission is granted only for the use specified in your request. No additional uses are granted (such as derivative works or other editions). For any other uses, please submit a new request.

If credit is given to another source for the material you requested, permission must be obtained from that source.

ROYAL SOCIETY OF CHEMISTRY LICENSE TERMS AND CONDITIONS

Aug 13, 2015

This is a License Agreement between Jessie Sun ("You") and Royal Society of Chemistry ("Royal Society of Chemistry") provided by Copyright Clearance Center ("CCC"). The license consists of your order details, the terms and conditions provided by Royal Society of Chemistry, and the payment terms and conditions.

All payments must be made in full to CCC. For payment instructions, please see information listed at the bottom of this form.

License Number	3687270641282
License date	Aug 13, 2015
Licensed content publisher	Royal Society of Chemistry
Licensed content publication	Soft Matter
Licensed content title	Self-assembly and gelation properties of α-helix versus β-sheet forming peptides
Licensed content author	A. Saiani,A. Mohammed,H. Frielinghaus,R. Collins,N. Hodson,C. M. Kielty,M. J. Sherratt,A. F. Miller
Licensed content date	Oct 16, 2008
Volume number	5
Issue number	1
Type of Use	Thesis/Dissertation
Requestor type	academic/educational
Portion	figures/tables/images
Number of figures/tables/images	2
Format	print and electronic
Distribution quantity	10
Will you be translating?	no
Order reference number	None
Title of the thesis/dissertation	Hydrophobic Payload Encapsulation and Release Effects on Self-Assembling Hydrogel
Expected completion date	Sep 2015
Estimated size	130
Total	0.00 USD

Title: Enhanced Mechanical Rigidity of Hydrogels Formed from Enantiomeric Peptide Assemblies

Author: Katelyn J. Nagy, Michael C. Giano, Albert Jin, et al

Publication: Journal of the American Chemical Society

Publisher: American Chemical Society

Date: Sep 1, 2011

PERMISSION/LICENSE IS GRANTED FOR YOUR ORDER AT NO CHARGE

This type of permission/license, instead of the standard Terms & Conditions, is sent to you because no fee is being charged for your order. Please note the following:

- Permission is granted for your request in both print and electronic formats, and translations.
- If figures and/or tables were requested, they may be adapted or used in part.
- Please print this page for your records and send a copy of it to your publisher/graduate school.
- Appropriate credit for the requested material should be given as follows: "Reprinted (adapted) with permission from (COMPLETE REFERENCE CITATION). Copyright (YEAR) American Chemical Society." Insert appropriate information in place of the capitalized words.
- One-time permission is granted only for the use specified in your request. No additional uses are granted (such as derivative works or other editions). For any other uses, please submit a new request.

If credit is given to another source for the material you requested, permission must be obtained from that source.

ELSEVIER LICENSE
TERMS AND CONDITIONS

Aug 13, 2015

This is a License Agreement between Jessie Sun ("You") and Elsevier ("Elsevier") provided by Copyright Clearance Center ("CCC"). The license consists of your order details, the terms and conditions provided by Elsevier, and the payment terms and conditions.

All payments must be made in full to CCC. For payment instructions, please see information listed at the bottom of this form.

Supplier	Elsevier Limited The Boulevard,Langford Lane Kidlington,Oxford,OX5 1GB,UK
Registered Company Number	1982084
Customer name	Jessie Sun
Customer address	201 DuPont Hall NEWARK, DE 19711
License number	3687320881657
License date	Aug 13, 2015
Licensed content publisher	Elsevier
Licensed content publication	Current Opinion in Structural Biology
Licensed content title	Molecular gymnastics: serpin structure, folding and misfolding
Licensed content author	James C Whisstock,Stephen P Bottomley
Licensed content date	December 2006
Licensed content volume number	16
Licensed content issue number	6
Number of pages	8
Start Page	761
End Page	768
Type of Use	reuse in a thesis/dissertation
Portion	figures/tables/illustrations
Number of figures/tables/illustrations	1

ELSEVIER LICENSE
TERMS AND CONDITIONS

Aug 13, 2015

This is a License Agreement between Jessie Sun ("You") and Elsevier ("Elsevier") provided by Copyright Clearance Center ("CCC"). The license consists of your order details, the terms and conditions provided by Elsevier, and the payment terms and conditions.

All payments must be made in full to CCC. For payment instructions, please see information listed at the bottom of this form.

Supplier	Elsevier Limited The Boulevard,Langford Lane Kidlington,Oxford,OX5 1GB,UK
Registered Company Number	1982084
Customer name	Jessie Sun
Customer address	201 DuPont Hall NEWARK, DE 19711
License number	3687391314982
License date	Aug 13, 2015
Licensed content publisher	Elsevier
Licensed content publication	Current Opinion in Colloid & Interface Science
Licensed content title	Controlled food protein aggregation for new functionality
Licensed content author	Taco Nicolai,Dominique Durand
Licensed content date	August 2013
Licensed content volume number	18
Licensed content issue number	4
Number of pages	8
Start Page	249
End Page	256
Type of Use	reuse in a thesis/dissertation
Intended publisher of new work	other
Portion	figures/tables/illustrations

From: **PNAS Permissions** PNASPermissions@nas.edu
Subject: RE: Figure Permission Request for Thesis Use
Date: August 19, 2015 at 12:33 PM
To: Jessie Sun

PP

Permission is granted for your use of the figures as described in your message. Please cite the PNAS article in full, and include "Copyright (2007) National Academy of Sciences, U.S.A." as a copyright note. Because this material published between 1993 and 2008, a copyright note is needed. There is no charge for this material, either. Let us know if you have any questions.

Best regards,
Kay McLaughlin for
Diane Sullenberger
Executive Editor
PNAS

-----Original Message-----
From: Jessie Sun
Sent: Thursday, August 13, 2015 10:28 PM
To: PNAS Permissions
Subject: Figure Permission Request for Thesis Use

Hello!
I'm requesting the permission for the use of two figures from Haines-Butterick et. al's paper for my Ph.D thesis. In the remaining email, I've filled out the provided form on the PNAS Permission site.

Thank you for all your help!
Happy Thoughts,
Jessie Sun

1. Jessie Sun, University of Delaware, Graduate Student
2. 201 DuPont Hall
   a. Newark DE, 19711
   b. Ph: 484-324-8537
3. Vol.104, no. 19, May 8, 2007
4. Controlling Hydrogelation Kinetics by Peptide Design for Three-dimensional encapsulation and injectable delivery of Cells
5. Lisa Haines-Butterick, Karthikan Rajagopal, Monica Branco, Daphne Salick, Ronak Rughani, Matthew Pilarz, Matthew S. Lamm
6. p.7793, p. 7794
7. Figure 2 & Figure 5a

1. Hydrophobic Payload Encapsulation and Release Effects on Self-Assembling Peptide Hydrogel
2. Jessie Sun
3. UMI
4. --
5. 10
6. Educational Use
7. Non-Profit

ROYAL SOCIETY OF CHEMISTRY LICENSE TERMS AND CONDITIONS

Aug 13, 2015

This is a License Agreement between Jessie Sun ("You") and Royal Society of Chemistry ("Royal Society of Chemistry") provided by Copyright Clearance Center ("CCC"). The license consists of your order details, the terms and conditions provided by Royal Society of Chemistry, and the payment terms and conditions.

All payments must be made in full to CCC. For payment instructions, please see information listed at the bottom of this form.

License Number	3687390590107
License date	Aug 13, 2015
Licensed content publisher	Royal Society of Chemistry
Licensed content publication	Soft Matter
Licensed content title	Injectable solid hydrogel: mechanism of shear-thinning and immediate recovery of injectable β-hairpin peptide hydrogels
Licensed content author	Congqi Yan,Aysegul Altunbas,Tuna Yucel,Radhika P. Nagarkar,Joel P. Schneider,Darrin J. Pochan
Licensed content date	Sep 9, 2010
Volume number	6
Issue number	20
Type of Use	Thesis/Dissertation
Requestor type	academic/educational
Portion	figures/tables/images
Number of figures/tables/images	1
Format	print and electronic
Distribution quantity	10
Will you be translating?	no
Order reference number	None
Title of the thesis/dissertation	Hydrophobic Payload Encapsulation and Release Effects on Self-Assembling Hydrogel
Expected completion date	Sep 2015
Estimated size	130
Total	0.00 USD